Underground Coal Thermal Treatment

Task 6 Topical Report, Utah Clean Coal Program

Reporting Period Start Date: October 2009

Report Period End Date: September 2011

Principal Authors: P.J. Smith, M. Deo, E.G. Eddings, A.F. Sarofim, K. Gneishen, M. Hradisky, K. Kelly, P. Mandalaparty, H. Zhang

Issue date: January 11, 2012

DOE Award Number: DE-NT0005015
Project Officer: David Lang

University of Utah
Institute for Clean & Secure Energy
380 INSCC
155 South, 1452 East
Salt Lake City, UT 84112

DISCLAIMER

ABSTRACT

The long-term objective of this work is to develop a transformational energy production technology by in-situ thermal treatment of a coal seam for the production of substitute natural gas (SNG) while leaving much of the coal's carbon in the ground. This process converts coal to a high-efficiency, low-GHG emitting gas fuel. It holds the potential of providing environmentally acceptable access to previously unusable coal resources. This topical report discusses the development of experimental capabilities, the collection of available data, and the development of simulation tools to obtain process thermo-chemical and geo-thermal parameters in preparation for the eventual demonstration in a coal seam. It also includes experimental and modeling studies of CO_2 sequestration. Efforts focused on:

- Constructing a suite of three different coal pyrolysis reactors. These reactors offer the ability to gather heat transfer, mass transfer and kinetic data during coal pyrolysis under conditions that mimic *in situ* conditions (Subtask 6.1).
- Studying the operational parameters for various underground thermal treatment processes for oil shale and coal and completing a design matrix analysis for the underground coal thermal treatment (UCTT). This analysis yielded recommendations for terms of targeted coal rank, well orientation, rubblization, presence of oxygen, temperature, pressure, and heating sources (Subtask 6.2).
- Developing capabilities for simulating UCTT, including modifying the geometry as well as the solution algorithm to achieve long simulation times in a rubblized coal bed by resolving the convective channels occurring in the representative domain (Subtask 6.3).
- Studying the reactive behavior of carbon dioxide (CO_2) with limestone, sandstone, arkose (a more complex sandstone) and peridotite, including mineralogical changes and brine chemistry for the different initial rock compositions (Subtask 6.4). Arkose exhibited the highest tendency of participating in mineral reactions, which can be attributed to the geochemical complexity of its initial mineral assemblage. In experiments with limestone, continuous dissolution was observed with the release of CO_2 gas, indicated by the increasing pressure in the reactor (formation of a gas chamber). This occurred due to the lack of any source of alkali to buffer the solution. Arkose has the geochemical complexity for permanent sequestration of CO_2 as carbonates and is also relatively abundant. The effect of including NH_3 in the injected gas stream was also investigated in this study. Precipitation of calcite and trace amounts of ammonium zeolites was observed. A batch geochemical model was developed using Geochemists Workbench (GWB). Degassing effect in the experiments was corrected using the sliding fugacity model in GWB. Experimental and simulation results were compared and a reasonable agreement between the two was observed.

TABLE OF CONTENTS

LIST OF FIGURES

LIST OF TABLES

LIST OF ABBREVIATIONS

BTX	Benzene, Toluene, and Xylene
C	Celsius
CAD	Computer Aided Design
CCR	Conduction, Convection, Reflux
CFD	Computational Fluid Dynamics
CO_2	Carbon Dioxide
DEM	Discrete Element Methods
DQMOM	Direct Quadrature Method of Moments
EDS	Energy Dispersive X-Ray Spectroscopy
EOR	Enhanced Oil Recovery
FBR	Fixed-Bed Reactor
G	grams
GHG	Greenhouse Gas
GWB	Geochemist's Work Bench
IC	Ion Chromatography
ICPMS	Inductively Coupled Plasma Mass Spectroscopy
IPCC	Intergovernmental Panel on Climate Change
K	Kelvin
LES	Large Eddy Simulations
LLNL	Lawrence Livermore National Laboratory
M	Meters
mg/l	Milligrams per Liter
PCX	Phenol, Cresol, and Xylene
ppm	parts per million
psi	pounds per square inch
RANS	Reynolds-Averaged Navier-Stokes
RF	Radio frequency
SEM	Scanning Electron Microscope
SO_2	Sulphur Dioxide
SNG	Substitute Natural Gas
UCG	Underground Coal Gasification
UCTT	Underground Coal Thermal Treatment
V/UQ	Validation, Uncertainty Quantification
µm	Micrometers
XRD	X-ray diffraction

EXECUTIVE SUMMARY

The long-term objective of this work is to develop a transformational energy production technology by in-situ thermal treatment of a coal seam for the production of substitute natural gas (SNG) while leaving much of the coal's carbon in the ground. This process converts coal to a high-efficiency, low-GHG emitting gas fuel. It holds the potential of providing environmentally acceptable access to previously unusable coal resources. This topical report discusses the development of experimental capabilities, the collection of available data, and the development of simulation tools to obtain process thermo-chemical and geo-thermal parameters in preparation for the eventual demonstration in a coal seam. This work includes the evaluation of underground coal thermal treatment (UCTT) for the production of SNG along with subsequent sequestration of CO_2.

The *experimental activities* for this subtask centered on the construction of a suite of three reactors for studying coal pyrolysis under *in situ* conditions. These reactors included 1) a fixed-bed reactor capable of operation at 1000 psi and 1000^{o}C with samples sizes up to ¾" in diameter, 2) a block reactor capable of operation up to 600^{o}C at low pressures with blocks up to 6" on a side, and 3) a rubblized-bed reactor capable of operating at 1500 psi and 600^{o}C with blocks up to 6" in diameter. All reactors are equipped with temperature and pressure control and sampling ports for kinetic studies.

Initial studies utilizing the low-pressure block reactor focused on mass transfer resistance effects that occur during coal pyrolysis in large blocks. Observation of coal structure near the heated surface and deep within the heated block suggest fundamentally different methods of void fraction development depending upon the ease of mass transfer. Near the heated surface, void volume is generated by pore growth and maturation, whereas near the block center, void volume is generated by microfracturing. There is also preliminary evidence that secondary pyrolysis plays an important role in coal block pyrolysis.

The *collection of existing data* included an extensive literature review of above and under-ground coal treatment. The literature for underground thermal treatment of oil shale is also highly relevant to in-situ conversion of coal. An evaluation of the literature yielded a set of guidelines for design and operating conditions that are desirable for the underground coal thermal treatment (UCTT):

Targeted Coal Rank:	Preferably high volatile bituminous coals.
Conversion Approach:	Conduction heating using an externally generated hot gas; or convection heating using an externally generated hot gas; or a combined approach.
Well Orientation:	Parallel to the targeted coal seam
Rubblization:	Not necessary
Presence of Oxygen:	Not necessary and preferably not.
Temperature:	The temperatures that favor the formation of different products are: a. Maximum 600-700°C (1100-1300°F), a temperature range at which the volatile yield approaches an asymptotic value;

b. Coal-bed methane, less than 300°C (570°F);
c. Liquid Products, less than 390°C (730°F);
d. Moisture, less than 400°C (750°F);
e. Methane, 400-500°C (750-930°F);
f. Hydrogen, above 500°C (930°F);
g. Tar, above 400°C (750°F) and peak at 550°C (1020°F);
h. Tar gasification, above 550°C (1020°F);
i. Syngas (H_2+CO), 450-700°C (840-1300°F).

Pressure: The pressure for underground gasification should be maintained below the lithostatic pressure to prevent outleakage of gas and contamination of groundwater. Lithostatic pressures of 3.5MPa to 15-30MPa (500 to thousands of psi) are not uncommon. The effects of pressure on yield are:

a. Liquid products are maximized at low pressure;
b. Gas products are maximized at high pressure;

Heating Sources:

a. Fossil fuel is currently the major energy source for heating;
b. In the future, solar, wind and renewable are possible alternatives;
c. The process can be made self-sufficient in energy by using product gas as the heat source;
d. Heating requirements can be reduced by aggressive heat management, such as using the waste heat in the coal ash product.

The *simulation* approach is to apply computational fluid dynamics (CFD)-based simulation tools to UCTT. The ultimate goal is to build a simulation tool that captures the relevant physical processes and to collect data from an experimental system (Subtask 6.1) for validation/uncertainty quantification (V/UQ). In the past year we were able to modify our geometry as well as a solution algorithm to achieve long simulation times of a rubblized coal bed by resolving the convective channels occurring in the representative domain. The ability to predict heat transfer, in particular, convective heat transfer in a coal bed is critical. Preliminary simulations of in situ processes using a reservoir simulation-type approach (e.g. fluid flow through porous media) showed that such an approach is at times insufficient to resolve key physics affecting production rates, particularly convective heat flow patterns. Once the coal bed is sufficiently fractured, the dominant heat transfer mode occurs through the convective channels. In the case of UCTT, there is a distribution of coal size in the production bed and those pieces of coal are packed such that convective currents heat the bed.

Carbon dioxide (CO_2) sequestration is considered to be at least a partial solution to decrease CO_2 emissions to the atmosphere, thus stemming the rapid rise in atmospheric CO_2 concentrations. The process has been conceptualized as being able to inject large quantities of CO_2 into saline aquifers, since saline aquifers offer the most storage capacity. Mineralogical sequestration, where CO_2 gets mineralized to a carbonate or related component, is the permanent storage mechanism. However, as the reactions occur, there are changes in rock properties that can impact the operation of the process. The formation

into which CO_2 is being injected governs the ultimate fate of CO_2. Injection of CO_2 into four different formations has been studied: limestone, sandstone, peridotite, and arkose. The effect of NH_3 in the injected stream was also investigated.

An experimental program was designed to study the rock and injection gas compositional effects. A high-temperature and high-pressure reaction system was built, and reactions were carried out at 100^0C and 2000 psia for multiple times under identical conditions. In the limestone experiments, the absence of the any source for cations rules out the possibility of any secondary precipitation reactions. Thus the primary modes of sequestration in this case are either structural trapping or ionic trapping. In the case of sandstone, silicate dissolution reactions dominate, which is indicated by the increase in the pH of the brine. Kaolinite formation was also observed. In the case of peridotite, carbonation reactions dominate yielding magnesite crystal formation. Numerous changes were observed in the case of arkose. Reprecipitation of calcite after initial dissolution, analcime formation was an important observation. In all the cases, very good correlation between brine and rock chemistries was observed.

INTRODUCTION

Underground Coal Thermal Treatment (UCTT) is a relatively new approach to subsurface coal utilization. Although UCTT is similar to underground coal gasification because it aims to produce valuable fuel gas from an in situ source, it is envisioned as an enhanced form of coal bed methane recovery. A UCTT operation would introduce heat into a deeply buried coal seam in the absence of an oxidation source, favoring the formation of high H:C ratio gases over oxidized species such as CO and CO_2. The selective extraction of high-value carbon from the coal deposit will lower the overall carbon footprint of the process. The carbon char retained in the ground should have the further benefit of minimizing surface subsidence issues and reducing the mobilization of contaminants such as mercury and cadmium into surrounding aquifers.

Pyrolysis in a subsurface environment introduces a number of effects not typically seen in conventional powdered coal pyrolysis. Lithostatic and hydrostatic pressures at reservoir depths combine to volumetrically constrain coal, preventing possible thermal swelling of the coal structure. Mass transfer is limited to movement through native pores and cleats, making product evolution far more difficult than in a high surface area powder. Heat transfer in coal blocks is also hindered due to the reliance upon conduction over larger length scales. As a result of these transport resistances, describing pyrolysis in coal blocks is more difficult than what is typically reported from powdered systems.

The work is focused on developing a group of investigative tools that will more accurately describe UCTT under realistic conditions.

METHODS

Subtask 6.1 – Bench-Scale RF Thermal Treatment

Subtask 6.1 focused on the design of several reactors capable of performing coal pyrolysis under conditions that would mimic in situ pyrolysis. The pyrolysis reactors described here offer the ability to study global pyrolysis kinetics in mass transfer-limited coal systems while also examining the effects of various modes of heat transfer including conduction and free convection. Collectively, the data sets derived from this suite of reactors should provide enough information to guide the preliminary design of a UCTT field test. The project initially focused on a broad literature survey to better define the important processing parameters, followed by the sequential design and implementation of each reactor. Described below are the results of the literature survey and the design considerations given to each reactor system to most accurately mimic the UCTT process.

Literature Survey Results

Coal pyrolysis is an extensively studied subject due to its importance in a wide range of industrial processes such as coal combustion and gasification, and coke production. In the context of the UCTT process, several parameters appear to be important when considering reactor design, including:

- Temperature – how does ultimate temperature affect yields and composition?
- Heating rate – how sensitive are yields to heating rates at relevant in situ conditions?
- Pressure – what effect will the natural formation pressure have on pyrolysis?
- Coal type – how does coal rank affect product yields and composition?
- Heating source – do different heating methods produce different pyrolysis chemistries?
- Coal size – do extended coal domains introduce secondary pyrolysis effects?

Survey results for these parameters are discussed below.

Temperature

In general, it can be stated that increasing peak temperature leads to increasing volatile yield during coal pyrolysis (Yu 2007). Figure 1 shows the yields of various volatile species from a bituminous coal when heated to varying ultimate temperatures at a constant heating rate of 10^3 Ks^{-1}. Although this result holds true for all coal types, the actual yields as well as compositions are complex functions of both heating rate and residence time at the peak temperature. 300^{o}C is the typical threshold temperature for the onset of pyrolysis, but beyond that, little can be concluded purely from the peak temperature achieved during heating.

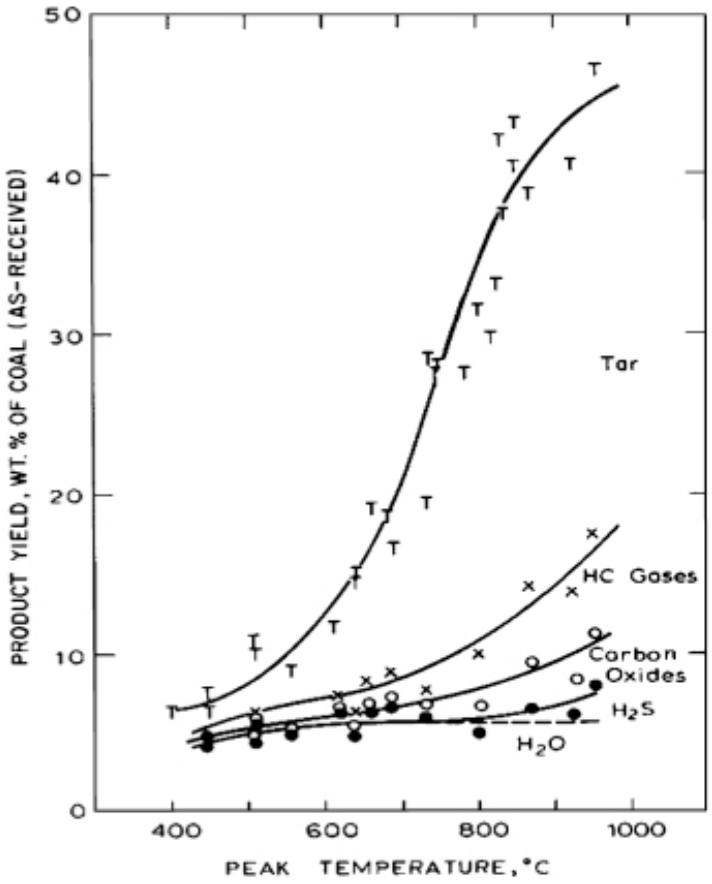

Figure 1. Volatile yields from pyrolysis of a Pittsburgh bituminous coal at a heating rate of 10^3 Ks^{-1} (Suuberg 1977). Overall yields increase as the temperature increases.

Heating Rate

Heating rate appears to be a crucial parameter in assessing the extent of devolatilization and the resulting product compositions in coal pyrolysis. Increased heating rate leads to a substantial increase in the volatile yield across a wide range of coals (Howard 1981). At the highest heating rates (~10^4 K s^{-1}), fragmentation of the coal structure is severe enough to carry fixed carbon into the vapor phase, giving yields higher than what is suggested via proximate analysis of the coal (Kimber 1967). At the slower heating rates that would be relevant to a UCTT process, devolatilization would tend to occur at lower temperatures, suggesting a greater retention of fixed carbon and an increased importance of secondary pyrolysis reactions in determining final product yields.

Pressure

Pressure has a very substantial affect on yield and composition during coal pyrolysis. Increased pressure decreases the overall yield of volatile matter from coal (Wall 2002). Figure 2 shows the yields of various volatile species during the pyrolysis of a bituminous coal at 1000°C. The lost yield is derived from the

reduction in tar yields because hydrocarbon gas yields are seen to increase at increased pressure. At the anticipated formation pressure of a deep coal seam (> 1000 psi), the pressure effect would be substantial, possibly decreasing tar yields by over 50% and increasing gas yields by over 50% when compared to pyrolysis at atmospheric conditions.

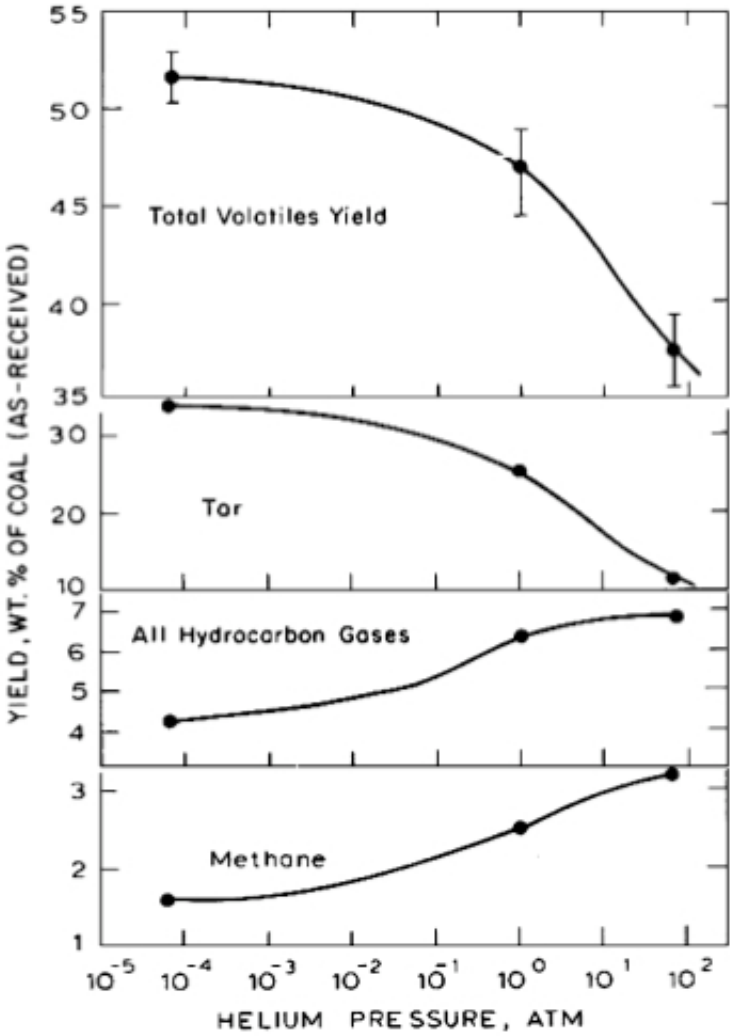

Figure 2. Pyrolysis species yields as a function of pressure from a Pittsburgh bituminous coal heated to 1000°C (Suuberg 1977).

Coal Type

Coal rank and seam location tend to offer some broad clues regarding the pyrolysis behavior of the coal. In general, increasing coal rank leads to decreases in volatile matter and moisture content (Neavel 1981). However, especially as it pertains to volatile matter, the effective volatile yields winds up being a function of the pyrolysis method and may increase or decrease from those measured via proximate analysis.

Typically, proximate analysis is measured by pyrolysis of a packed bed of coal particles, promoting some level of secondary cracking of volatiles on the bed surface. The tendency for cracking to occur is not a clear function of coal type, thus it is difficult to precisely correlate coal rank to effective volatile yields (Howard 1981). In a UCTT process, secondary pyrolysis reactions are expected to be important so effective volatile yields should decrease from what is measured via proximate analysis.

Heating Source

There is little evidence to suggest that the heating method affects yield or composition during coal pyrolysis. Microwave and radio frequency (RF) radiation frequencies, the two most likely candidates for electromagnetic field-based hydrocarbon production, function by the absorption of radiation into specific chemical bonds, leading to increases in rotational and vibrational energies of the affected molecules. Microwave frequencies are most strongly absorbed by water while RF is weakly absorbed by most bitumen components (Mutyala 2010). This observation suggests that microwave radiation would dissipate rapidly at the nearest region of high moisture content while RF would promote a more general heating over a larger volume. In either case, no evidence exists to suggest that either of these modes of heating leads to direct bond rupture, so composition and yield would be functions of heating rate, pressure and temperature as described above.

Coal Size

Increased coal particle size has been shown to have an effect similar to that of increased pressure (Yu 2007). Total volatile and tar yields decrease while gas yields increase. These effects are attributed to increased mass transfer resistances and additional secondary pyrolysis reactions. Little work has been done on coal domains larger than 1"; however, an experiment on large blocks of lignite suggested that the product distribution of carbon oxides and hydrocarbons could only be explained by the substantial role of self-gasification reactions as incipient moisture vaporized and diffused back through the pyrolysis front (Westmoreland 1984). The drying of coal blocks has also been studied via forced convection of hot air. Permeability was seen to increase by two orders of magnitude after drying completed (Vanderborgh 1978). This study did not examine the influence of pyrolysis on the permeability of coal blocks, but the UCTT project at the University of Utah is actively addressing this issue.

Literature Survey Conclusions

From a process perspective, UCTT is envisioned as a low-temperature, low-heating-rate, high-pressure pyrolysis method in large blocks of coal. Based upon the available evidence in the literature, these conditions will generally favor the formation of char and gases over tar and liquid products. The biggest question that remains is what heating rates can be achieved in large blocks of coal. Heat transfer is likely to couple with mass transfer and kinetics in determining the product yields in an *in situ* environment, making the simulation of UCTT conditions far more complex than what has been previously studied in the field of coal pyrolysis.

Changes to the Scope of Work

Based upon the results of the literature survey and discussions within the UCTT research group, two in-scope adjustments were made to the scope described in Subtask 6.1 of the Phase 2 Statement of Project Objectives. First, TGA studies of coal pyrolysis were removed in favor of work in a fixed-bed reactor (FBR). This was motivated by the inherently small sample sizes typically used in a TGA system. Because a TGA can really only handle powders, it was agreed that any such studies would basically be replicates of results that have already been published. The switch to the FBR system was seen as an upgrade in that it could provide the same basic data as a TGA with similar throughput of samples, but allow the use of large coal lumps that could introduce more realistic heat and mass transfer resistances. Second, the design of an RF-based reactor was abandoned and replaced with an electrically heated reactor. This was jointly motivated by the difficulty in finding a partner to produce an affordable RF heat source for heating coal blocks and by a lack of evidence in the literature that electromagnetic heating would produce unique results.

Reactor Design

Based upon the literature survey and UCTT group discussions, three unique reactors have been implemented to fulfill the scope of work for this subtask. The basic capabilities of each reactor are outlined in Table 1. Each reactor is discussed in greater detail below.

Table 1. UCTT pyrolysis reactor capabilities.

Reactor	Max. Temperature (^oC)	Max. Pressure (psi)	Coal Geometry	Sample Size (kg)
Fixed-Bed	1000	1000	¾"-diameter cylindrical cores	0.1
High-Pressure Rubblized-Bed	600	1500	< 6" blocks	10
Coal Block	600	50	6" blocks	5

Fixed-Bed Reactor

The primary purpose of the FBR system is to measure global kinetic data for lump coal samples of interest to the UCTT project. The fixed-bed has a ¾" diameter and a 6" bed length. The FBR can be operated at pressures up to 1000 psi and temperatures up to 1000^{o}C. The system is integrated with an OPTO-22 control system that allows for user-defined heating rates and precise control of pressure and ultimate temperature. The FBR system can operate under a variety of atmospheres including N_2, He, Ar,

CO_2 and H_2O. The reactor exit has been designed to condense tar and liquid products, then route gas products to a gas chromatograph or total hydrocarbon analyzer for analysis.

Coal Block Reactor

The primary purpose of the coal block reactor is to study conductive heat transfer and mass transfer in blocks of coal up to 5 kg in weight (~ 6" cubed). A nitrogen purge and downstream bubbler train also permits the capture and analysis of condensable liquids and gases. The reactor is currently constructed with four electrical cartridge heaters and three thermocouples, all monitored externally by an OPTO-22 controller. Coal blocks for the reactor are cut to produce two parallel faces perpendicular to the bedding plane of the coal. Four ¼" diameter holes are drilled in a square pattern in the blocks to accommodate the cartridge heaters. Three thermocouple holes are drilled, two parallel to the heaters and one perpendicular to and beneath the heaters. The heaters are capable of heating rates up to 10 K min^{-1} and ultimate temperatures of 600°C. The coal block reactor is not designed for high-pressure operation, but can be operated at modest pressures above atmospheric. In a typical experiment, the four embedded heaters within a coal block are ramped at a user-defined rate until they have reached the ultimate temperature. The heaters are then held at this temperature for a defined length of time while temperature profiles are measured at various locations in the block. Products can be collected continuously, and the blocks are available for analysis after pyrolysis is complete. A schematic of the coal block reactor is shown in Figure 3.

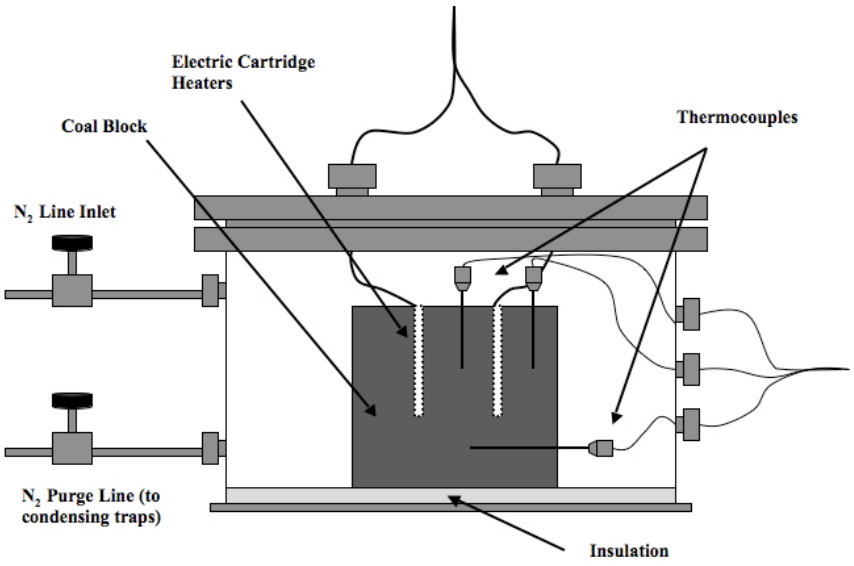

Figure 3. Schematic of the coal block reactor.

High-Pressure Rubblized Bed Reactor

The primary purpose of this reactor is to study free convective heating in a large bed of coal chunks at high pressures. The reactor is also equipped with sampling ports for analysis of product composition. The reactor will operate at pressures up to 1500 psi and temperatures up to 600°C. The rubblized bed reactor utilizes a unique two-vessel design to achieve its severe operating thresholds. The outer vessel is an 18" diameter pressure vessel that is built to withstand the maximum operating pressure at temperatures up to 300°C. Housed inside the pressure vessel will be a 6" diameter vessel that contains the rubblized coal bed. The inner vessel will have an electrical heat source that conductively heats adjacent coal blocks and induces convective currents in the free spaces between blocks. An array of thermocouples will give temperature data in various regions of the block. External lines through both vessels will permit a steady purge of N_2 so that gas samples can be collected during pyrolysis. This reactor will have the unique ability to simultaneously examine heat transfer, mass transfer and kinetics simultaneously during pyrolysis of a large coal bed. A cross-sectional schematic of the rubblized-bed reactor is shown below in Figure 4.

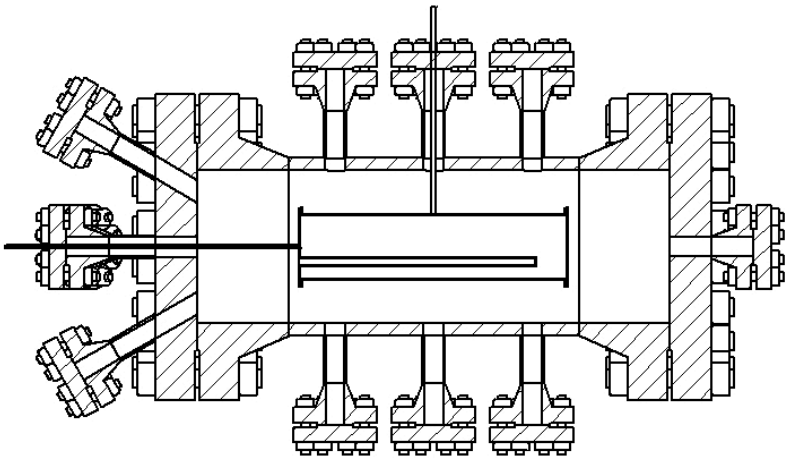

Figure 4. Cross-sectional schematic of the rubblized-bed reactor. An N_2 purge line enters the inner vessel from the left and vents through the top of the pressure vessel.

Subtask 6.2 – In-Well Heater Design Alternatives

This project focuses on UCTT, in contrast to underground coal gasification. Unlike coal gasification there is very little literature on UCTT. However, a large number of retorting techniques relevant to UCTT have been explored for underground oil shale thermal treatment (Bartis et al. 2005; Crawford et al. 2008; Liu et al. 2009; Qian and Wang 2006; United States Department of Energy, 2007). In addition, a number of publications summarized the operation conditions and product yields using various types of lab-scale apparatus. These publications are highly relevant to our investigation in UCTT processes.

The first task was to review the existing technology used for underground thermal treatment of oil shales, which was highly relevant to UCTT. Oil shale has been treated in-situ since 1970s. The treatment concepts can be divided into four major categories according to the heating techniques: internal combustion, wall conduction, externally generated hot gas, and volumetric heating. Combined approaches were also used for oil shale. For example, ExxonMobile's Electrofrac technology is a combined approach of volumetric heating and wall conduction, and an integrated conduction heating and internal combustion approach was used by Energy Partners in their geothermic fuel cells.

The second task was a review of the physical, chemical and geological properties of various coal resources. Coal properties provide insights into the best design parameters for its conversion. Coal shows very different properties in comparison with those of oil shales. Therefore, adjustments in design parameters are necessary. For example, the thickness of coal seams is usually much less than that of shales. In general, coal seams are less than 30 meters thick (100 feet) with multiple single layers.

The third task focused on experimental data from lab-scale coal treatment and identified the relationships between operational parameters and product yields and distribution. The available data for product yields at varying temperature, pressure, heating rates and other coal treatment parameters include contradictory results. We examined and compared the available data to establish validation data.

Although there is very little literature in the field of underground coal thermal treatment, the literature on oil shale in-situ treatment, coal properties, and lab-scale coal treatments were highly relevant to the project. Therefore, this enabled the development of a set of design parameters for the underground coal thermal treatment.

Subtask 6.3 – LES in Reacting Porous Media

The approach included: the evaluation and selection of appropriate simulation tools, preliminary simulations, the development of a representative geometry, simulations with simplified and extended domains, the development of boundary conditions, the study of temperature evolution, and the development of a strategy to deal with dramatically different time scales.

Software tools

The initial approach was to develop a simulation tool using a statistical approach to model the geometry involving voids and physical pieces of coal in ARCHES. ARCHES is a highly scalable, finite-volume large eddy simulation code developed at the Institute for Clean and Secure Energy. However, we determined that having a simulation involving the actual geometry of pieces of coal would provide a better representation of this process, but performing this type of simulation in ARCHES is difficult due to the complex geometry. The commercially available simulation software Star-CCM+, created by CD-adapco, is a simulation tool that has been developed to handle complex geometries and can be used to model the convective currents through the channels of a rubblized bed of coal. Scaling studies performed

on Star-CCM+ showed reasonable scalability up to 768 processes. Because of these capabilities, we have determined that Star-CCM+ would be more appropriate tool to achieve our project objectives.

We have identified a set of experimental data of rubblized pieces to serve as the preliminary validation geometry, based on which we are creating our simulation. The efforts of Subtask 6.1 are also concentrating on creating an experiment with rubblized pieces of coal, which we plan to use for V/UQ. Therefore, all efforts have centered on creating a rubblized coal geometry with pipe heating elements. To simulate the rubblized coal bed heated through pipes, we are using a suite of commercial software tools, including Matlab, Gambit, ICEM-CFD, and Star-CCM+. Using a discrete element method (DEM) software tools, we are able to simulate the random coal distribution inside this test domain. Particles can be randomly packed based on input distributions of particles sizes and on particle physics. In the early stages of creating the rubblized bed geometry we have successfully used the commercial software EDEM. However, during the course of this project, CD-adapco implemented a DEM solver into the more recent versions of Star-CCM+, enabling recreation of rubblized coal geometry using this DEM solver. Therefore, during this project, we have shifted our efforts from using the EDEM software to the DEM solver capabilities available in Star-CCM+.

Preliminary simulations

Initially, in order to create CFD simulations for validation studies, the computational efforts focused on three main tasks: 1) correctly modeling heat transfer in the fluid region of the computational domain, including flow around obstacles, 2) correctly model heat transfer inside the solid regions, and 3) coupling physics for both the fluid and solid regions into one simulation. The initial fluid simulations were two-dimensional, unsteady, using Reynolds-Averaged Navier-Stokes (RANS) turbulence model. The test geometry, along with the developing velocity field, is shown in Figure 5. Figure 6 shows the temperature distribution for the same simulation. Both the velocity and temperature results for the initial 2-D case were satisfactory, as expected. This allowed us to extend the simulation into a three-dimensional space. Using the same model and same simulation setup, we have obtained similar results.

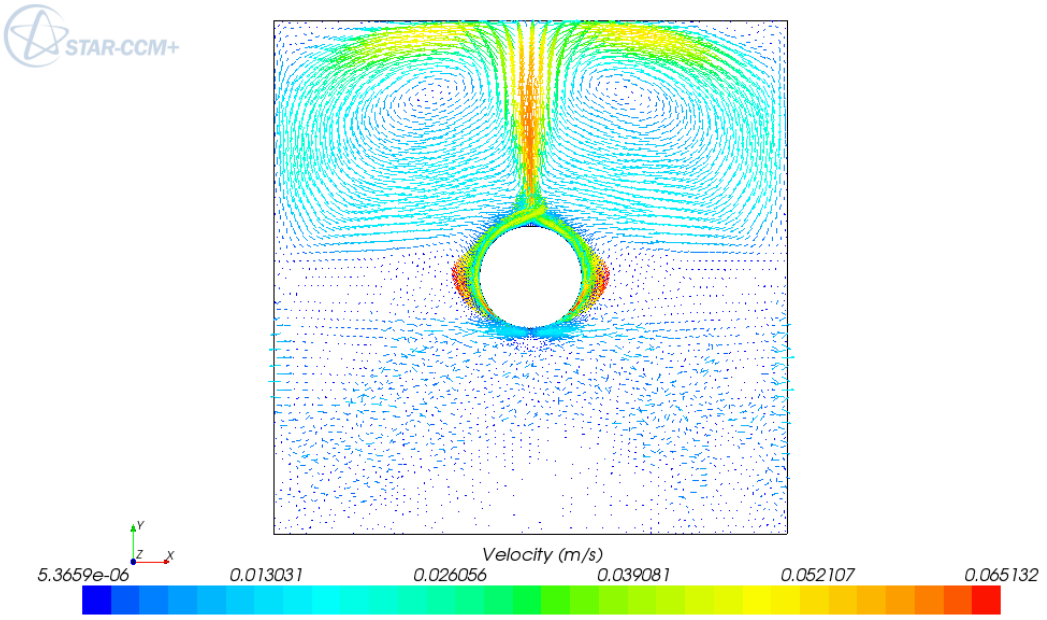

Figure 5. Velocity field for the initial 2-D RANS simulation.

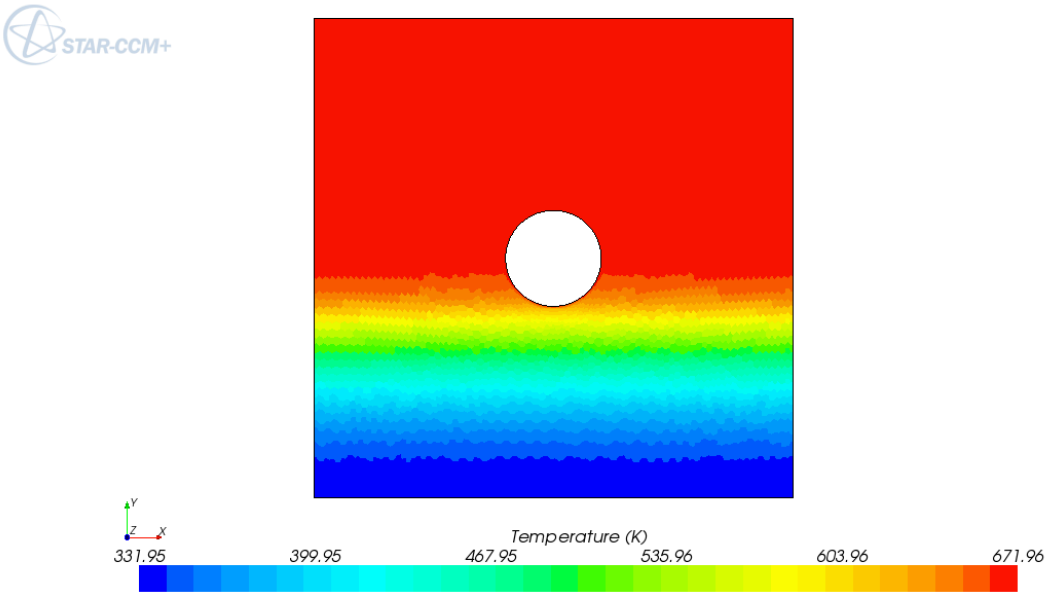

Figure 6. Temperature distribution for the initial 2-D RANS simulation.

In the next step we introduced solid objects generated in EDEM into the domain, shown in Figure 7, and we changed from RANS models to Large Eddy Simulation (LES) turbulence models. LES models are

able to resolve the unsteady vortex structures, which contribute to the overall heat transfer and can greatly contribute to providing a more accurate answer in comparison to RANS models. The rubblized chunks of coal inside the representative domain shown in Figure 7 are represented by eight cubes generated using the EDEM software. While this is an extremely simplified geometry, it helped determine the capabilities of our simulation tools as well as to provide a starting point in creating more complex geometries and simulations. The preliminary results from this simulation showed the expected heat transfer within the computational domain, shown in Figure 8.

Development of Representative Geometry

To further improve the simulation results and to achieve higher fidelity results, we explored the geometry and meshing capabilities of EDEM, Gambit, and Star-CCM+ simulation tools. First, we create our representative rubblized geometry using the DEM simulation capabilities of Star-CCM+ and export these results into Gambit meshing software, which allows efficient processing of the DEM results into the actual geometric representation of the coal bed. This geometry is then exported back to Star-CCM+, with the appropriate boundary conditions, where the CFD simulation is performed. This streamlined process for geometry creation allows us to side-step memory limitations, which occur when processing the DEM simulation results directly in Star-CCM+. Figure 8 shows a more complex geometrical representation of the rubblized coal volume. We have also evaluated two geometry and meshing strategies that would allow us to: 1) eliminate the problematic corner areas by using the surface-wrapping meshing model, and 2) preserve the sharp geometric features by further refining the mesh.

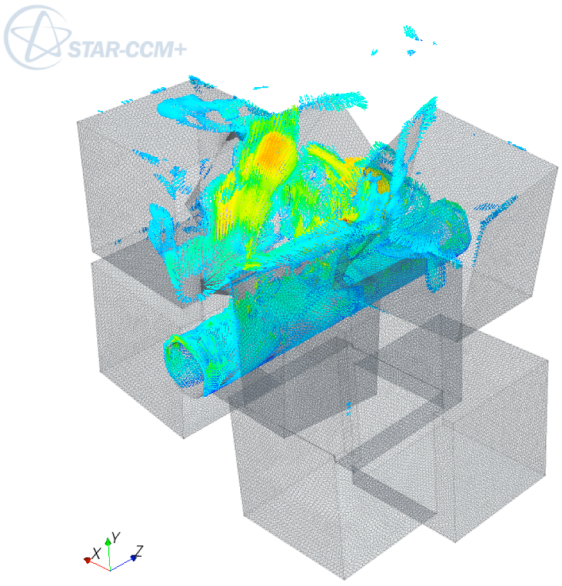

Figure 7. Initial 3-D LES simulation with obstacles. Also shown are velocity vectors for the preliminary simulation.

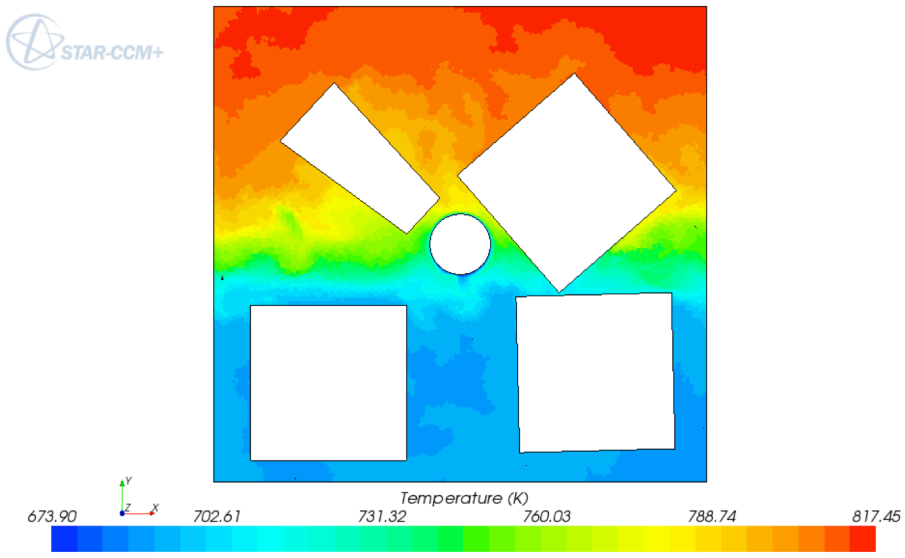

Figure 8. Temperature contours from the preliminary 3-D LES simulation.

Surface Wrapping. Surface wrapping is generally used to wrap problematic details in the geometry, such as a corner of a cube or a sharp angle between two pieces of coal. Surface wrapping corrects the sharp areas of the geometry or eliminates difficult areas by combining regions. Figure 10 compares the previous geometry details in the simple eight-piece coal case to the wrapped surface geometry. Figure 10 also shows an example of the corner of a cube being merged into the cube below it. This helped to increase contact angles and helped the meshing process by eliminating problematic areas. However, the surface-wrapping model created new difficulties in preserving independent pieces of coal.

Figure 9. Complex coal geometry created using EDEM, Matlab, Gambit, and Star-CCM+

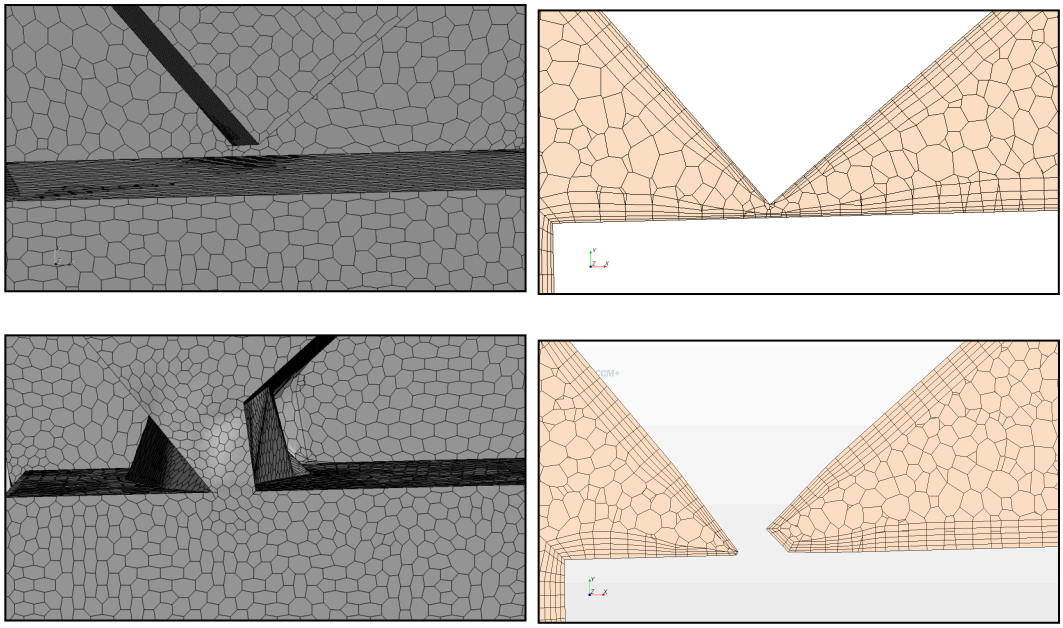

Figure 10. Comparison of original geometry and mesh (top) with newly-adapted wrapped surface geometry and mesh (bottom). The new approach eliminates the problematic areas.

Mesh Refinement. Figure 11 and Figure 12 show images of a refined mesh that was used to decrease the temperature fluctuations present in the solution due to sharp corners and small spaces by eliminating

highly skewed cells. This meshing strategy preserved the complex geometrical features by decreasing the computational cell size. However, this mesh led to an excessive number of cells and thus greatly increased the computational time required to obtain a converged solutions. Additionally, neither of these methods addressed a problem that occurs in the more complex geometric representations of the rubblized coal: the presence of internal gas volumes trapped among multiple pieces of coal.

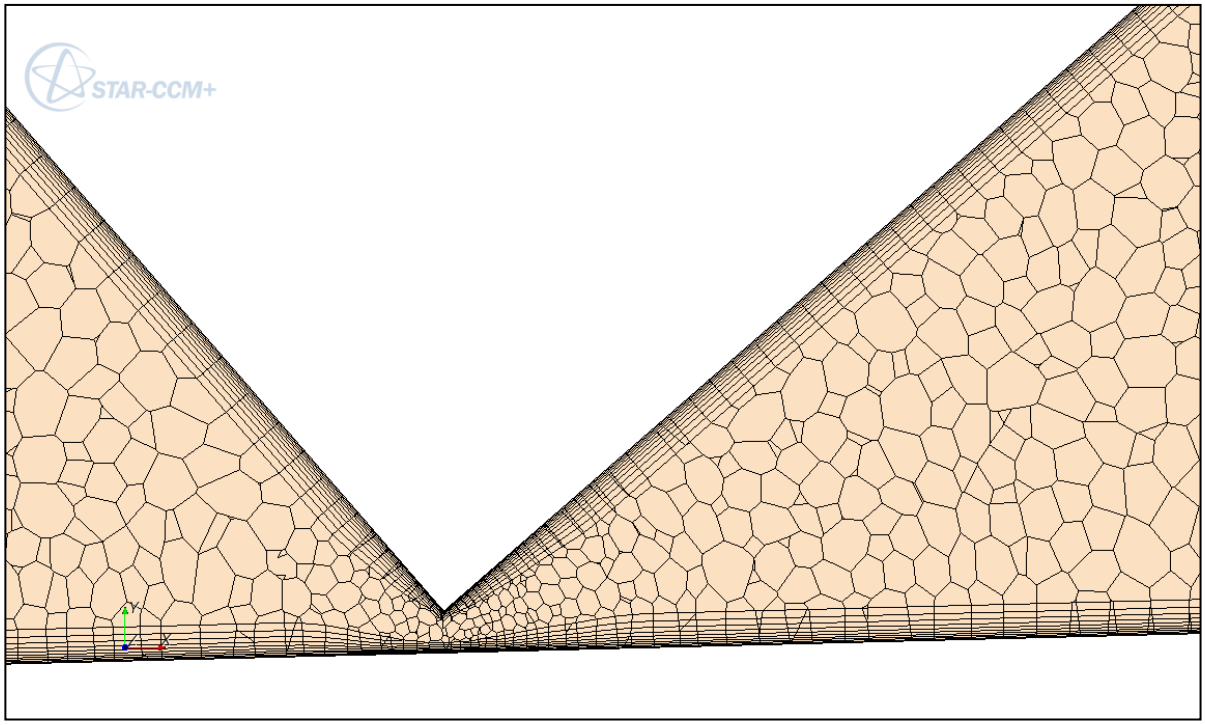

Figure 11. Refined mesh – close up view of problematic area.

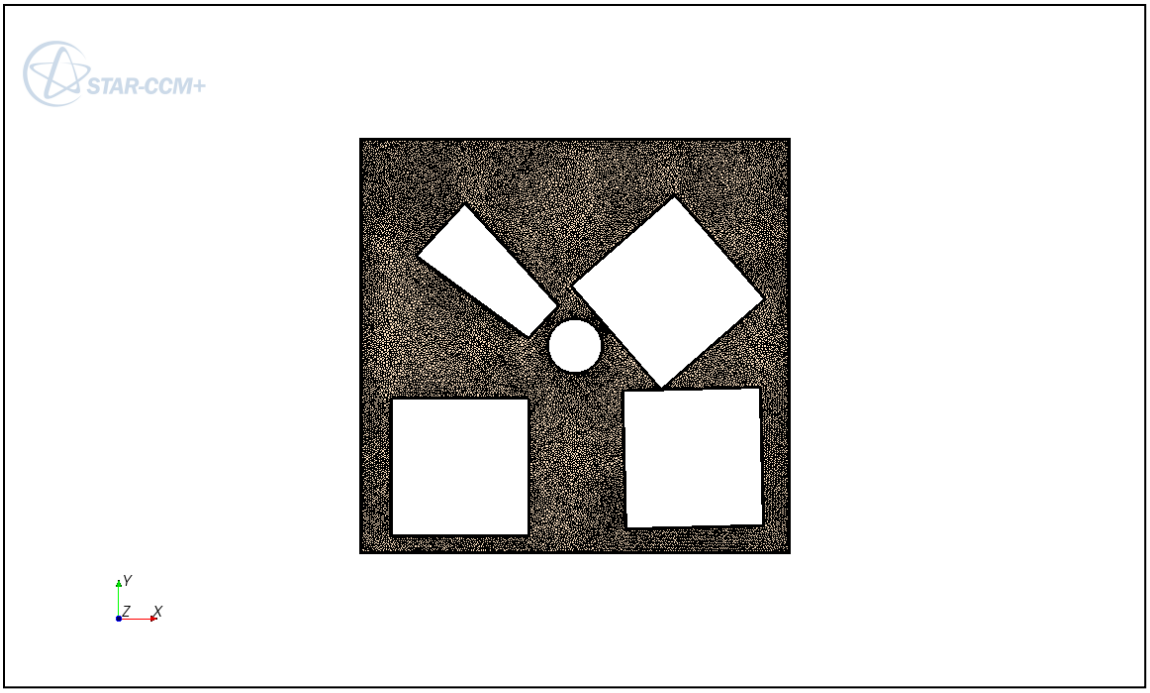

Figure 12. Refined mesh – view of a plane through the computational domain.

Development of Simplified Geometry

We have developed a simplified particle creation method that allowed us to develop the coal bed geometry in simplified form, therefore omitting the significant difficulties in creating successful mesh as previously discussed. A simplified particle representing a single piece of coal is shown in Figure 13. The decreased effort in creating the more suitable mesh for the flow and heat transfer simulation allowed us to move more rapidly toward obtaining a thermal profile inside our representative computational domain. To demonstrate the new Star-CCM+ DEM capabilities, first, we created a simplified computational geometry domain containing sixty-two particles, as shown in Figure 14. These particles are uniform in size and are distributed evenly throughout the inlet of the domain. After the DEM simulation was completed, a process of taking the data from the simulation and creating a computer-aided-design (CAD) of the geometry was done using Matlab, Gambit meshing software, and Star-CCM+. The new geometry was meshed in Star-CCM+ using the surface-wrapping model and a polyhedral volume mesh, with a total of 3.5 million cells. Because of the rounded edges on each particle, the meshing was a straightforward process with no extra time required to produce an improved simulation mesh. Unfortunately, this rapid prototyping with DEM does not allow for a realistic coal particle size distribution. The method discussed in the section on *Development of Representative Geometry* describes how to obtain realistic fractured coal geometries (Figure 8), but this method presents the problem of the presence of internal gas volumes trapped among multiple pieces of coal, which do not allow for a stable simulation. We are continuously improving the geometric representation of the representative rubblized coal geometry.

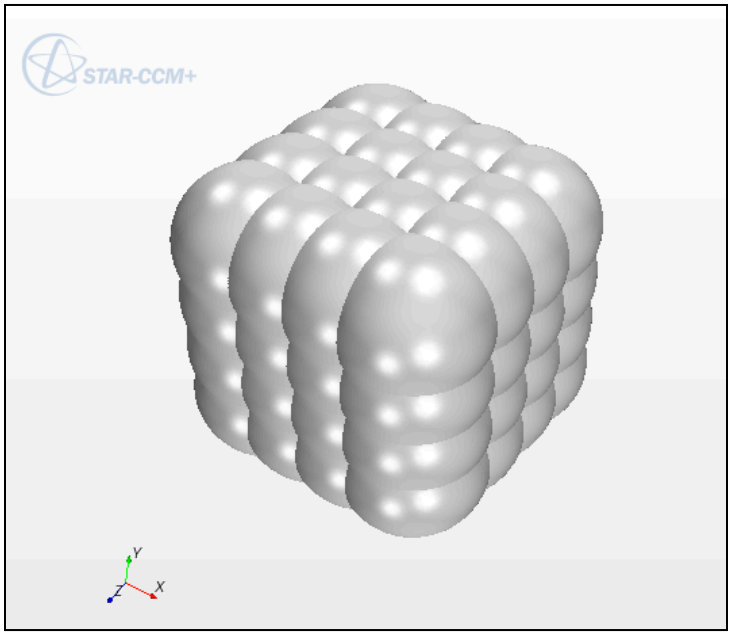

Figure 13. DEM shape formed from a grouping of spheres in Star-CCM+ used to show a simplified representation of one piece of coal.

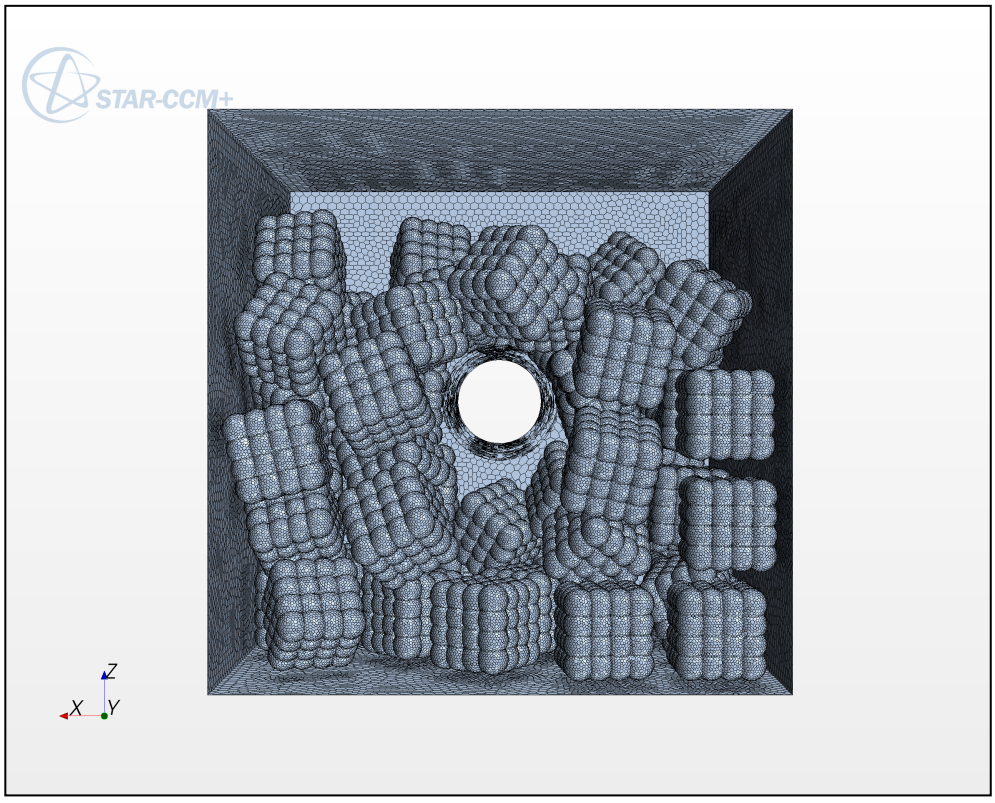

Figure 14. Image of the surface mesh created for the coal simulation bed in Star-CCM+.

For our initial development of the representative geometry we have used the Gambit meshing software. However, Gambit is no longer commercially available. Therefore, we are transitioning the meshing procedure to the new ICEM-CFD geometry and meshing tool. Thus far, we have transitioned the coal particle generation process using the simplified geometry from Gambit to ICEM-CFD. A sample coal particle geometry creation process is shown in Figure 15.

Simulations with simplified geometry

Initial flow simulations on the simplified geometry were performed using full transient flow simulations with heat transfer to both the fluid and solid phases. Figure 16 and Figure 17 show the velocity vectors in a plane within the geometry and the temperature profile in the coal and fluid regions at 22.5 minutes of simulation time. The results appear as expected, yielding an upward buoyant plume of hot air, interacting with the geometry and mixing throughout the domain. The pieces of coal in the pathway of the convective current of hot air show increased heating. This simulation used simplified thermal properties of coal, which do not vary with temperature. Nonetheless, the stable simulation demonstrated a proof-of-concept that we are able to produce a stable simulation with the expected thermal profile.

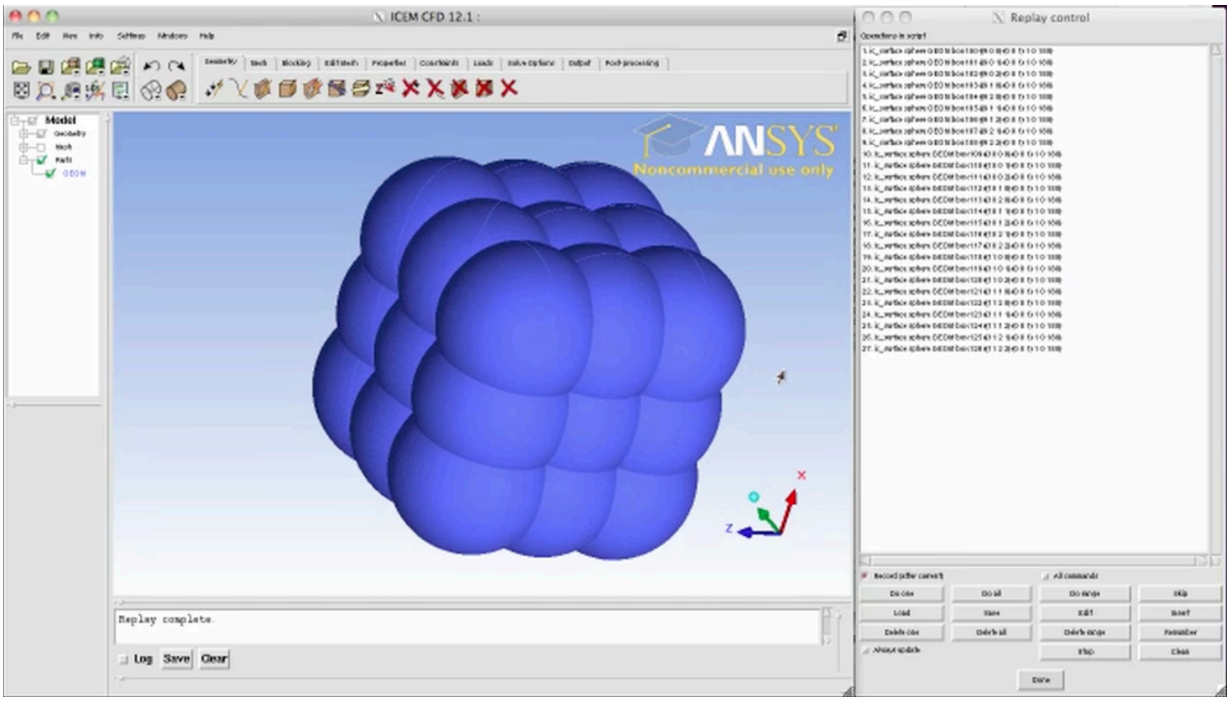

Figure 15. Sample particle generated in the new meshing and geometry software ICEM-CFD.

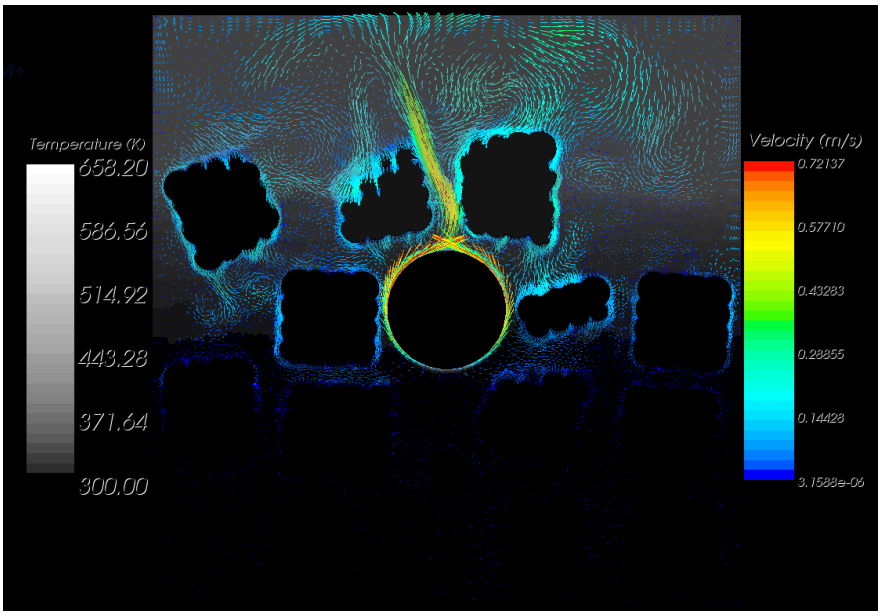

Figure 16. Velocity vectors in a plane inside the domain for the laminar simulation.

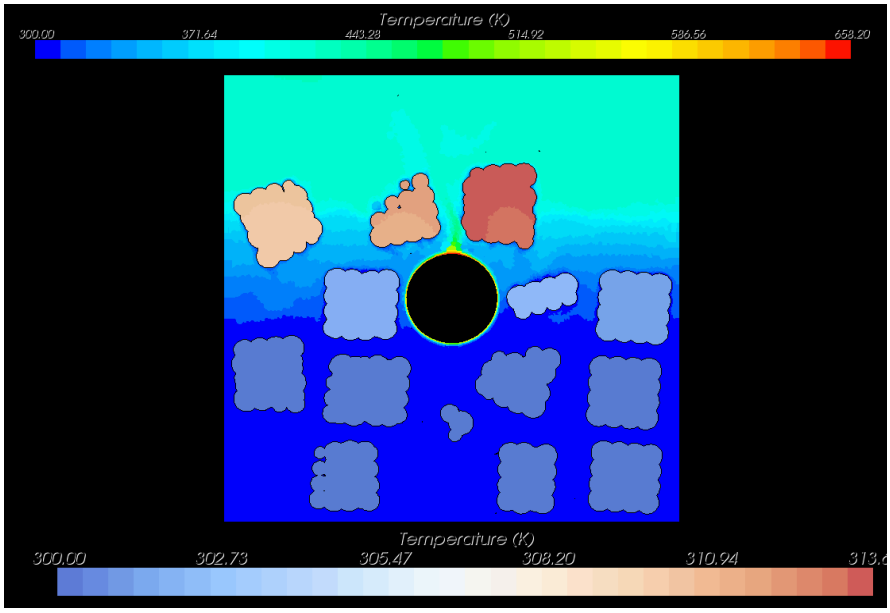

Figure 17. Temperature profile in both coal and fluid regions in a plane inside of the computational domain for the laminar simulation.

Extended-domain simulations

After obtaining a stable computational simulation with the simplified geometry domain, we created an extended-domain simulation, shown in Figure 18, to test the ability of Star-CCM+ to generate and handle larger numbers of particles. The extended domain features two heating elements instead of the single heating element in simplified domains. It contains close to 2,000 pieces of coal, but unlike previous geometries, each piece of coal is created from 27 spherical elements instead of the 64 spherical elements used in previous simulations. This reduced the computational cost of the DEM simulations as well as allowed the scale up of geometry by avoiding memory usage issues associated with a larger number of pieces of coal, which are more densely packed. The final computational mesh, including both the fluid as well as solid phases, contained 8.4 million polyhedral cells. All runs employed a laminar implicit solver for the fluid phase, with time step size of 0.1 seconds. In the previous runs, we used RANS and LES turbulence models; however, for geometric domains containing many pieces of coal, the fluid flow characteristics change, so we have employed the laminar model, which better characterizes the fluid flow present in the tightly packed rubblized coal bed. The simulation was run on 612 processors, with 1 minute of simulation time corresponding to about 300 minutes of real time. This highlights the large computational cost associated with simulations involving heat transfer in both the fluid as well as solid phases.

Figure 18. Extended computational domain used for solid and fluid simulations.

Figure 19 – Figure 21 show the coupled fluid/solid simulation results for the extended domain. Figure 19 and 20 are taken after 418 time steps, whereas Figure 21 is produced after 974 time steps. Results appear as expected, with buoyant velocities approaching 1.5 m/s in the convective channels. The upward buoyant plume of hot air interacts with the geometry and mixes throughout the domain. The pieces of coal located in the direct pathway of the convective current of the hot air show the largest temperature change. Of interest is also the difference between the heating time of the fluid and the solids. In the upper region of the domain the temperature of the fluid increased by about 100 K from the initial stage, while the temperature of coal in the same region increased only by only about 2 to 4 K. This highlights the vastly different heating time scales for the fluid and solid regions.

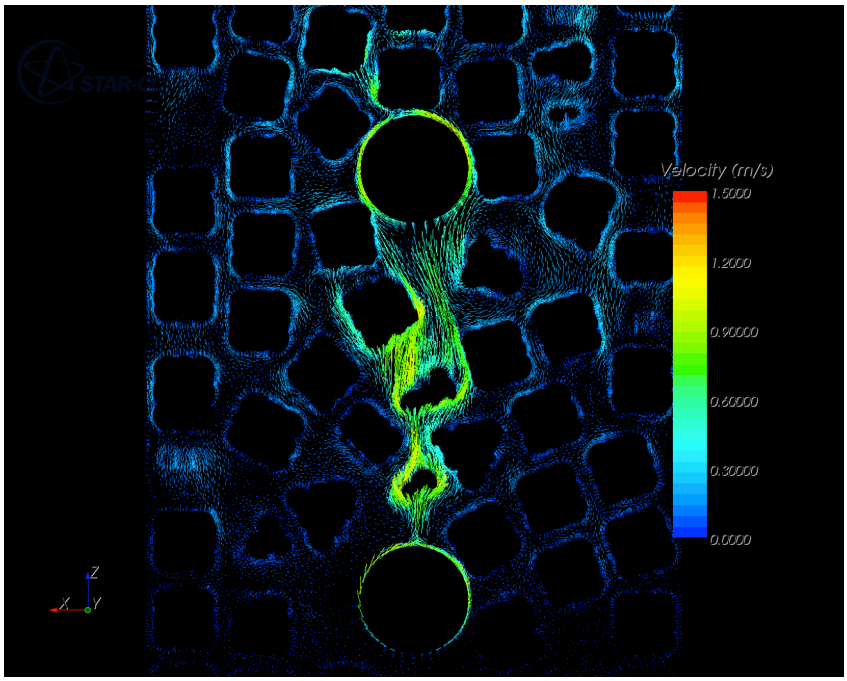

Figure 19. Velocity vectors for the extended domain simulation in a plane inside of the domain.

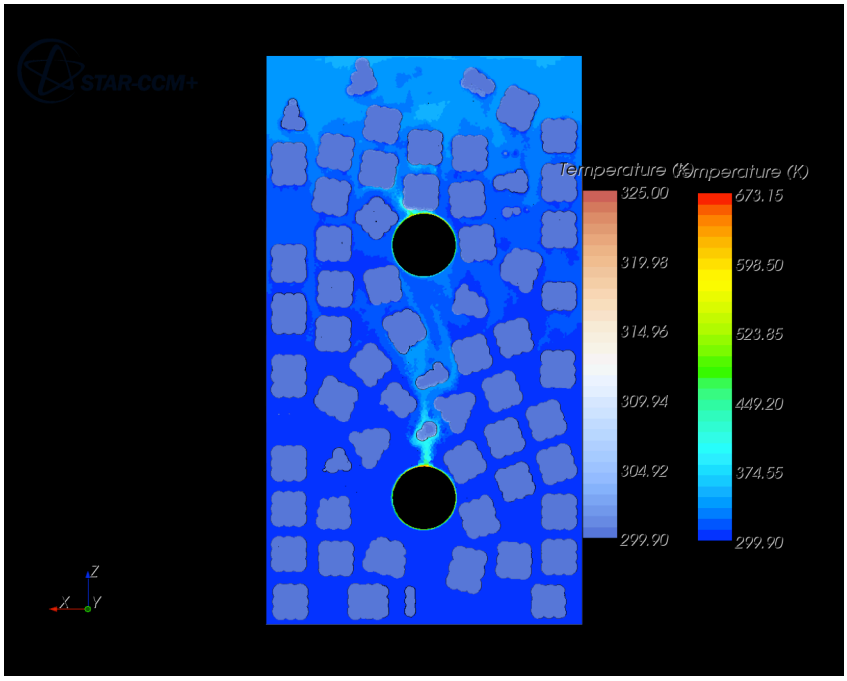

Figure 20. Temperature profile in both solid and fluid phases for the extended domain simulation.

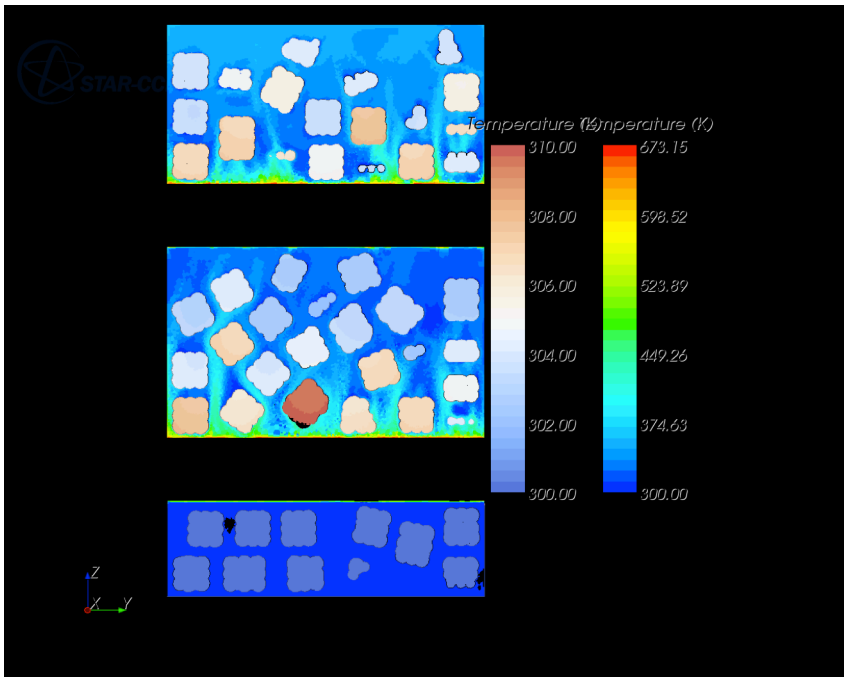

Figure 21. Side view of the temperature profile in the fluid as well as solid (coal) regions in plane inside the extended domain simulation.

Boundary conditions. The next phase of the research considered the effect of boundary conditions on the simulation results. Because of the large computational costs associated with simulations including extended domain and/or two phases, we have conducted the boundary sensitivity tests using the simplified domain shown in Figure 22 and considered only the fluid phase in the analysis. These simulations used a polyhedral mesh with approximately 14 million elements in the fluid region alone, coupled with the implicit laminar solver with time step of 1 second. We considered the following three scenarios: 1) adiabatic (perfectly insulated) boundaries for both the geometry domain as well as pieces of coal where no heat is allowed to escape the system, 2) adiabatic boundaries at the geometry edges and constant 300 K temperature boundary condition for the pieces of coal, and 3) constant 300 K temperature boundaries for both the geometry edges as well as pieces of coal. The constant 300 K boundaries for coal are based on the vastly different heating time scales for the fluid and solid regions, as described previously. Because of the relatively short simulation times for these tests, we assumed that the temperature increases in pieces of coal are negligible in comparison to the temperature increase in the fluid region, allowing us to reduce the computational costs of our simulations by omitting the simulation of solid heat transfer. The coupled simulation discussed under the extended-domain simulation section justifies this assumption. The constant 300 K temperature outer boundary scenario represents a very poorly insulated system. These three scenarios span the maximum possible extremes in boundary conditions expected for a UCTT system in reality.

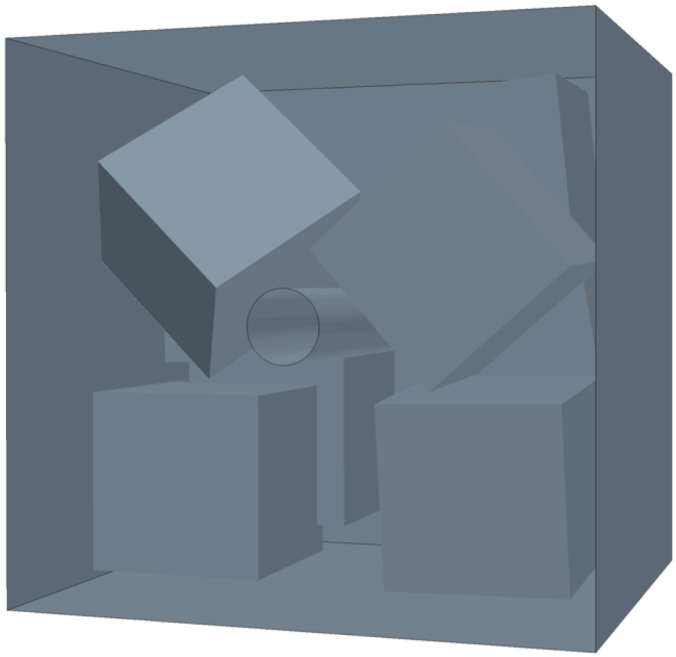

Figure 22. Simplified computational domain used in conjunction with fluid-only simulations to evaluate the effect of boundary conditions on the thermal profile inside of the domain.

Figure 23 – Figure 25 which were taken at the same simulation time of 8,861 seconds, indicate that the thermal profile inside the domain is very sensitive to the boundary conditions. As expected, the greatest temperature increase is seen in the perfectly insulated system, Figure 23, while the smallest temperature increase is seen in the non-insulated system, Figure 25. The most realistic scenario with mixed boundary conditions, shown in Figure 24, shows a temperature distribution between the insulated and non-insulated systems. Therefore, it is important to: 1) insulate the actual experimental system extremely well to reduce the heat loss and to increase the available amount of heat to effectively heat the pieces of coal, and 2) to develop very accurate description of experimental boundary conditions for a proper simulation-to-experiment comparison.

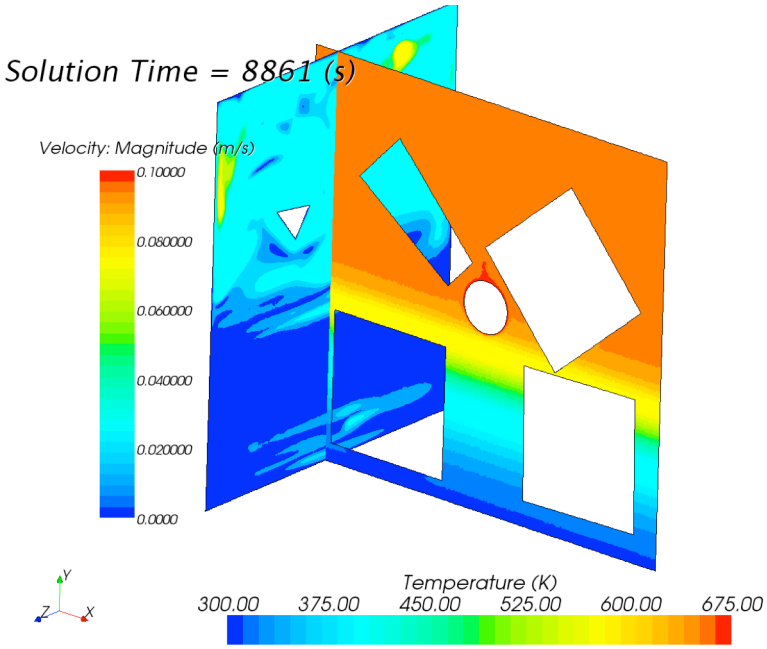

Figure 23. Temperature distribution inside a perfectly insulated domain.

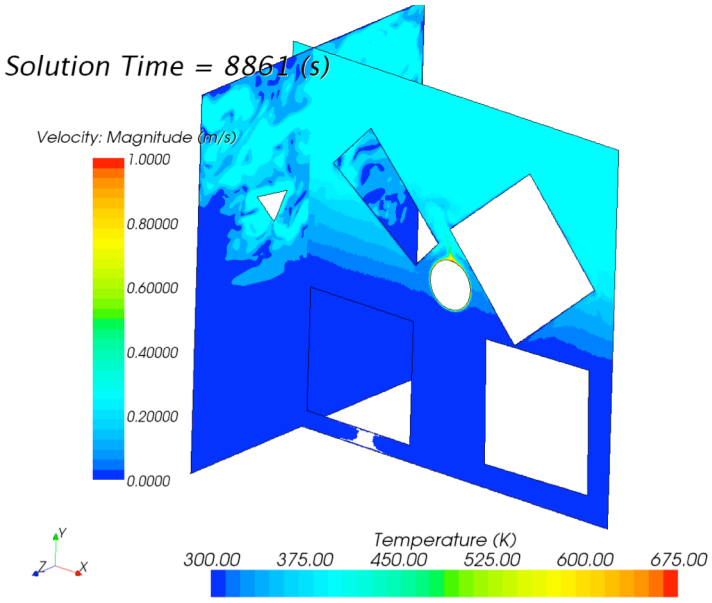

Figure 24. Temperature distribution inside a domain with perfectly insulated external boundaries, and pieces of coal fixed at constant temperature of 300 K.

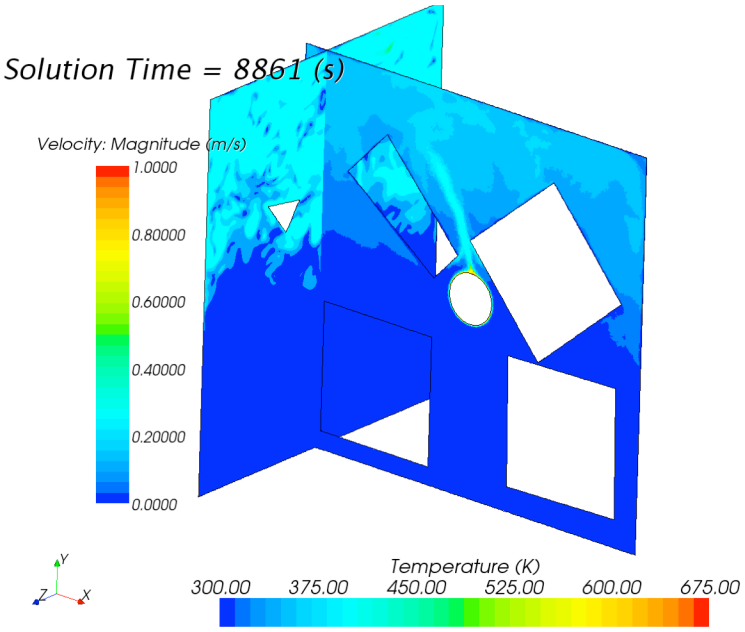

Figure 25. Temperature distribution inside a representative non-insulated domain.

Temperature evolution

To understand the time evolution of the temperature field inside the domain, we once again chose to use the simplified domain, with exactly the same simulation settings as described in the *Extended Domain Simulation* section, perfectly insulated boundaries, and pieces of coal set at a constant temperature of 300 K. The results are shown in Figure 26. The greatest heating occurs in the first 1,000 seconds of the simulation, then the overall heating rate inside the domain decreases considerably. The initial heating is caused by the buoyant mixing of the hot air supplied by the heat source that rises through the convective channels between the pieces of coal. As soon as the air above the heating element increases in temperature, the buoyancy effect decreases considerably, and most of the subsequent heat transfer occurs through conduction. After that, the heating progresses from the upper part of the domain to the lower part of the domain at a substantially reduced rate. This greatly decreases the overall heating rate as well as highlights another very important issue: because the conductive and convective heating time scales are of such different magnitudes, to completely simulate heating of the entire domain using conventional solution algorithms would require unfeasible amounts of computational resources. We address this particular issue later in the report. Even from the results of these preliminary simulations we can conclude that the best placement for the heating element would be as close to the bottom of the domain as possible. This would allow for more effective buoyancy-driven mixing, therefore increasing the overall temperature inside the bed more rapidly.

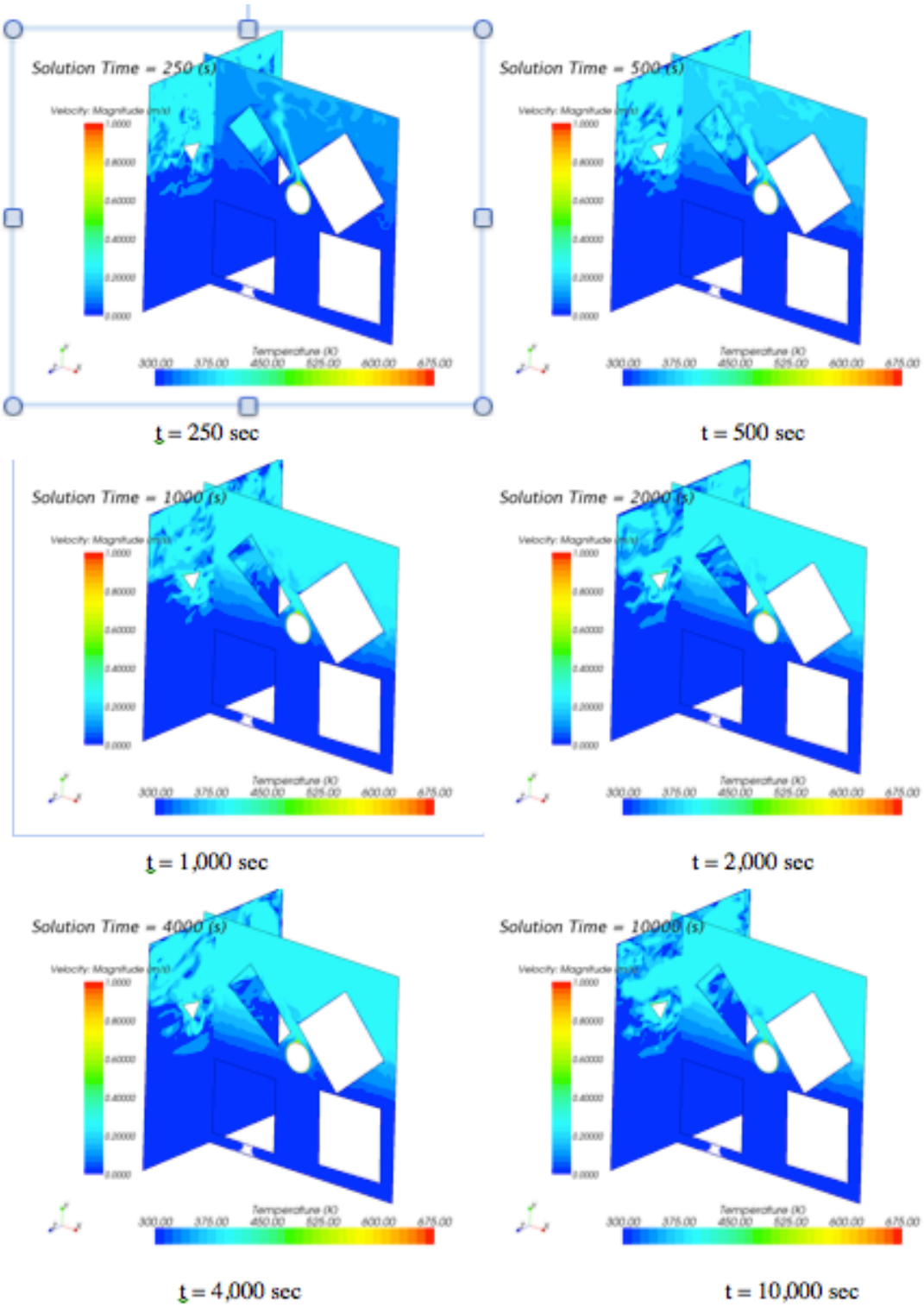

Figure 26. Time evolution of a thermal profile inside the simplified computational domain.

Addressing differing time scales

To address the issue of differing time scales in the simulation, we have modified our solution algorithm to include operator-splitting procedure. This solution technique allows the efficient simulation of the long-term thermal effects occurring inside the rubblized coal bed geometry. This algorithm implementation represents a significant step forward in efficiently, obtaining the temperature history of coal particles on the order of days and weeks instead of minutes, while using the same amount of computational resources. We were able to incorporate this algorithm because of the difference in the magnitude of time scales present in UCTT. The fluid convective time scales are much shorter than the fluid and solid thermal time scales. Therefore, for the simulation to remain numerically stable, the maximum overall time step was limited by the time stepping requirements of the smaller, fluid convective time scales. These time scales need to be on the order of a second or a fraction of a second for the computational fluid dynamics simulation to remain stable. However, once the simulation achieves a statistically steady state, effects of the faster, convective fluid currents decrease and the slower, thermal conductive effects, present in both fluid and solid phases, dominate.

Up until this point we have employed the traditional iterative solution algorithm shown in Figure 27. The solution for both smaller and larger times scales is advanced concurrently, thus restricting the maximum allowable time step required for the simulation to remain stable. For each time step, the fluid continuity and momentum equations are solved first, followed by the solution of the fluid energy equation and solid energy equation. Only then is the time step advanced. We have modified the solution algorithm to take advantage of the difference in magnitudes of the simulation time scales and thus have subdivided the algorithm into two sections: 1) we first employ the traditional solution algorithm, where we advance the fluid continuity and momentum equations along with the fluid and solid energy equations concurrently, until we obtain a statistically steady fluid flow and thermal solution; then 2) we disable the time-intensive computation of fluid continuity and momentum, and only solve the fluid and solid energy equations, a process which allows us to increase the numerically-stable simulation time step from seconds to multiple minutes, therefore significantly increasing the simulation computational speed. This algorithm is shown in Figure 15. After approximately hundred large time steps, we revert back to the traditional algorithm for a few time steps to allow for the fluid flow field solution to adjust based on the new temperature gradients. Once we achieve a statistically steady state solution, we once again revert back to solving only the fluid and solid energy equations while omitting the fluid continuity and momentum equations. We can repeat this solution strategy iteratively until we obtain converged thermal distributions inside the rubblized coal bed.

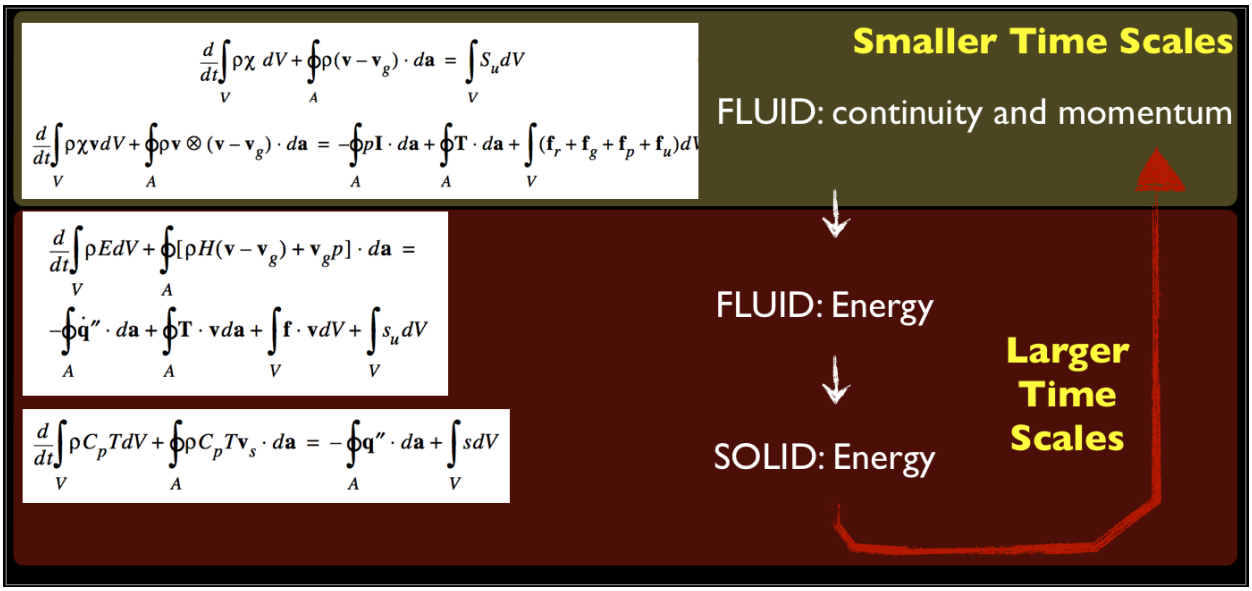

Figure 27. Traditional iterative solution algorithm for fluid convective currents, and fluid and solid thermal solutions.

Subtask 6.4 – CO_2 Sequestration Chemistry

Experimental setup

The experimental setup used in this study was described in detail in the UC3 topical report, Carbon Dioxide Sequestration: Effect of the Presence of Sulfur Dioxide on the Mineralogical Reactions and on the Injectivity of CO_2+SO_2 Mixtures, and is briefly summarized in Figure 28. The brine composition used in this study is described in Table 2. The different sets of experiments are tabulated in

Table 3. All the minerals were angular to circular in shape. They were ground to 100μm size, and a particle size distribution analysis revealed particles ranging from 40μm to100μm in diameter.

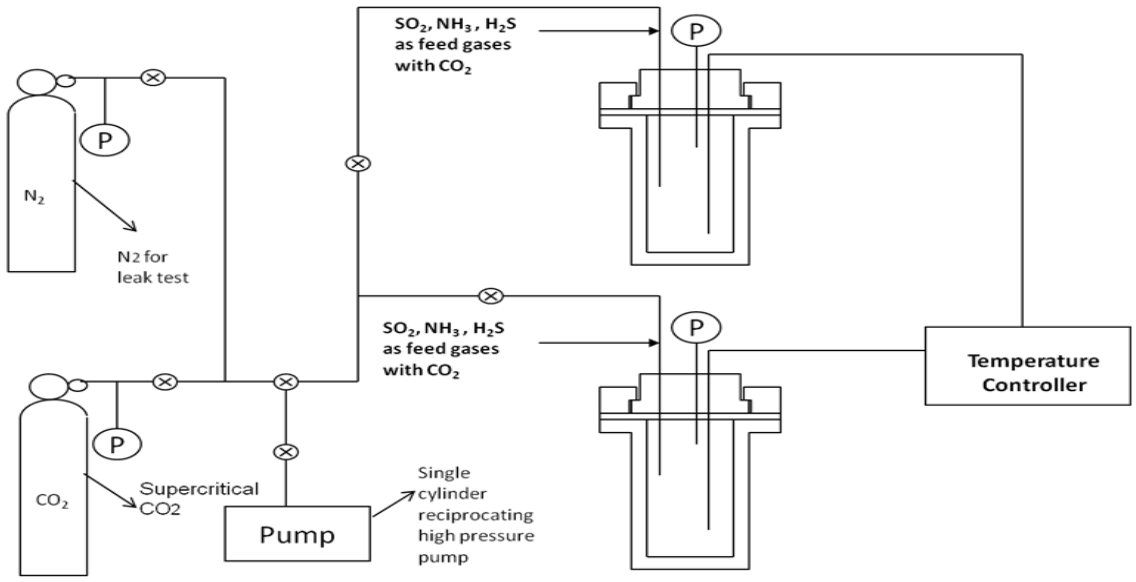

Figure 28. Schematic diagram of the experimental setup.

Table 2. Initial composition of the brine.

Na	Mg	K	Ca	Al	Mn	Fe	Ba	Si	S	Cl
mg/L	mg/L	mg/L	mg/L	µg/L	µg/L	µg/L	µg/L	mg/L	mg/L	mg/L
23032	1	<6	<4	<8	<1	54	<2	0.4	<6	26542

Table 3. Experimental conditions.

Expt	Rock used	Temperature	Pressure
Set A	Limestone	100^0C	2000 psi
Set B	Sandstone	100^0C	2000 psi
Set C	Peridotite	100^0C	2000 psi
Set D	Arkose	100^0C	2000 psi

All the experiments were carried out with 3g of rock. For the Arkose, the initial sample was prepared by mixing equal proportions of rock (0.5 grams each). The initial composition of Arkose is shown in Table 4. The brine to rock ratio in the experiments was 10:1.

Table 4. Composition of the arkose.

Rock	Quartz	Andesine	Dolomite	Chlorite	Microcline	Calcite
Formula	SiO_2	$Na_xCa_yAlSi_2O_8$	$CaMg(CO_3)_2$	$(Fe, Mg, Al)_6(Si, Al)_4O_{10}(OH)_8$	$KAlSi_3O_8$	$CaCO_3$
Class	Silicates	Silicates	Carbonates	Silicates	Silicates	Carbonates
Group	Quartz	Feldspar	Dolomite	Chlorite	Feldspars	Calcite
Composition as seen by XRD	22.7%	13.1	8.5	20.2	22.5	13.2

After each experiment, samples were retrieved from the reactor by detaching the bottom (wherein, the sample rests in a cap). The sample is taken out carefully without disturbing the precipitate. The sample was dried overnight at 50^0C, a temperature not high enough to alter the structure of any phases that might have grown during the experiment. The sample is retrieved, cooled down and divided into equal parts for XRD and SEM/EDS analyses. The quantitative estimates of the minerals before and after the experiments were obtained by XRD. Since small amounts of precipitates were formed, attempts to quantify produced solids proved difficult. Hence the changes in the initial mineral assemblage and the mineral assembly after the reaction were evaluated. These changes can be corroborated with the precipitated minerals seen in the SEM/EDS analyses, and a reaction mechanism leading to the precipitation of new minerals can therefore be postulated. The brine samples were diluted and filtered using Whatman 40 filter paper (retention capacity of 4μm) in a vacuum filtration setup. The sample was then divided into equal fractions for all cation and anion analyses. The sample was acidified by addition of sulfuric acid to prevent any further precipitation. All the dissolved cations were analyzed using ICPMS and dissolved anions by ion chromatography. All the solids are washed with deionized water before analysis. The major changes, which occur due to degassing the reactor, are the changes in the saturation states of the minerals in the brine, which may lead to secondary precipitation of minerals in the solid phase, change in the pH of the brine because of CO_2 degassing. The possibility of these changes was evaluated and explained for each case.

Geochemical modeling

Experimental analyses of the long-term behavior of CO_2 injected into saline aquifers are not possible with relatively short-term laboratory experiments. The fundamental issues of long-term geological carbon sequestration, which are the key to full scale CO_2 injection into a geological repository, can be understood through simulation and geochemical modeling. Comprehensive numerical models that incorporate the physics of CO_2 behavior in porous media and the geochemical interactions of free and dissolved CO_2 in the brine with the host rock are necessary to effectively monitor the fate of injected CO_2 on geological time scales. These geochemical models must accurately represent the underlying processes over a broad range of spatial and temporal scales. They should also successfully integrate short-term injection with

long-term transport and reaction.

In this report, a batch reaction geochemical model was used to assess the fate of CO_2 injected into geologic formations. Since the analytical measurements were carried out at ambient conditions after degassing the reactors, degassing simulations were also carried out to assess the retrograde reactions that might occur when the reactor was depressurized and also long-term quenching reactions that might have taken place during this process. An attempt has also been made to compare the modeling results with the experimental results. The degassing simulations also provided the corrections that need to be taken into account before the comparison between the modeling and experimental results could be made. Batch geochemical modeling was conducted using the commercially available, flexible, and multipurpose geochemical software; Geochemist's Workbench (GWB) (Bethke, 1998). Simulations of water-rock-gas interactions under no flow conditions are important for identifying the reactions that are most important for trapping CO_2 in the geological formations and for identifying the parameters that have the greatest influence on the quantity and form of sequestration. Detailed descriptions of the modeling follow.

GWB is a chemical reactor type, module based software that simulates chemical reactions under both equilibrium and kinetic conditions. It is a set of software tools for manipulating chemical reactions, calculating stability diagrams and the equilibrium states of natural waters, tracing reaction processes, modeling reactive transport and plotting the results of these calculations. The GWB package was developed at the Department of Geology of the University of Illinois at Urbana-Champaign under the guidance of Craig Bethke.

GWB can be used for equilibrium, reaction path and kinetic modeling of CO_2-brine- mineral reactions. Equilibrium modeling can be used to determine the ultimate fate of CO_2 in the aquifer. Kinetic modeling calculates the pace of the reactions based on the appropriate kinetic parameters i.e., reactive surface areas and kinetic rate constants. It also calculates the time it takes to approach dynamic equilibrium.

Since the geochemical modeling was an attempt to verify the numerous experimental cases, the modeling conditions were chosen to match those of the experiments. Reactions involving the gases CO_2 and CO_2+ SO_2 were modeled. The temperature of the system was assumed to be isothermal and set at 100^0C for reaction path and kinetic modeling. This geochemical modeling for arkose was used to investigate the impact of CO_2 fugacity, mineralogy, temperature and pressure on mineral dissolution and precipitation and the mode of sequestration for each case. The main constraints are the mass of water, amount of minerals in the system, fugacities of any gases at their known partial pressure, the amount of any component dissolved in the fluid and the activities of species such as H^+ as determined by pH measurement. The intermediate products from a complex set of sequestration reactions can be evaluated using reaction-path modeling. The progress of the possible reactions is traced by reacting several minerals with CO_2 enriched brine. This is important to investigate the precipitation and dissolution of phases as the reaction progresses because this has implications on the porosity evolution and integrity of the geochemical repository.

The GWB has a rich database that is capable of simulating many common chemical reactions. The database is compiled from work done at the Lawrence Livermore National Laboratory. In the modeling, the equilibrium constants are tabulated based on eight principal temperatures for any given reaction. For temperatures outside of the principal values, a polynomial fit was used to calculate the equilibrium constants. The GWB provides default datasets where the equilibrium constants are only valid at 1 bar from 0-100°C and steam saturation pressures thereafter. These geochemical models do not have a built in method to adjust the values of the equilibrium constants as a function of temperature and pressure explicitly.

Kinetic modeling considers the rates of reactions based on appropriate rate constants and reactive surface areas. The algorithm computes the time needed by the system to initiate CO_2 consumption and CO_2 trapping as mineral precipitates. The time required by the system to approach steady state or dynamic equilibrium is also calculated. The GWB has an internal thermodynamic database and requires user input of kinetic rate data. The following rate equation was adopted for the modeling (Lasaga 1995)

$$Rate = \frac{dn_i}{dt} = KA_{\min} \exp\left(\frac{-E_a}{RT}\right)\left(\frac{Q}{K_{eq}} - 1\right)$$

Where, K is the rate constant (mol/cm^{2}s), A_{min} is the reactive surface area (cm^2), E_a is the activation energy (J/mol), R is the gas constant (J/Kmol), T is the absolute temperature (K), Q is the activity product and K_{eq} is the equilibrium constant.

This rate law assumes that the surface reaction is the rate-controlling step in the reaction mechanism chain. It is derived from the transition rate theory, which states that the mineral dissolves, by a mechanism involving the creation and subsequent decay of an activated complex. The rate at which the activated complex decays controls how quickly the mineral dissolves. The dissolution rates of the minerals do not depend on the saturation state. The precipitation rate, on the other hand, varies strongly with saturation exceeding the dissolution rate only when the mineral is supersaturated. It is also of interest that when A_{min} is zero, the reaction rate vanishes. Therefore, a mineral that does not exist cannot begin to precipitate unless crystal nuclei form.

Rate constants for the kinetic reactions were compiled from the published literature based on laboratory experiments. However, these rates can be several orders of magnitude greater than the rates of weathering measured in the field (Lasaga 1995). To check the validity of the model and the kinetic parameters used in this model the modeling results were compared to the experimental results. It was observed that the rate constants for the same mineral varied greatly depending on the literature source. Hence kinetic parameters from different sources were used and the results were compared with each other and also with the experimental results. The measured rate constant reflects the dominant reaction mechanism in the experiment from which the constant was derived.

The GWB requires that the CO_2 pressure be input directly as fugacity. The fugacity (f_{CO2}) was calculated using the CO_2 solubility model developed by Duan and Sun (2003). The investigation of how geochemical reactions vary as a function of f_{CO2} can approximate the sequence of reactions and the reaction progress as fugacity decreases with increasing distance from the injection site and also over time.

Reactive surface areas were calculated from geometric approximations and also adopted from literature measurements. For the geometric approximations, the grains were assumed to have a spherical geometry, and an average diameter of 100 μm was assumed. For a spherical grain the specific surface area is given by A*ν/V*MW, where A is the sphere area, ν is the molar volume, V is the sphere volume and MW is the molecular weight. For sheet silicate minerals like clinochlore (chlorite), an average grain diameter of 2μm was assumed which corresponds to sheet silicate size. Interactions with the minerals are generally expected to occur only at selected sites on the surface and the difference between total surface area and the reactive surface area can be between 1 to 3 orders of magnitude (White and Peterson 1990). Hence a scaling factor of 0.001 was used for all minerals to account for this difference.

Activity coefficients were calculated using the B-dot equation (an extension of the Debye Huckle equation). The virial method (Pitzer equations) is better suited to high ionic strength solutions such as the brine under consideration, but the GWB's application of the Pitzer equations does not take into account the distribution of species in solution, only recognizes free ions as if each salt has fully dissociated in solution, nor does it take into consideration SiO_2 and Al^{3+} species. Those assumptions preclude use with minerals like albite, quartz, and feldspar (Zerai et al. 2006).

RESULTS AND DISCUSSION

Subtask 6.1 – Bench-Scale RF Thermal Treatment

Three reactor systems have been constructed to study various aspects of fuel production from a UCTT process. The status and preliminary results from these reactors are discussed below.

Fixed-Bed Reactor

The FBR system was completed and tested in conjunction with the research group of Prof. Kevin Whitty (University of Utah), who purchased the system from a laboratory in Finland. Due to its European design, retrofitting the FBR for an American power source and control system proved to be a major undertaking. After several months of work, the system was successfully tested for both pyrolysis and steam gasification. Figure 29 shows sample data for gas yields during pyrolysis of a Utah bituminous coal sample. The system was also adapted to collect condensable liquid and tar species although an analysis algorithm has yet to be developed for these products. The FBR system is currently undergoing a few minor modifications to ensure minimal tar deposition in the downstream pipe and valve system.

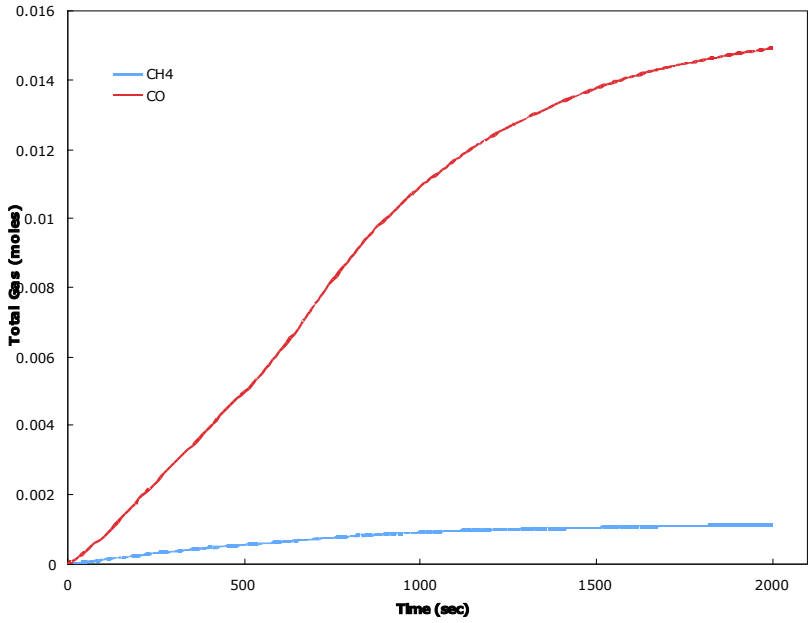

Figure 29. Total gas yields during the pyrolysis of a Utah bituminous coal at 800°C in a fixed-bed reactor system.

Rubblized-Bed Reactor

The rubblized bed reactor was designed and submitted for construction to local ASME-certified pressure vessel manufacturer Mark Steel Corporation. The design criteria for the reactor are described above in the

Approach section. An isolation room for the reactor has also been constructed at the university's downtown combustion facility. The room features two layers of sandbag walls and a blast door and routing in the ceiling to channel gases upward and out of the building in the event of an unexpected pressure release. The layout of the isolation room is shown in Figure 30. The high-pressure vessel, shown in Figure 31, has now been completed, hydro-tested and certified for pressure operation, and has been installed in University of Utah off-campus Industrial Combustion and Gasification Test Facility.

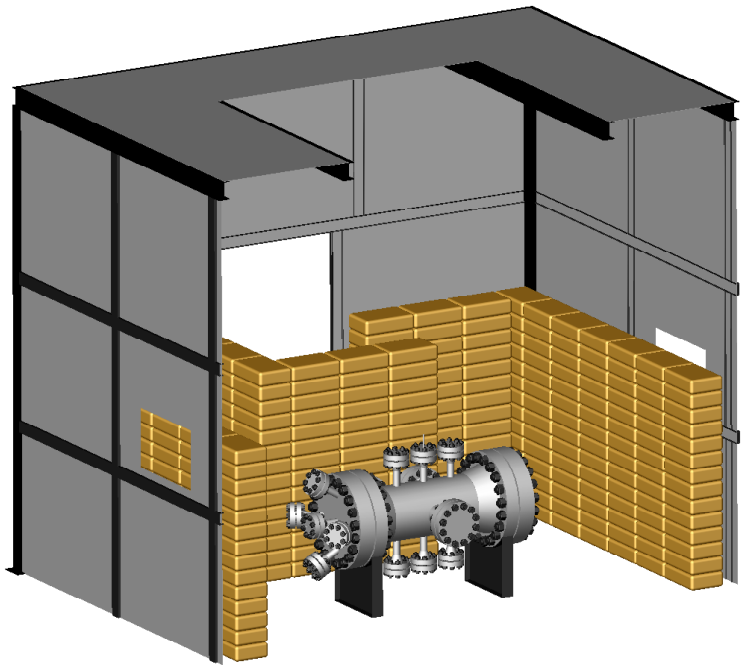

Figure 30. Arrangement of the isolation room for housing the high-pressure rubblized-bed reactor.

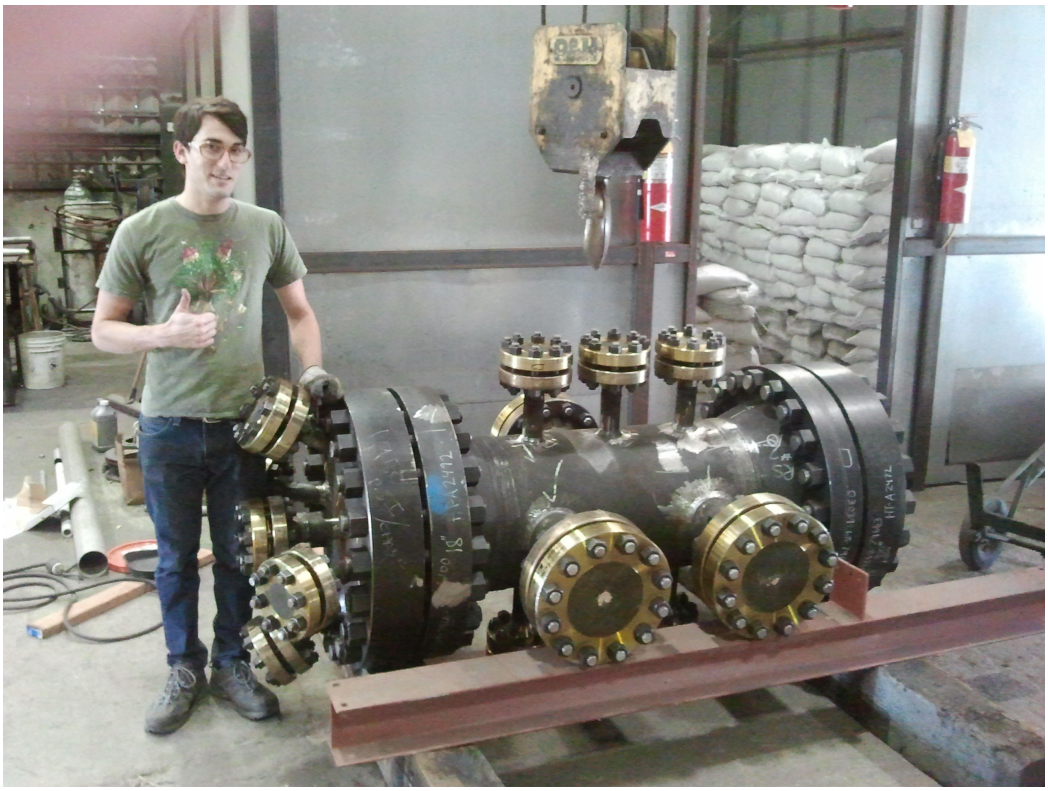

Figure 31. The high-pressure rubblized-bed reactor after pressure testing and certification, and prior to placement in the isolation room.

Coal Block Reactor

The coal block reactor has been the most-extensively used reactor to date of the three. Numerous studies have been conducted to better understand the heat transfer and mass transfer dynamics in coal blocks. The preliminary data are suggesting several key effects that are not typically seen in powdered coal pyrolysis, but that would have significant effect on the final product distribution of a UCTT process.

As a sample coal system, large blocks of Utah bituminous coal from the Skyline Mine have been obtained. This coal has the advantage of significant structural integrity, making it easy to cut and drill blocks as necessary for pyrolysis experiments. The blocks have been prepared as described in the Approach section. Each block was heated at a rate of 5 K min^{-1} to an ultimate heater temperature of either 500 or 600^{o}C. Upon reaching the final heater temperature, the heaters were held constant for 2 or 5 hours. The blocks were then cooled at 10 K min^{-1} to prevent rapid thermal contraction and subsequent fracturing.

Thermocouple data show the heat transfer resistances created by the block during pyrolysis. Figure 32 plots heater and block center temperatures for two different final heater temperatures. It is interesting to note that despite a nearly 20% larger heat flux for the case of the 600^{o}C heater temperature, the

temperature response in the center of the block is nearly uniform for both cases. It is also interesting to note that the block center temperature appears to level out at the threshold for pyrolysis in both cases. Currently, it is unclear whether this asymptote represents the steady-state temperature profile for the system or whether heat flow is being inhibited by a substantial reaction endotherm. If the later is true, it would demonstrate a much larger impact of secondary pyrolysis reactions on the product distribution than what is typically observed in powdered systems, which are typically viewed as energy neutral.

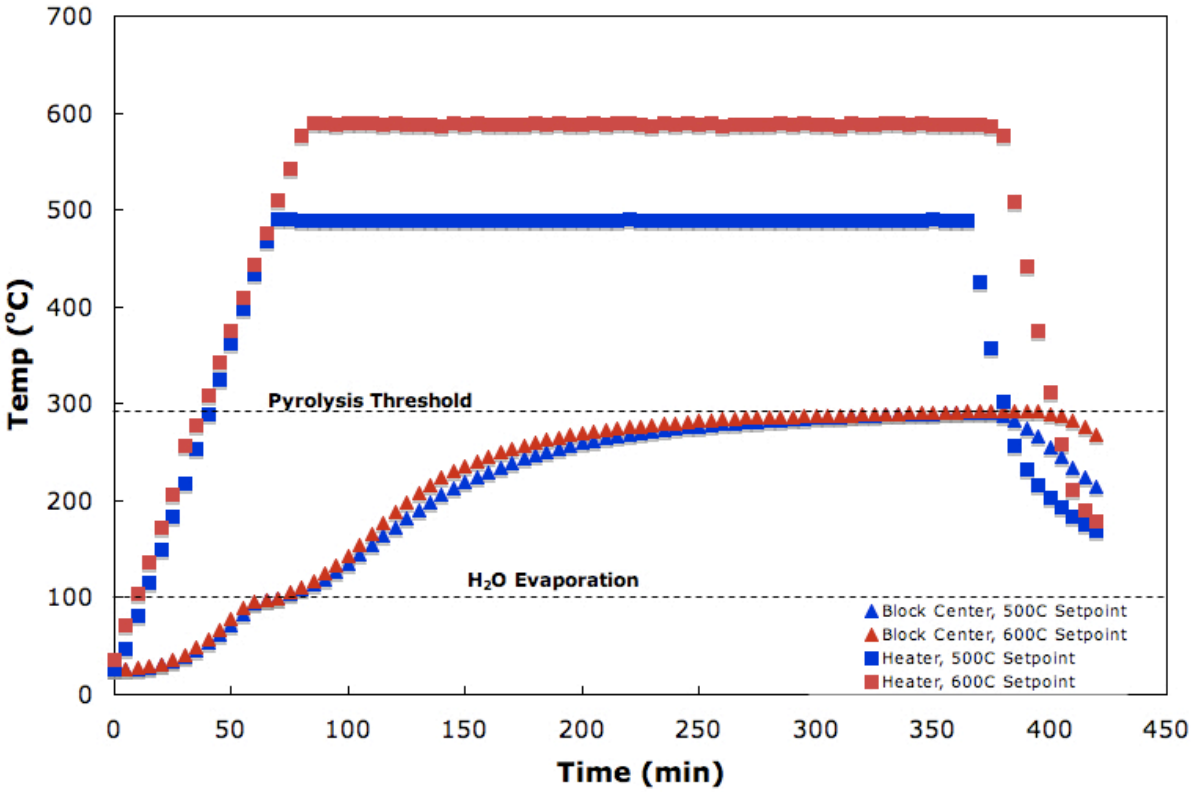

Figure 32. Time-temperature data from the coal block reactor. Despite different heater temperatures, both blocks shown here are heated at similar rates in their centers.

The coal block reactor has also yielded interesting data demonstrating changes in the pore structure and internal void fraction of coal blocks as they are pyrolyzed. The results suggest an important role of secondary pyrolysis reactions in determining the final pore structure of coal. To examine the changes in pore structure, samples were removed from pyrolyzed blocks in areas adjacent to the heaters and in the block centers. Samples were washed in warm xylenes to remove any debris and dissolve any labile tars off the surface of the samples. Once washed, each sample was examined by scanning electron microscopy. The microscope offers good resolution of pores down to the order of 100 nm.

The porosity changes observed in the pyrolyzing coal blocks differs from that typically seen in pyrolyzing powders. Adjacent to the cartridge heaters, the porosity initially develops in a manner consistent with a swelling coal powder, however over time this porosity is reduced and diminished. Figure 33 shows a

series of micrographs depicting changes from unpyrolyzed coal to 5 hours of pyrolysis at 500°C. These images were taken of coal slightly removed from the surface that was directly exposed to the heaters. There is a dramatic reduction in the size and openness of pores after 5 hours. The reduction is attributed to the deposition of tars on the pore surface. These tars likely originated deeper within the coal block and had a fairly extended residence time at pyrolysis temperatures, increasing the likelihood that they would undergo secondary pyrolysis. The reversal of porosity development in the char closest to the heat source is very different from single coal particles that will typically mature to a final large pore size distribution.

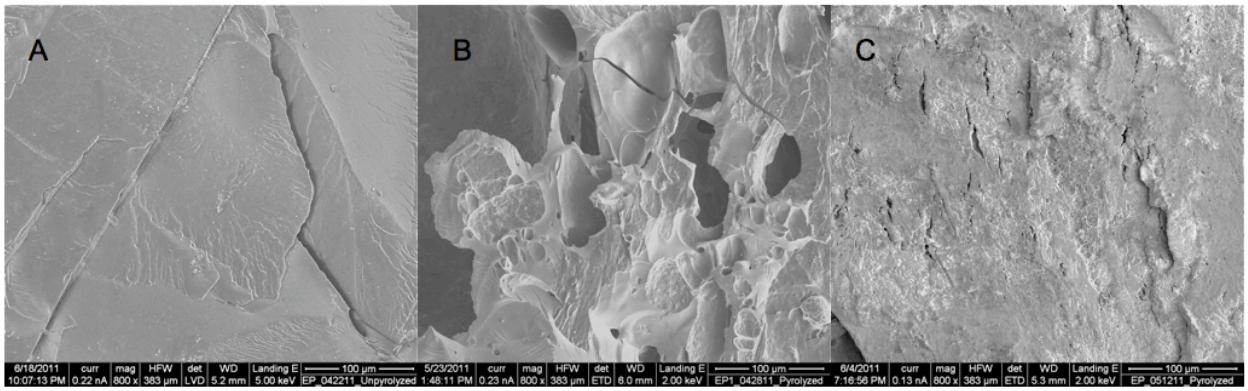

Figure 33. Porosity changes in a coal block adjacent to the heat source. All micrographs are at 800x magnification with a scale bar (lower right) corresponding to 100 μm. A) Unpyrolyzed coal. B) 2 hrs at 500°C. C) 5 hrs at 500°C.

The porosity changes observed in the center of pyrolyzing coal blocks are radically different from that observed near the heat source. Figure 34 shows a series of micrographs depicting changes in coal structure in the block center at times up to 5 hours of pyrolysis. After two hours, the block center has not yet reached pyrolysis temperatures and shows little change in overall porosity. However, after 5 hours, the coal appears to have become severely fractured. The fractures are almost entirely filled with deposited tars such that very little open space is available for molecular transport near the block center. Further examination of the deposited tars suggest that channels of < 100 nm width do exist for gas to pass through, but liquid transport would certainly be hindered. Little in the way of porosity development is seen at the block center. Instead, it appears that fracturing is the predominant mode of void fraction development in the internal regions of pyrolyzing coal blocks. The tortuous channels required to move tars from within the center of coal blocks would seem to suggest severe transport limitations, increasing the likelihood that secondary tar pyrolysis is an important factor in determining gas yields from coal block pyrolysis.

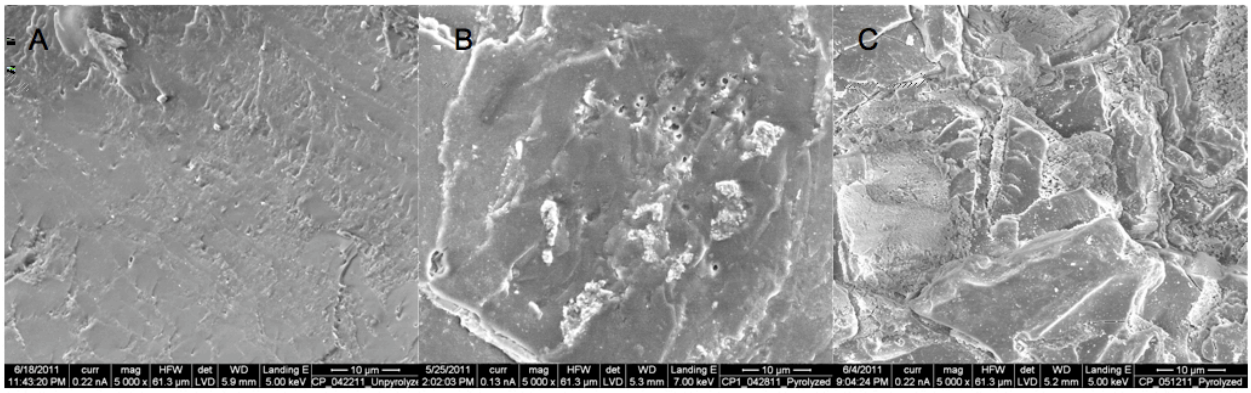

Figure 34. Porosity changes in a coal block near the block center. All micrographs were taken at 5000x magnification with a scale bar (lower right) corresponding to 10 μm. A) Unpyrolyzed coal. B) 2 hrs with a maximum temperature of 220°C. C) 5 hrs with a maximum temperature of 290°C.

Subtask 6.2 – In-Well Heater Design Alternatives

Technical approaches developed for underground oil shale thermal treatment can be easily adapted for underground coal thermal treatment. Some of the parameters need to be adjusted because of the difference in properties between coal and oil shale.

Review of Underground Oil Shale Thermal Treatment Technologies

Conversion Technologies

The shale conversion concepts can be divided into four major categories according to the heating techniques: internal combustion, wall conduction, externally generated hot gas, and volumetric heating. Combined technologies of these four categories were also explored by industrial companies. Table 5 and Table 6 summarize the advantages and disadvantages of these approaches, which are further discussed in the following subsections.

Table 5. Operational information for various hydrocarbon underground conversion approaches.

Company/Tech	**Site**	**Heating**	**Fracturing**	**T, °C (°F)[a]**	**P, MPa psi[c]**	**Efficiency**
Occidental Petroleum	CO	Internal combustion	Rubblized			
Geokinetics	UT	Internal Combustion	Rubblized			
Shell ICP[b]	CO, Jordan	Conduction; electrical; 2-4 y		340-400 (650-750)	0.2-3.4 (30-500)	
Electrofrac		Conductant; planar conduction, 7-8 y	Hydraulically	400 (750)	16.3 (2400)	50-80% extraction rate
Geothermic Fuel Cell		Fuel cell	Yes, Raised T			
Taiyuan Tech U	China	Hot Alkane Convection	Yes	400-700 (750-1300)		
Chevron CRUSH		CO2 Convection	Yes			
EGL CCR		Hot Alkane Convection	Yes	400 (750)	13.6 (2000)	
Petroprobe, omnishale		Hot Air => Shale Gas Convection	Yes			
Mountain West Energy In situ Vapor Extraction		Natural Gas Convection; 2-4 years	Yes	400 (750)	88 (1300)	extraction efficiency can be up to 90%
Radio Frequency		Volumetric heating, 1-2 months		low		
Microwave		Volumetric heating				
Total Resource Energy Extraction		Coal gasification Flue gas	Yes	725 (1340)		

[a] Kerogen decomposition rate depends on temperature: 90% decomposition occurs within 5000 minutes at 370°C (700°F) and within 2 minutes at 500°C (930°F).

[b] Frozen wall is 3.1m thick; freeze-wall wells are 2.5m apart from each other; refrigerant at -40°C (-40°F); stabilized within 1.5-2 years; maintained for 6.5-8 years.

Heater wells are 7.8m apart; the heating rate is 0.5°C (0.9°F) per day; Heat loss to overburden is relatively small;

At atmospheric pressure and ICP heating rate, 80% of FA oil yield can be reached; at higher pressure, 60% of FA oil yield was reported; Shell reported a 66% of the FA oil yield from test plots.

Hydrocarbons travel to production well in vapor form, then was pumped to the surface as liquid at ~200°C (390°F).

After production ceased, water is flushed to the production wells for 20 times of pore volumes to recover mobile HCs.

[c] Pore pressure cannot exceed the lithostatic pressure that applied to pore space from the overlying formation.

Table 5. continued.

Company/Tech	Product[a]	Quality	Water/oil production[b]	Depth, 100m (1000ft)	Emission	Energy Bal. Out:In
Occidental Petroleum						
Geokinetics						
Shell ICP	2/3 liquid + 1/3 syngas	> 30 API	3 to 1	3-6 (1-2)	21%-47% more C than petroleum	1.2-3.5:1
Electrofrac	Gas + Liquid					
Geothermic Fuel Cell	Electricity, gas, oil					18:1
Taiyuan Tech U	Oil, Gas and Water					
Chevron CRUSH						
EGL CCR						
Petroprobe, omnishale	Hydrogen; 1000 BTU methane; condensate; and water	45 API		9 (3)		
Mountain West Energy In situ Vapor Extraction	Gas only					
Radio Frequency	Oil and gas					Twice as other processes
Microwave						
Total Resource Energy Extraction	Oil yield 88.7% of assay					

[a] For a 0.1l/kg (26.7 gal/ton) shale, the Fischer Assay yield is 84% oil, 6% gas, and 10% char. The FA involves heating the shale to 500°C (930°F) at 12°C (21.6°F) per minute and holding at that temperature for 10 minutes. Higher pressure, lower temperature, and slower heating leads to lower oil yield and higher gas yield. Synthetic crude has a high H:C ratio of 1.9:1.

[b] Underground water that fills the porosity and fractures needs to be removed as much as possible because the heat capacity of water is 4 times that of shale. After all drainable water has been removed, water will occupy ~7% of shale bulk volume.

Table 6. Advantages and drawbacks of various hydrocarbon underground conversion approaches.

Company/Tech	Advantages	Drawback	Ref
Occidental Petroleum	Utilizing more of the heat and chemical values; capture sulfur dioxide. IRR 20% ⇔ $23-35/barrel		a
Geokinetics			b
Shell ICP	Lower up-front cost; low pollution; lower reclamation cost; available tested technology	Complex configuration; low thermal efficiency; excessive electricity consumption; low extraction rate	c
Electrofrac	Fracturing to increase permeability; by-product of NA_2CO_3; higher thermal efficiency of planar heating; reduced surface footprint	No mention of ground water protection; excessive electricity consumption;	d
Geothermic Fuel Cell	Even heating; self-sustainable; producing electricity; $14/barrel; lower air emission (SO_X, NO_X, particle, toxic); minimal water usage; minimal surface footprint		e
Taiyuan Tech U	Fracturing to increase permeability; low demand for water; even heating		f
Chevron CRUSH		High water usage; pollution	g
EGL CCR	High thermal efficiency; low pollution; self-sustainable		h
Petroprobe, omnishale	Fracturing to increase permeability; Low Pollution; self-sustaining; minimal surface footprint		i
MWE's In situ Vapor Extraction	Natural gas is soluble in shale; even heating; some control in product distribution; fewer wells	Heating efficiency is unknown	j
Schlumberger and LLNL's Radio Frequency	Short time heating; neutral carbon footprint; tunable process; targeted products	excessive electricity consumption to generate RF	k
Global Resource Corp's Microwave	Short time heating; volumetric heating; selective heating; low pollution; very high extraction rate		l
Total Resource Energy Extraction	Using coal syngas for heating; sulfur reduction by 60%; product quality can be altered		m

a. Agarwal, 1986; Hulsebos et al. 1988; Johnson et al. 2004; Lee et al. 2007; United States Department of Energy, 2007; United States Office of Technology Assessment, 1980.
b. Lekas, 1979.
c. Colorado Division of Reclamation and Mining Safety, 2007; Nair et al. 2006; Shell Frontier Oil and Gas, Inc., 2006.
d. Symington et al. 2008.
e. Savage, 2006.
f. Taiyuan University of Science and Technology, 2006.
g. Chevron USA, Inc., 2006; Green Car Congress, 2006; United States Department of Interior, 2006.
h. E. G. L. Resources, Inc., 2006.
i. Earth Search Science, Inc., 2010; Green Car Congress, 2009.
j. Reuters, 2008; Shurtleff and Doyle, 2008.
k. Burnham, 2003; Carlson et al. 1981; Raytheon, 2006; Moon, 2008.
l. Global Resource Corp., 2007.
m. Covell and coworkers, 1984.

Internal Combustion. In 1972, Occidental Petroleum became the first company in the US to conduct a viability study of a modified in-situ process at Logan Wash, Colorado (Agarwal, 1986; Hulsebos et al. 1988; Johnson et al. 2004; Lee et al. 2007; United States Department of Energy, 2007; United States Office of Technology Assessment, 1980). Since then, several companies have tested internal combustion approaches which use a fire front moving through the oil shale deposit. The combustion of oil shale rocks generates energy to break down macromolecular hydrocarbon clusters into syncrude and gases. Major players include Lawrence Livermore National Laboratory (LLNL) Rubber In Situ Extraction (Burnham et al. 2006; Lewis and Rothman, 1975; Rothman, 1975), Rio Blanco (Berry et al. 1982), and Geokinetics Horizontal (Lekas, 1979). The internal combustion approach requires rubblization of an oil shale formation to create porosity that facilitates the flow of gas and oil toward the extraction wells before the combustion starts. A fraction of the shale deposit needs to be removed to allow oil shale expansion during the rubblization. In the LLNL rubble in situ extraction demonstration, 20% of an oil shale deposit was mined for this purpose. Explosives were often used for rubblization.

Companies have also tested internal combustion in underground coal conversion, which is generally known as underground coal gasification (UCG). There are significant efforts ongoing on UCG, which, while encouraging, are beyond the scope of this subtask.

Wall Conduction. Underground thermal treatment using heated pipes has been explored by several companies for oil shale conversion, including Shell's In-situ Conversion Process in 1997 at Piceance Creek Basin, Colorado (Colorado Division of Reclamation and Mining Safety 2007; Nair et al. 2006; Shell Frontier Oil and Gas, Inc. 2006), and the Conduction, Convection, Reflux (CCR) Process by American Oil Shale (formerly E. G. L.) at Western Colorado (E. G. L. Resources, Inc. 2006).

This technique has later been adapted to coal deposits. Underground coal thermal treatment using a wall conduction heating was proposed by Shell Oil Company (Wellington et al. 2001). In their process, the coal was heated to 525°C (980°F) and high quality gas and oil were produced. The major products include a coal liquid with a API gravity over 30.

Geothermic Fuel Cell. An interesting extension of conduction heating and internal combustion was proposed by Independent Energy Partners (Savage 2006). The products of shale pyrolysis are used to generate the energy for shale pyrolysis as well as electricity in a "Geothermic Fuel Cell" to which an external oxidant is supplied. Independent Energy Partners proposed extraction wells consisting of stacked fuel cells producing electricity at the same time as hydrocarbon extraction.

Externally Generated Hot Gas. In 2006, Chevron developed an underground retorting technique, the Recovery and Upgrading oil from Shale (CRUSH) process that circulated heated CO_2 through the shale formation (Chevron USA, Inc. 2006; Green Car Congress 2006; United States Department of Interior 2006). Externally generated hot gases used by other companies for in situ shale oil production include superheated pressurized air and shale gas by General Synfuels International's Omnishale technology (Earth Search Science, Inc. 2010; Green Car Congress 2009), and the combustion products of natural gas

by Mountain West Energy's In situ Vapor Extraction (Reuters 2008; Shurtleff and Doyle 2008) and alkane gases by Taiyuan University of Science and Technology (2006).

Coal seams have also been treated using externally generated hot gases. Calderon and Laubis (2010) proposed in situ coal pyrolysis using a heated hydrogen-rich recycle gas to extract syncrude and syngas, and subsequently to convert in-situ (CO_2 to CO, SO_2 to S, NO_x to N_2) using the residual coal char with a gas stream consisting of CO_2 and air.

Volumetric Heating. Researchers have also explored the possibilities using radio frequency and microwaves to heat oil-shale formations (Kinzer, 2008). In 1970s, the Illinois Institute of Technology and later Lawrence Livermore National Laboratory developed in situ oil shale radio wave heating technique (Burnham 2003; Carlson et al. 1981). Raytheon and CF Technologies developed another approach using radio frequency heating and critical fluid flushing (Raytheon, 2006), which was transferred to and further developed by Schlumberger (Moon 2008). Global Resource Corporation is testing a similar concept using microwave heating (Global Resource Corp. 2007).

ExxonMobil Electrofrac. ExxonMobil developed a combined approach of wall conduction and volumetric heating by injecting an electrically conductive material into the fractures of an oil shale formation (Symington et al. 2008). This conductive material forms the heating element of the electrically heated underground oil shale retort.

Co-processing Approach. Covell et al. (1984) at Western Research Institute developed an approach of coal and oil shale in-situ co-processing. In many locations around the world, including Wyoming (Covell et al. 1984) and Liaoning, China (He, 2004), coal and oil shale layers are in the vicinity of each other. The approach was named Total Resource Energy Extraction, and uses the heat generated from an underground coal conversion (combustion or gasification) process to heat and produce hydrocarbon gases and oils from oil shale.

Thermal Treatment

Two steps are needed to establish an underground retort for in situ oil shale processing. Naturally occurring oil shale has almost no permeability and a vast resource of kerogen is locked up and will not flow under normal conditions. Therefore, the oil shale formation must be massively fractured before implementing a second step of heating the fossil rock to produce the shale oil.

Fracturing. Hydraulic fracturing is a mature technique that has been applied in the petroleum industry over the last 60 years to more than 1 million wells (Halliburton 2008; Oil & Gas Journal 2008). To create fractures, a fracturing fluid is pumped down to the wellbore to generate pressure downhole to break the formation rock. The fracturing stimulates the flow of hydrocarbons to achieve a higher well production. Water, often mixed with sand, gels, foams and other chemicals, is commonly used as a fracturing fluid. Conventional approaches used small volumes of fracturing fluid until the invention of high-volume horizontal slick-water fracturing in 1990s. The fracturing fluid in the new technology contains a lower

amount of gelling agent, but adds friction reducers. To maintain the opening after fracturing, a proppant is usually introduced after the injection. Hydraulic fracturing has been widely used in underground shale processing such as in ExxonMobil's Electrofrac (Symington et al. 2008) and Taiyuan University of Science and Technology's Hot Alkane Convection (2006) technologies.

Explosives were also used to create a rubblized shale formation such as in Occidental Petroleum's modified in situ oil shale processing (Hulsebos et al. 1988). Occidental Petroelum's underground retorts, with dimensions of 50 m wide × 50 m deep × 85 m high, were constructed by mining 3 retort void volumes (upper, intermediate, and lower) to provide the expansion space for the shale formation after the detonation of explosives that were placed underneath the retort.

Shockwaves can also be generated for oil shale rubblization using high pressure gas explosion and expansion (Cha, 2010). A combustible gas mixture was proposed to be injected into an oil field, oil shale and sand formation to create a shock wave after detonation.

The temperature and pressure at which a shale rock formation fractures depend on the rock properties. For example, Liushuhe oil shale sample fractures under the pressure between 4.5 and 13 atmospheres (65 and 190 psia), in comparison with 80 atmospheres (1180 psia) for Fushun samples (Zheng et al. 2008).

The particle size after rubblization is usually on the order of 10 cm.

Heating Sources. Electrical heating was used in Shell's ICP. The electricity cost alone for oil shale retorting was estimated to be $16-17 per barrel (crude oil equivalent) in this study, in comparison with the estimation by Bartis et al. (2005) of $12-15 per barrel. The electricity can be generated near the retorting facilities using coal, gas, nuclear power and renewable energy sources. Around the oil shale rich Green River Formation in Colorado, Utah, and Wyoming, coal is the cheapest fuel for electricity production as coal deposits are often in the vicinity of oil shale formations (Covell et al. 1984). Coal-fired plants, however, have socio-political and environmental consequences as they generate a significant amount of greenhouse gases and air pollutants. The produced gas generated from underground oil shale thermal treatment is a natural source of fuel for a gas-fired power-plant. Similar conclusions can be reached for underground coal thermal treatment.

Waste gases generated during coal conversion can be heated and injected into the coal seam as a heat carrier. For approaches using externally generated hot gases, gaseous hydrocarbon fuels are often used as the heat source, because product gases such as water vapor, nitrogen and carbon dioxide are relatively less soluble in oil shale (Petroleum Research Center 2008; Shurtleff and Doyle 2008). This hydrocarbon-rich stream of gases was also recommended to augment coal conversion even when electrical heating is used. The recycled gas can diffuse into the formation and be exhausted to the surface after heat exchange with coal.

Product gas can be used to fire a gas turbine to generate electricity in addition to providing a carrier for recycling energy. Underground oil shale retorting can usually achieve self-sustaining production cycles

after an initialization stage by replacing the injection hydrocarbon gas with the producer gas (Earth Search Science, Inc. 2010; Green Car Congress 2009). If coal seams exist near an oil shale retorting site, then coal-generated gases can be used for heating (Covell et al. 1984). Therefore, no gas needs to be imported to the production site.

Recently, solar and wind technologies have shown great promise for future energy need. Chinese solar companies using photovoltaic technology have bid a state contract for only 10 cents per kilowatts (Chemical & Engineering News, 2010). Land-based wind turbines are able to generate electricity at a comparable cost to coal-fired power stations (Businessweek 2010). Therefore, besides the onsite generation of energy sources, wind and solar show promise for coal and oil shale underground thermal treatment. The intermittent supply of energy from solar energy and wind is less of a problem for underground coal thermal treatment than in providing electricity to the grid.

Review of Physical, Chemical and Geological Properties

After reviewing the chemical, physical and geological properties of various coal samples reported in the literature, the investigators identified the most relevant properties are coal rank, coal seam depth and thickness, and coal permeability.

Targeted Coal Rank

Coal composition presents various challenges towards production of coal liquids in an economical and environmentally acceptable way using UCTT. Moisture is an energy barrier to UCTT as water has a heat capacity 4 times that of dry coal. Typically lignite and sub-bituminous coals contain high moisture contents, often over 20%. Approximately 50% of energy input is consumed to dry a 20% moisture content coal. Oxygen content correlates closely with pollutant formation and CO_2 emissions. A low oxygen content is preferred, which usually found in bituminous and anthracite coals. Hydrogen content determines the quality of UCTT products, since higher hydrogen corresponds to lighter syncrude and less carbon pollution. Usually anthracite coals have a 40% lower hydrogen content compared to other coal ranks. Therefore high-volatile bituminous coals are target resources when UCTT technology is first commercialized.

Coal Thickness and Piping Orientation

The US thickest recorded single coal layer was discovered in the Wasatch Formation near Lake DeSmet on the western edge of the Powder River Basin, and it was estimated to be 75 meters (250 feet). However, the coal is too deep and currently not extractable. A coal seam usually consists of many single coal layers with rock layers in between. In comparison, shale is more uniformly distributed in the rock without separating into different layers. Therefore, when a heating and extraction piping system is designed for UCTT, the pipe orientation should consider the structure of the coal seam. To avoid wasting energy in the rock layers between the coal layers, pipes parallel to the coal layer make most sense. It might not be economically feasible to apply UCTT to thin coal seams separated by rock layers. Thick layers parallel to

the surface, such as in the Big George Deposit in the Powder River Basin, are candidates for UCTT. An additional benefit of such a deposit is that many of them are already tapped for coal bed methane coal-bed methane. This provides the additional advantages of existing seismic characterization of the sites, a large number of wells that can serve as conduits in the UCTT process, and a dewatered deposit after the coal-bed methane has been extracted.

Coal Permeability and Need for Rubblization. Rubblization is usually needed for underground oil shale thermal treatment due to its lower permeability and porosity. In contrast, rubblization was determined as not being necessary in Shell's UCTT patent (Wellington et al. 2001), as high permeability and porosity in coal seams will develop during devolatilization.

Adsorbed water, methane and light hydrocarbons are first removed by physical processes. The water vapor will further catalyze the removal of hydrocarbons from pores. Starting with the removal of water, the permeability in coal seams develops. The temperature during the heating stage will pass through a plateau when the moisture in the coal is evaporated (Westmoreland and Dickerson 1980) and then increase steeply with time.

When the temperature exceeds 270°C (520°F), hydrocarbons start to be removed by chemical reactions. As the pyrolysis process continues, more labile-phase compounds are removed, and the coal permeability grows rapidly. The extent of growth in permeability is remarkable. When the temperature reaches 390°C (730°F), the permeability of the coal formation can be a factor of 1000 higher than at ambient temperatures (Wellington et al. 2001).

Coal Permeability and Selection of Process. Coal permeability is also determined by the way the coal is heated. Wall conduction using hot pipes leads to very uniform thermal heating, which generates a uniform distribution of porosity and a higher permeability. When the coal formation is heated by the combustion of gases, channeling is usually observed with a non-uniform distribution (Wellington et al. 2001). Therefore, wall conduction heating has an advantage over heating using combustion gases.

Review of Lab-Scale Coal Treatment Data

There is abundant literature on the coal conversion yields as a function of temperature and pressure. In general, the volatile yield increases with temperature and decreases with pressure.

Temperature

The kinetic data for kerogen decomposition was collected by Berchenko et al. (2006), Campbell et al. (1978) and Shih and Sohn (1980). The Berchenko et al. data were directed at obtaining the time needed to decompose 90% of the kerogen, which depends strongly on temperature. For one sample at 370°C (700°F), the target decomposition occurred within 5,000 minutes; at 500°C (930°F), it occurred within 2 minutes.

Similar information can be found for coal devolatilization. In general, coal conversion increases when the temperature increases. Farage et al. (1987) determined that amounts of extractible carbonaceous materials increased with ultimate temperature as more volatiles are released from the coal at higher temperatures. An asymptotic volatile yield is approached at temperatures above 700°C (1300°F), at which temperature less than 10% of the ultimate volatile yield remains. The time needed in Farage's experiment was less than 1 minute. This observation is supported by McCown and Harrison (1982) and Suuberg and coworkers (1980) for Louisiana and Montana lignites.

A slower heating rate to a relatively low temperature reduces heating and facility costs. Therefore, the target retort temperatures for underground oil shale processing in most approaches were set to an operational range between 340 and 400°C (650 and 750°F) for both above-ground and underground treatments (E. G. L. Resources, Inc. 2006; Nair et al. 2006; Shurtleff and Doyle 2008; Symington et al. 2008). UCTT will require a higher temperature as observed by Calderon and Laubis (2010) because coal is a less volatile material than oil shale.

In the Taiyuan University of Science and Technology's Hot Alkane Convection and Western Research Institute's Total Resource Energy Extraction approaches, the convection gases were heated to 700°C (1300°F). This gas temperature will probably lead to similar shale temperatures as other approaches.

Pressure. The underground pore pressure, in theory, should not exceed the lithostatic pressure that is applied to the void space realized by the overlying formation. In the western United States, the overburden layer can be up to 300 meters (1000 feet, Bartis et al. 2005) in comparison with the overburden between 30 and 90 meters) (100 and 300 feet) at the Liushuhe site, Daqing, China (Zheng et al. 2008). Due to the different overburden thickness and various operational considerations, the underground pressure was reported to be 0.2-3.5 MPa (30-500 psia) in the Shell ICP process (Berchenko et al. 2006; Brandt 2008), 16 MPa (2400 psia) in ExxonMobil's Electrofrac process (Symington et al. 2008), 9 MPa (1300 psia) in Mountain West Energy's In-situ Vapor Extraction process (Shurtleff and Doyle 2008).

Shell reported that its UCTT process is maintained under pressures up to 3.5 MPa (500 psia, Wellington et al. 2001). Selection of a high retorting pressure sometimes is a natural choice of the overall process design. When a stream of syngas is produced from UCTT, the gas product is often used to fire a gas turbine for electricity. A produced gas stream needs to be pressurized for power generation. Therefore, a selection of a high operation pressure (of steam, CO_2, air or O_2) in underground retorting unit does not increase the overall cost much.

Selection of operation pressure is also influenced by other design considerations, such as safety of personnel and equipment. During the underground heating stage, volatile matter vaporizes, and the porosity volume increases dramatically inside the coal and oil shale formation. Therefore, subsidence and compaction of the formation becomes a possibility, which endangers the surface workers and underground equipment. A high operation pressure in the formation will prevent a subsidence, thus preventing damage of drilling and well equipment.

Pressure selection determines the product yield, distribution, and overall quality. In general, higher pressure leads to lower yield of coal liquids but with a higher quality. Higher pressure stimulates secondary reactions that result in a higher yield of gaseous products.

Injection Gas

Biagini and Tognotti (2006) studied the separate processes of direct oxidation (with air) and devolatilization followed by char oxidation. The devolatilization step was operated under an inert atmosphere. They found that devolatilization was favored over direct oxidation by rapid heating rates because 1) the effective heating rate is faster than oxygen diffusion, and 2) the volatile material forms a cloud that further slows down the diffusive mechanism. On the other hand, under the same reference heating-rate, the presence of oxygen enhances the thermal breakage of chemical bonds, in addition to the exothermic nature of oxidation reactions that heats up the reacting samples. The effect of oxidizing environment is evident in terms of the weight loss curves in Figure 35 that is shifted to the low temperature region. The direct oxidation leads to higher reactivity of chars than those obtained from devolatilization in inert environments, as shown by the relative earlier peak of derivative thermogravametric curve in comparison with the devolatilization/char oxidation process.

For non-oxidizing environments, many researchers (Christsora et al. 1987; Sharma et al. 1986; Tyler 1980) reported that substituting an atmosphere of argon, hydrogen, carbon dioxide, and steam for inert gases has almost no impact on the tar and hydrocarbon gas yields. Khan and Hshieh (1989), however, discussed the influence of steam presence on the gasification reactivity. At the two temperatures they tested, steam presence had a significant influence at 950°C (1740°F) on the weight loss of sub-bituminous coals, most likely due to the catalytic effect of the exchangeable cations present in low-rank coal. Steam enhances the gasification process of coal/char. They also found that the weight loss is a strong function of heating rate in the presence of steam, with larger weight loss associated with lower heating rate because of the reaction between steam and coal. The reactivity of char formed at 650°C (1200°F) is higher in the presence of steam in comparison with the inert condition. The char formed at 950°C (1740°F) in the presence of steam, by contrast, leads to lower reactivity, likely due to the loss of volatile material during the pyrolysis step.

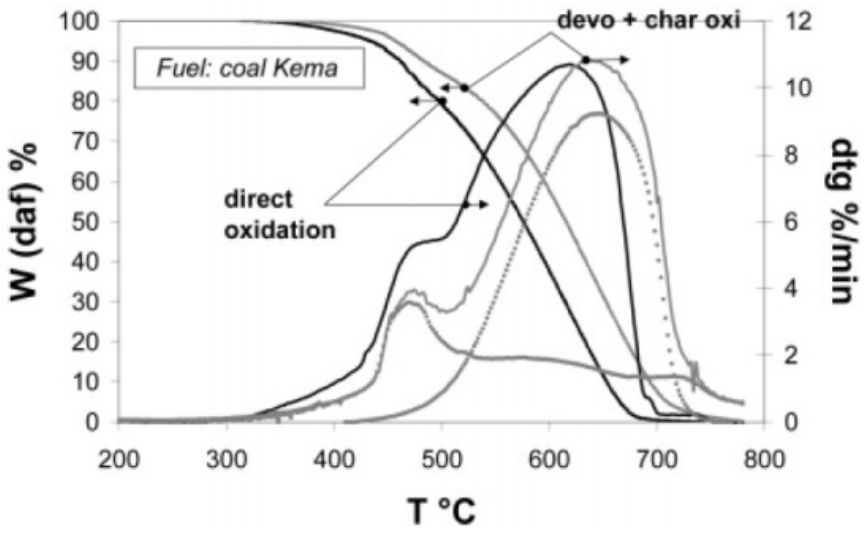

Figure 35 Weight loss and derivative (dtg) curves for direct oxidation (black curves), separate steps of devolatilization and char oxidation (dotted gray curves), and the weighted sum of separated steps (Biagini and Tognotti 2006).

Two atmospheres, CO_2 and N_2, were used in Avid et al.'s experiment (2002), and CO_2 purging gas yields a higher weight loss of coal due to the catalytic effects of alkali metals. The CO_2 reactivity is not significant, however, when the devolatilization temperature was lower than 550°C (1020°F).

Wu and Harrison (1986) found large differences in the pyrolysis liquid composition from Louisiana lignite samples under nitrogen and hydrogen atmospheres. Under hydrogen atmospheres, the yield of alkane/alkene compounds decreased with a significant increase in the production of one-ring aromatic compounds (Figure 36). Although the authors tried to eliminate secondary reactions by controlling the hydrogen gas flow rate, the preferred formation of aromatic fragment rather than re-deposition onto char is a clear evidence of active secondary reaction under hydrogen atmosphere, possibly including hydrogen addition, beta scission, and ring opening.

Graff and Brandes (1984) and Sharma et al. (1986) reported the increase of tar yields with steam in coal devolatilization. In Sharma's experiments, the yield of volatile increased with pressure (up to 66 bars) linearly in steam and hydrogen atmospheres, and decreased with pressure in an argon atmosphere, as shown in Figure 37. The high-pressure argon environment decreased the reactivity due to re-condensation of primary volatile products on the coke surface. A hydrogen environment led to the largest gain in the yield of volatiles since the hydrogen stabilized the primary product from thermal degradation. Secondary reactions via hydrogenated aromatics were proposed. Due to the cost of using hydrogen gas, the authors have proposed a few alternatives. First, they found that by adding high-pressure steam into the hydrogen gas stream will increase the volatile yields. Second, the mixture of 5% red mud with coal enhanced the volatile production probably due to the catalytic effects of 37% Fe_2O_3 (hydrogen dissociation reaction possible on surface) content in the red mud. Third, the synthetic gas also increased the yield of volatiles

due to water-gas shift reaction that produce activated hydrogen gas catalyzed by the mineral and metal walls; the water-gas shift reaction was evident by the gas product composition.

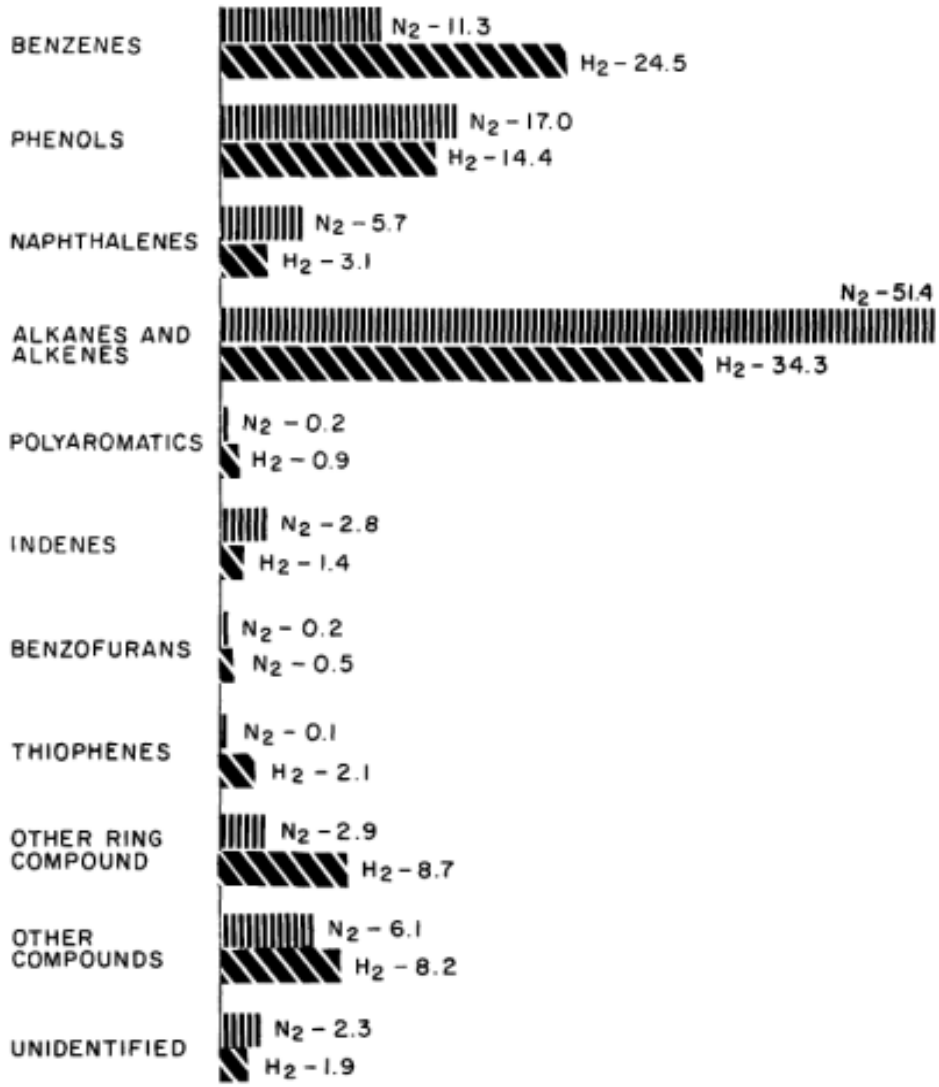

Figure 36 The pyrolysis liquid composition under nitrogen and hydrogen reactor atmospheres (Wu and Harrison 1986).

Wellington et al. (2001) also suggested that hydrogen gas can be injected into coal formation to improve product quality. Like the results reported by Graff and Brandes (1984), hydrogen will stabilize the pyrolysis intermediates and facilitate secondary reactions. A more hydrogen-rich product can be produced, indicating a higher quality and volatility (Khan 1989).

Chen et al. (1999) also concluded that hydropyrolysis gives higher tar yields. A very detailed study by Cypres and Furfari (1982) focused on the pyrolysis yields of oil, gas, char and water from a low-

temperature devolatilization of a bituminous coal. They found the oil production increased exponentially with the hydrogen partial pressure, while the total char yield decreased exponentially and the water yield increased rectilinearly with the hydrogen partial pressure. Their results (Figure 38) are different from those of Graff and Brandes (1984) in terms of the non-linearity of their yields on hydrogen pressure. The authors found that the methane in the reactor acted as an inert gas and showed very little reactivity. The positive effect of a hydrogen atmosphere can be explained by the prevention of condensation (polymerization of primary pyrolysis products) and enhanced upgrading reactions of coal fragmentation due to hydrogenation of free radicals.

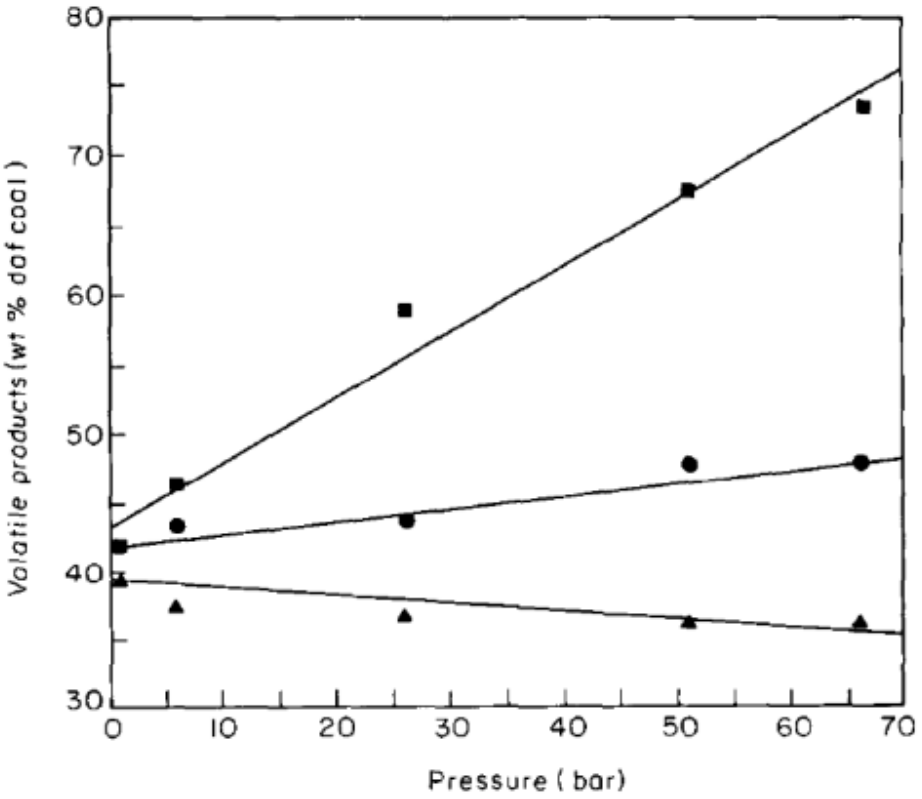

Figure 37 Pressure dependence of volatile yields from coal devolatilization in hydrogen (upper curve), steam (middle) and argon (lower) (Sharma et al. 1986).

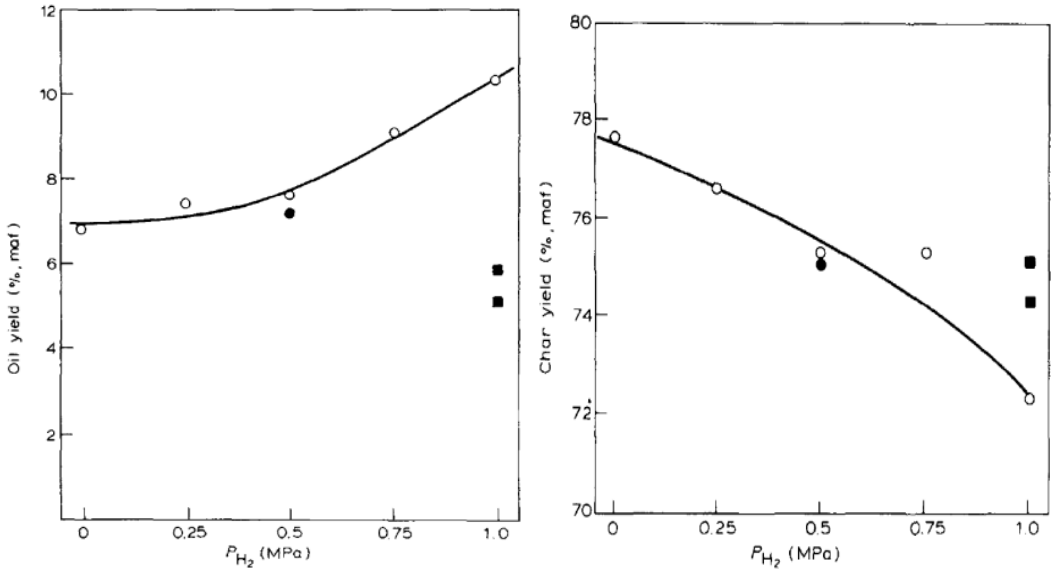

Figure 38 Effect of hydrogen partial pressure on pyrolysis yields of oil and char at 1 MPa and 580°C (1020°F) under a mixing atmosphere of hydrogen and methane (Cypres and Furfari 1982). The solid circle corresponds to a mixing atmosphere of hydrogen and nitrogen. Squares represent results under a total pressure of 4 MPa.

Liao and coworkers (1998) compared the devolatilization of a Chinese lignite for various reactor atmospheres under the same total pressure or partial hydrogen pressure. They concluded that a hydrogen atmosphere is the most effective in the coal devolatilization, as the pyrolysis yields decreased when a coke oven or a synthesis gas under the same total pressure was used. However, if the hydrogen partial pressure of the replacement atmosphere was equal to the total pressure of hydrogen atmosphere, the larger total pressure in the replacement atmosphere resulted in a higher yields of pyrolysis oils. It is interesting to note that the BTX (benzene, toluene, and xylene) and naphthalene yields in the pyrolysis oils are almost the same under hydrogen and coke oven gas atmospheres, although the relative abundance of these species are different. In hydropyrolysis, the benzene fraction is the smallest, and xylene fraction is the largest; in contrast, with coke oven gas, the reverse order is observed (Table 7). The authors concluded that methane in the coke oven gas reacts with CO and H_2 that yielded an increasing oil yields and improved oil quality through an increase of the BTX, PCX (phenol, cresol, and xylene) and naphthalene content. However, the conclusion is not in line with those of Chen et al. (1999) who suggested that methane acts as an inert gas. Indeed, the inertness of methane can be concluded from the Liao et al. (1998) data, which indicated that coke oven gas atmosphere resulted in an almost identical oil composition (BTX, PCX, and naphthalene) as that obtained from hydropyrolysis.

Table 7. Major fractions in pyrolysis oils from a Chinese Xianfeng lignite with hydrogen and coke oven gas with a reference heating rate of 5°C/min (41°F/min) and an ultimate devolatilization temperature of 650°C (1202°F) (Liao et al. 1998).

Tar components[a]	H_2 (3 MPa)		COG (3 MPa)		COG (5 MPa)		N_2 (3 MPa)	
	Content	Yield	Content	Yield	Content	Yield	Content	Yield
Benzene	2.98	0.86	7.04	1.65	5.88	2.10	2.01	0.14
Toluene	4.71	1.35	5.04	1.19	6.02	2.15	2.80	0.24
Xylene	6.08	1.76	4.74	1.11	5.90	2.11	5.09	0.48
BTX	13.77	3.97	16.82	3.96	17.80	6.36	9.90	0.86
Phenol	10.22	2.94	9.56	2.25	15.62	4.13	18.43	1.59
Crysol	16.07	4.63	13.12	3.08	15.62	5.58	21.28	2.10
Xylenol	7.30	2.10	6.56	1.54	7.63	2.73	10.75	0.99
PCX	33.59	9.68	29.24	6.87	34.79	12.45	50.46	4.68
BTX + PCX	47.36	13.65	46.06	10.83	52.59	18.81	60.36	5.54
Naphthalene	4.48	1.29	5.45	1.28	5.92	2.12	3.80	0.33

[a] Content: MK%; yield: wt%, daf

Minkova et al. (1991), Angelova et al. (1981), and Angelova and Minkova (1986) have shown that pyrolysis liquid yields from the low temperature devolatilization of lignite and bituminous coals and oil shales increased in a steam atmosphere by 20-50%. They also found that the steam treatment provides a significant desulfurization effect on solid fuels and their liquid products. Sulfur content in the coal is transformed into H_2S. Therefore, pyrolysis of coals and oil shales yields pyrolysis gases with higher concentrations of H_2, CO_2, and H_2S and lower contents of CO and CH_4. The possible water-gas shift reaction of steam with CO is, therefore, not excluded.

Yardim et al. (2003) applied steam pyrolysis to four Turkish sub-bituminous coals and found the same conclusion as earlier studies: the yields of pyrolysis liquid and gases species increased significantly with steam treatment. Elemental analysis identified increased hydrogen content in the steam-treated coal products, which was explained by possible chemical alternation between stream and the core coal structures. They also reached the same conclusion regarding the considerable de-sulfurization effect after steam treatment. They also concluded that the enhanced production of volatiles from the coals leads to a significantly higher void volume, specific surface area and adsorption capacity towards iodine of the resultant semi-cokes (Figure 39).

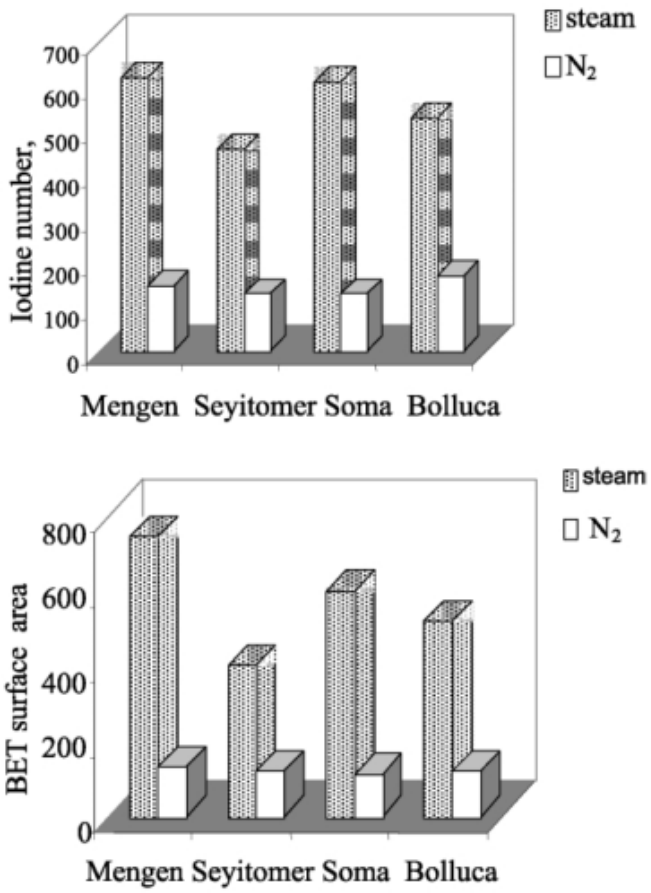

Figure 39. The specific surface area (BET) and adsorption capacity towards iodine with steam treatment are compared with the data under inert atmosphere (Yardim et al. 2003).

Heating Rate

The relation between coal-derived product yields and heating rate has been extensively studied, and sometimes, contradictory observations were reported in the literature. Peters and Bertling (1965) reported significantly higher volatiles from a rapid coal pyrolysis than those from slow heating rate processes. Some researchers (Anthony et al. 1975; Avid et al. 2002; McCown and Harrison 1982) found no significant effects of heating rates on the final yields of volatile matter from Montana, Louisiana and Mongolian lignites, which was calculated by the weight loss. In contrast, Khan and Hshieh (1989) studied the weight loss of devolatilization in the presence of steam for Pittsburgh No. 8 and Wyodak coals, and they found it was a strong function of heating rate, with larger weight loss associated with lower heating rate. Khan and Hshien concluded that the longer residence time at slower heating rate stimulated the secondary reactions that further decompose the coal and coal liquids in favor of gaseous products during transport process out of coal particles.

Khan (1989) used a different set of data reached the same conclusion. The weight loss of devolatilization was 50% at a heating rate of 5 C/min, which decreased to 37% when the heating rate is 50 C/min (Table 84). In contrast, the heating rate had no statistical significance on weight loss under a helium atmosphere, which indicates hydrogen content in the gaseous phase is critical to secondary reactions including steam reformation and water-gas shift reactions (Westmoreland and Dickerson 1980).

Table 8. Effect of steam and heating rate on the pyrolysis weight loss of Pittsburgh No. 8 coal up to 900°C (1650°F) (Khan, 1989).

Effect of Steam and Heating Rate on the Pyrolysis Weight Loss of Pittsburgh No. 8 Coal Up To 900°C

Heating Rate (°C/min)	Weight Loss During Pyrolysis Up To 900°C	
	He	Steam
5	38.0	50.0
10	37.0	44.5
20	37.0	40.5
50	37.0	37.0

A slow heating rate to above about 390°C (730°F) was also increased the ratio of the yield of gas to condensable hydrocarbons (Wellington et al. 2001). The production of methane can be significantly enhanced by minimizing the yield of condensables. This is a huge advantage because process can be altered according to market demands.

For underground retorting processes, slow heating rates were chosen to reduce the upfront cost of surface facilities. In Shell's oil shale *In-situ* Conversion Process (ICP), the heating period is 2-4 years (Shell Frontier Oil and Gas, Inc. 2006), which corresponding to less than 0.5°C/day (0.9°F/day). The heating period for Shell's ICP is typical among shale conversion approaches, including a 7-8 year heating period for ExxonMobil's Electrofrac (Symington et al. 2008), and 1-2 years for Mountain West Energy's *In-situ* Vapor Extraction (Shurtleff and Doyle 2008) processes.

Numerical Simulations and Engineering Calculations

Subtask 6.3 is performing numerical simulations of underground coal conversion.

The investigators have performed engineering calculations for various design parameters. Due to the often contradictory information found in coal literature, we have been cautious in using published coal data, and sometimes carried out our own calculations to verify literature results.

One important aspect of shale conversion is to determine what grade of shale is economically feasible for conversion. We calculated the heat value of various rocks and the cost to convert them, and reached a conclusion that 0.06L/kg is the division between rich and lean rock. This is consistent with literature values from a dozen sources. Details of this calculation are not included in this report.

In another calculation, the investigators determined the electricity cost to heat underground hydrocarbon formation in Shell Oil's In-situ Conversion Process. Our results showed the cost (heating energy cost alone) is higher than that claimed by Shell. Considering other costs associated with the heating (up-front investment, working capital, drilling, pumping, transportation, human resources, environmental, etc.), the cost may be much higher than what was reported in the literature. See section *on* Thermal Treatment for additional detail.

Environmental Impacts of UCTT

Because this process is still in the early design phases, the environmental impacts of the various design alternatives are highly uncertain. However, the following subsections highlight some differences between UCTT methods.

Criteria pollutant and Greenhouse Gas emissions

The pollution and emission issues were discussed for various design parameters in Table 5 and in the text. For example, we concluded that oxygen content correlates closely with pollutant formation and CO_2 emissions; therefore a low oxygen-content coal is preferred. We also concluded that a higher hydrogen-content coal corresponds to lighter syncrude and less carbon pollution (Section on Targeted Coal Rank).

Water Consumption

Water consumption is a less important issue in underground hydrocarbon conversion processes. The vast resources of US coal and shale are located in water-scarce regions, e.g., Green River Formation and Powder River Basin. However, any conversion process will require a dewatering step (Section on Coal Thickness and Piping Orientation) because water in the formation is a more efficient heat absorber than coal and becomes an energy barrier for conversion (Section 2 on Targeted Coal Rank). The produced water can be used in various aspects of conversion processes. The problem of water becomes one of eliminating its environmental impact: cleaning a large amount of produced water and recycling it into the formation is time consuming and costly. The focus should also be on the prevention of water leakage into the dewatered zone, e.g., using a frozen wall in Shell's In-Situ Conversion Process.

Land Use Impact

The dewatering step that depletes the underground water in the work zone might pose a threat to surface vegetation. Sometimes this is not the case since rock layer in the overburden often separate the underground retort and surface ecosystem. This evaluation is not included in this report.

Since we have determined that fracturing is not necessary for underground coal conversion, there is minimum impact on the land topology. Topological changes are possible up to 2 miles if a fracturing process using explosives is required. This evaluation is not included in this report.

Selection of operation pressure is important for the safety of personnel and equipment. During underground heating, volatile matter vaporizes, and the porosity volume increases dramatically inside the coal and oil shale formation. Therefore, subsidence and compaction of the formation becomes a possibility, which endangers the surface workers and underground equipment. A high operating pressure in the formation will prevent subsidence (Subsection entitled Pressure).

Subtask 6.3 – LES in Reacting Porous Media

Simulation results obtained using the newly developed operator-splitting algorithm and the geometric and meshing lessons learned are shown in Figure 40, which shows simulation results at solution times of 0.5 seconds, 83 seconds, 183 seconds, 14,998.5 seconds, and 112,500 seconds. For the first 83 seconds we used the traditional iterative solution algorithm to advance the solution at a time step of 0.5 seconds to initialize both the convective as well as thermal fields. After 83 seconds, we stopped solving the fluid continuity and momentum equations, and only advanced the solution for fluid and solid energy equations at a time step of 100 seconds. At a simulation time of about 14,900 seconds, we once again decreased the simulation time step to 0.5 seconds and solved all continuity, momentum, and energy equations until achieving a statistically steady state. At that time we once again stopped iterating the fluid continuity and momentum equations, and only solved the energy equations with a time step of 500 seconds. This allowed us to advance our simulation solution to 112,500 seconds (31 hours of simulation time). Even when using a time step of 500 seconds, we are able to resolve the large scales that occur within the computational domain and thus capture the heat transfer within the fluid as well heat transfer between the fluid and solid particles. We also observe a significant increase in temperature of the coal particles. In the past it would not have been possible to advance the simulation to this point without using excessive computational resources.

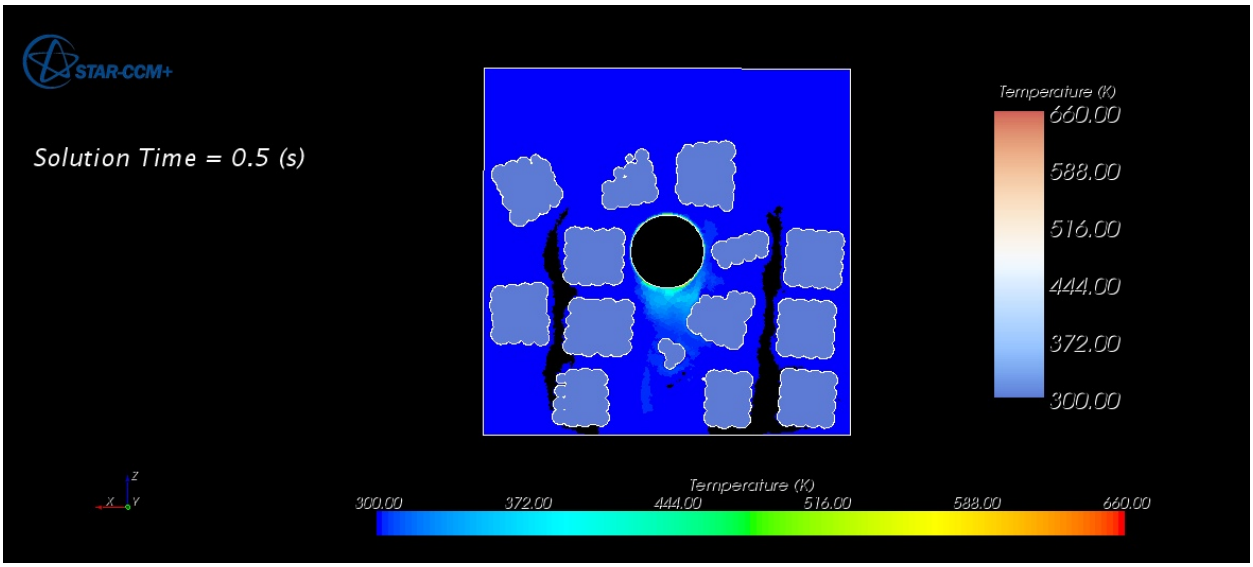

(a) Solution time of 0.5 seconds.

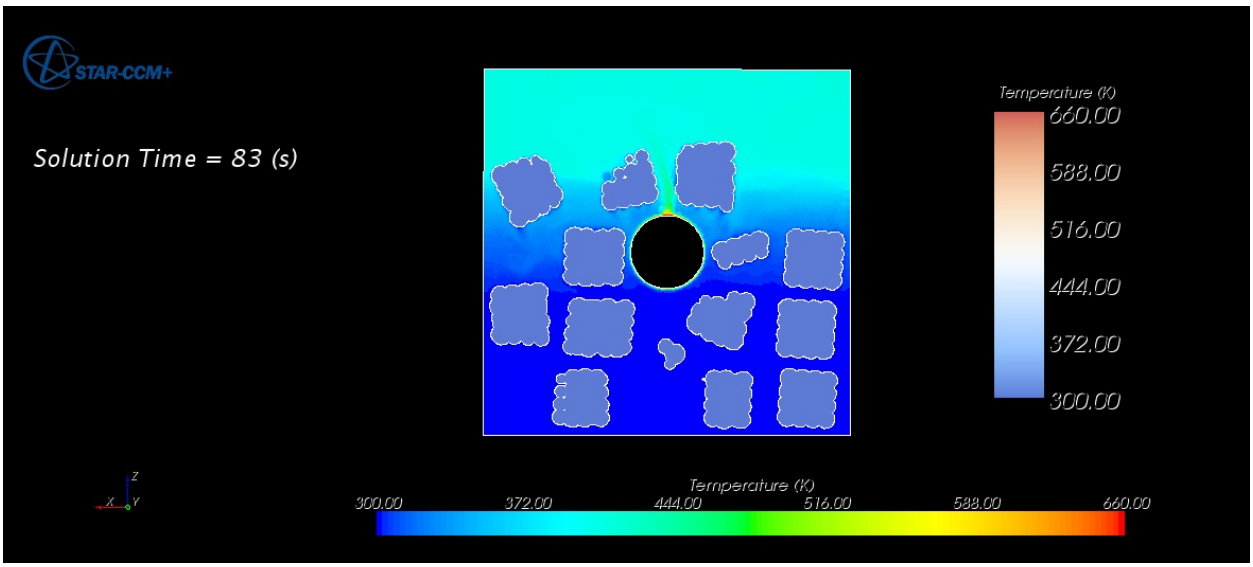

(b) Solution time of 83 seconds.

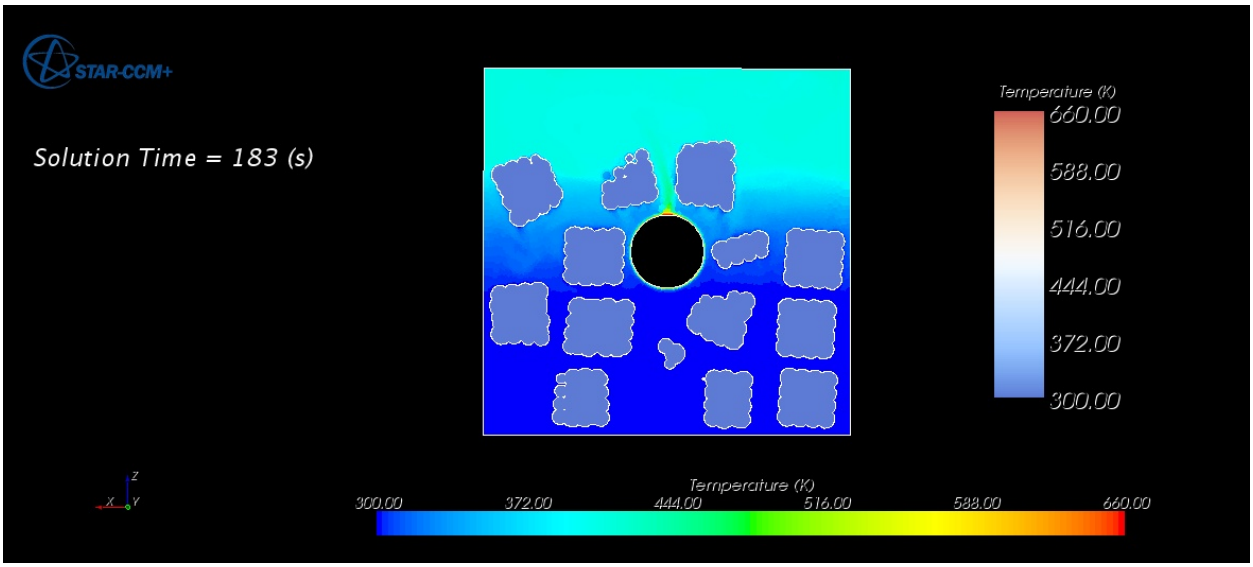

(c) Solution time of 183 seconds.

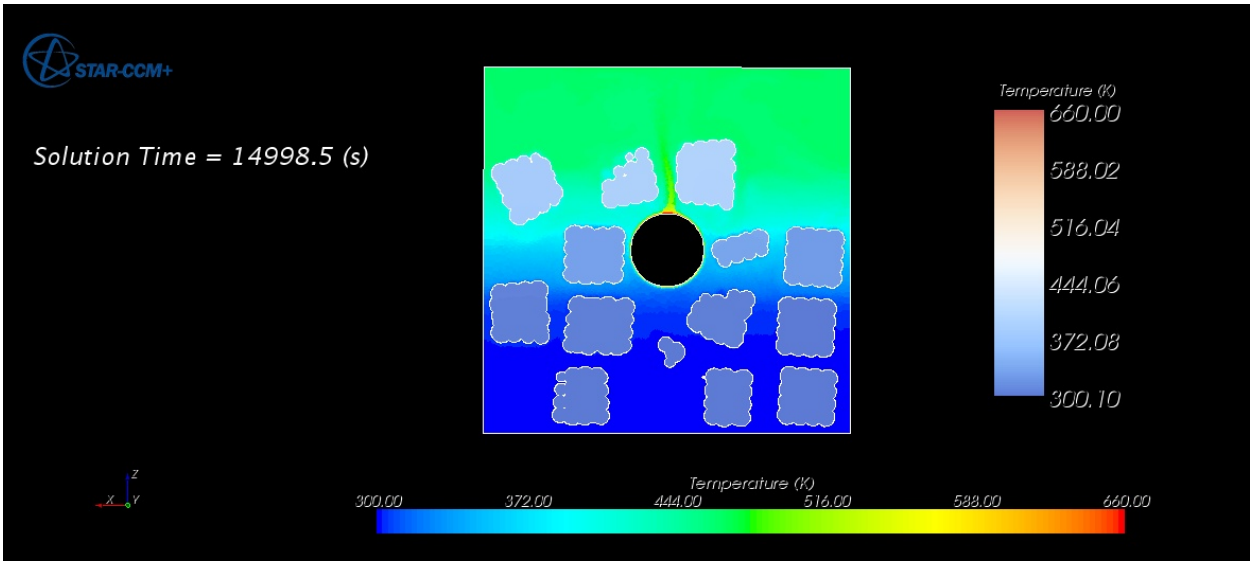

(d) Solution time of 14,998.5 seconds.

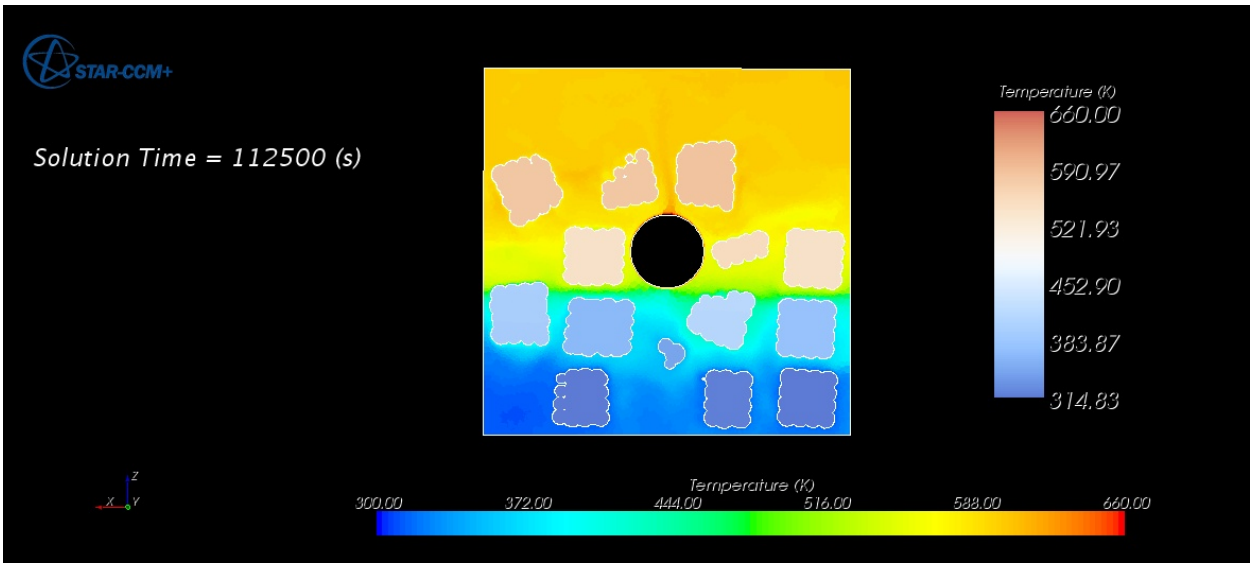

(e) Solution time of 112,500 seconds.

Figure 40. Simulation results obtained using the newly implemented operator splitting algorithm.

Subtask 6.4 – CO_2 Sequestration Chemistry

Set A: Experiments with pure Limestone

Initial XRD and SEM analysis (Figure 41) of limestone revealed it to be 98.4 calcite, 1.2% dolomite and 0.4% quartz. During the experiment, which was carried out for a period of 42 days, the pressure increased to 2060 psi after 17 days and 2090 psi after 42 days. This can be attributed to a four-step process indicated by the following reactions:

(Eq 1) $CO_2(g) \leftrightarrow CO_2(aq)$

(Eq 2) $H_2O + CO_2 \leftrightarrow H_2CO_3$

(Eq 3) $H_2CO_3 \leftrightarrow H^+ + HCO_3^-$

(Eq 4) $CaCO_3 + H^+ \leftrightarrow Ca^{2+} + HCO_3^-$

The CO_2 dissolves in water to form carbonic acid (Eq1 and Eq 2). This leads to a decrease in pH. pH decreased from a value of 5.4 to about 4.9 after 28 days and increased to 5.2 after 42 days. Because of this increased acidity calcite, which is sensitive to changes in pH, undergoes dissolution to release carbonate and bicarbonate ions (Eq 3 and Eq 4). The absence of feldspars and clays, which serve as a

source for cations for secondary precipitation of carbonates, rules out the possibility of any precipitants and also mineral sequestration of CO_2. XRD analysis revealed a reduction in both calcite and dolomite indicating that significant dissolution of these components has occurred. These dissolution patterns are almost omnipresent (Figure 41) through out the sample when the SEM analysis was carried out.

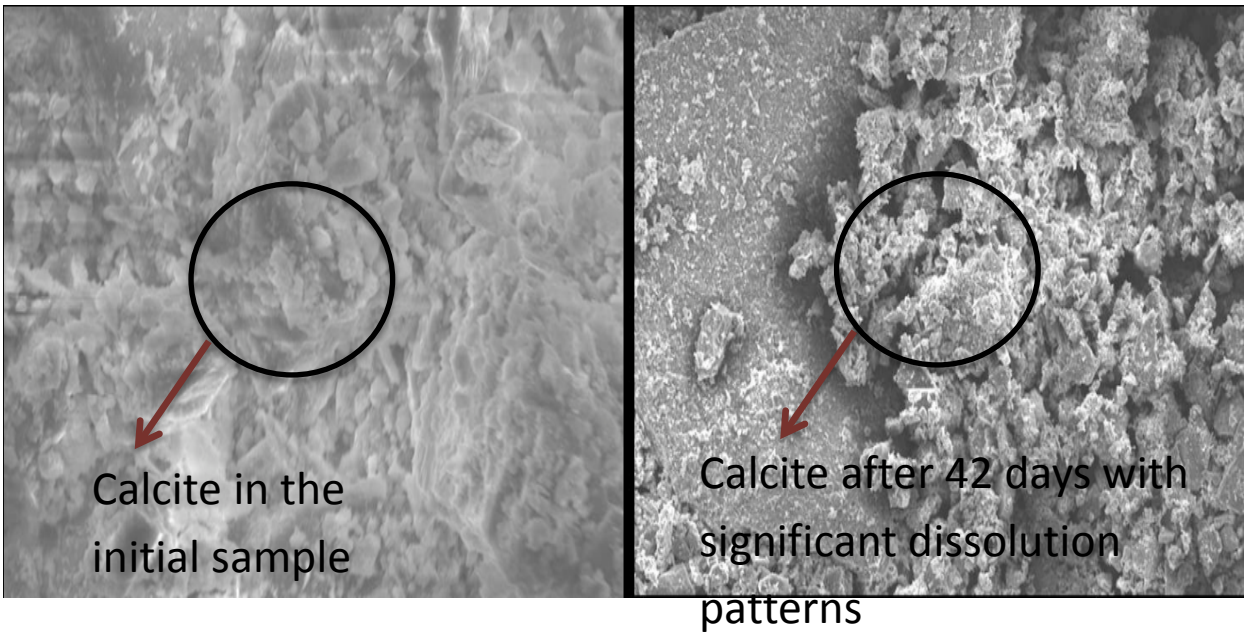

Figure 41. SEM analysis of initial calcite (left) and the reacted calcite after 42 days: dissolution patterns are almost omnipresent with deep etching and rough edges of the surfaces.

The primary cations tracked here are Ca ion and Mg ion (Figure 42). The Mg ion is derived from dolomite, which was present as traces in the initial mineral assemblage. The continuous increase in the concentrations of both the principal ions indicates dissolution of calcite and dolomite. The pH of the system initially decreased due to CO_2 dissolution in brine and increased subsequently because of carbonate dissolution (Eq 4). Carbonate chemistry buffers the brine by consuming a H+ ion and decreases the acidity of the system. The relative scarcity of cations nullifies the possibility of occurrence of precipitation reactions. The primary modes of sequestration in these aquifers are structural trapping and ionic trapping.

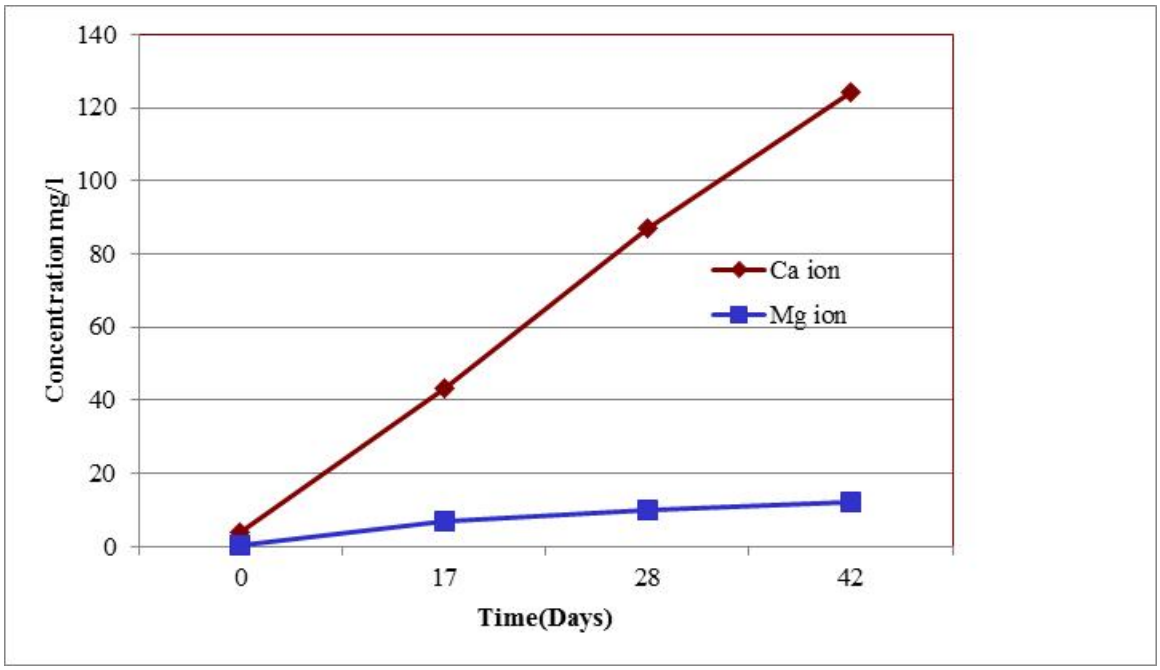

Figure 42. Principal changes in brine chemistry in the limestone experiments.

Set B: Experiments with Sandstone

Initial XRD analysis of the sandstone revealed 44% calcium feldspar, 26.2 % Na feldspar and the rest potassium feldspar. During the experiments, pressure was constant around 2000 psi after 17 days and remained stable for the rest of the experiment. The pH increased from a value of 5.4 to about 5.9 after 28 days and 6.4 after 42 days. The principal reactions in this case can be formulated as follows.

(Eq 5) $2H^+ + CaAl_2Si_2O_8 + H_2O \leftrightarrow Ca^{2+} + Al_2Si_2O_5(OH)_4$

(Eq 6) $CaAl_2Si_2O_8 + H_2CO_3 + H_2O \leftrightarrow CaCO_3 + Al_2Si_2O_5(OH)_4$

(Eq 7) $NaAlSi_3O_8 + 3\ H_2O \leftrightarrow NaAlSi_2O_6.H_2O + H_4SiO_4$

(Eq 8) $2KAlSi_3O_8 + 9H_2O + 2H^+ \leftrightarrow Al_2Si_2O_5(OH)_4 + 2\ K^+ + 4H_4SiO_4$

Dissolution of feldspar also decreases the acidity of the brine (Eq 5) (increases pH), which turned acidic because of the formation of the carbonic acid (Eq 1). This leads to the next sequence of reactions, which is the carbonation of calcium feldspars (Eq 6) leading to the precipitation of calcite and kolinite. At these temperatures and pressures albite undergoes phase change (Eq 7) to precipitate analcime, which was detected in the XRD analysis. Dissolution of potassium feldspars (Eq 8) also leads to precipitation of kaolinite (Figure 44). The primary product of these dissolution reactions is silica. This results in the brine becoming saturated and in some cases supersatured with silica. Hence when the samples are retrieved for

analysis this silica undergoes heterogeneous deposition as amorphous silica on the surface of other host minerals, which was evident in the EDS analysis on all reacted samples. There was also evident precipitation of halite on these samples (Figure 43 and Figure 44). Halite precipitates when the sample is prepared for analysis, i.e., drying overnight.

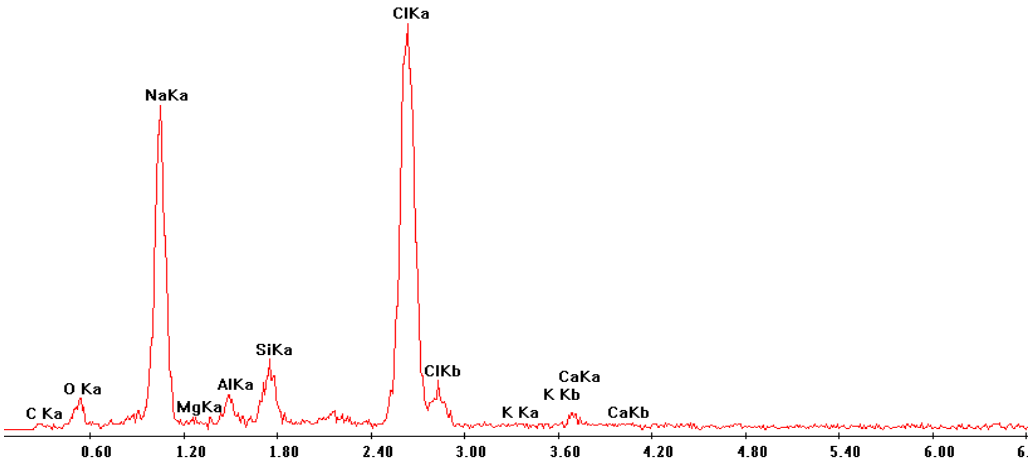

Figure 43. EDS analysis of halite.

Figure 44. Halite chunk on the left and deposition of kaolinite on plagioclase feldspar. Kaolinite is formed from the dissolution of potassium feldspar and was absent in the initial mineral assemblage.

Figure 45 shows the trend of principal ions Ca, K, Al and Si in the brine with plagioclase feldspar and microcline being the primary alumino silicates in the initial mineral matrix. The decrease in Al ion

indicates its precipitation in solid phase, which is evident from the precipitation of kaolinite, which is an aluminosilicate hydroxide. Analcime was detected in XRD but its precipitation was not evident in the reacted samples when subjected to SEM analyses. Si concentration increases continuously in the samples because of the dissolution of the alumino silicate minerals.

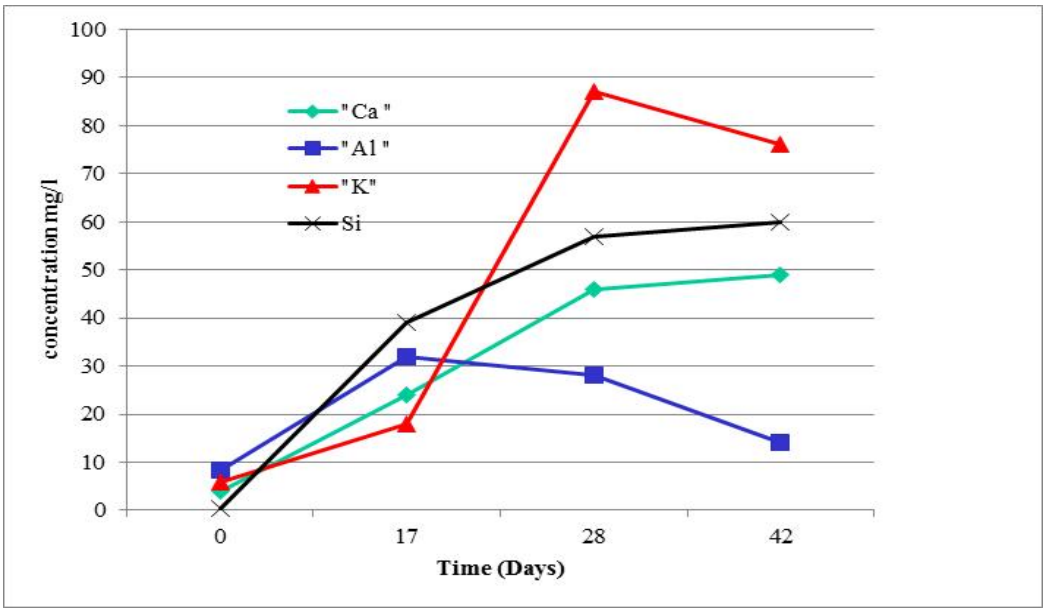

Figure 45. Principal changes in brine chemistry.

Set C: Experiments with Peridotite

Peridotite is composed largely of the minerals olivine [$(Mg, Fe)_2SiO_4$] and pyroxene [$(Ca, Mg, Fe)_2Si_2O_6$] which react with CO_2 and H_2O near the earth surface to form hydrous silicates (serpentine), iron oxides (magnetite) and carbonates (calcite, magnesite and dolomite). These reactions can be formulated as:

(Eq 9) $2Mg_2SiO_4 + Mg_2Si2O_6 + 4\ H_2O = 2Mg_3Si_2O_5(OH)_4$
(Mg-olivine) (Mg-pyroxene) (serpentine)

(Eq 10) $Mg_2SiO_4 + 2CO_2 = 2MgCO_3 + SiO_2$
(Mg-olivine) (Magnesite) (quartz)

(Eq 11) $Mg_2SiO_4 + CaMg_2Si_2O_6 + 2CO_2 + 2H_2O = Mg_3Si_2O_5(OH)_4 + CaCO_3 + MgCO_3$
(Mg-olivine) (Ca-Mg-pyroxene) (serpentine) (calcite) (magnesite)

Natural carbonation of peridotite by weathering and low temperature alteration is common. Evidence for natural, low-temperature hydration and carbonation of peridotite can be found in springs and associated travertines in catchments composed of peridotite and in outcrops of altered peridotite with abundant carbonate veins (Kellemen et al. 2008). High alkalinity, stable isotope ratios and formation of travertine

and carbonate cemented conglomerates in springs indicate ongoing serpentenization involving meteoric water at low temperature. Ground water reacting with peridotite in near-surface, open systems forms water rich in Mg^{-} and HCO_3^{-}, which upon continuous reaction with peridotite leads to precipitation of abundant magnesite and dolomite as veins. The resulting waters become progressively richer in Ca^{-} and OH^{-}. These waters emerge near surface to mix with Mg-HCO_3^{-} waters or react with the atmosphere; they precipitate abundant calcite and dolomite in near surface veins. Enhanced natural processes such as dissolution followed by the carbonation of feldspars, may provide an important alternative to mineral carbonation.

Peridotite was obtained as big green crystalline granules from the deposits in the Samail Ophiolite, Sultanate of Oman. The distinctive green color was due to the presence of significant portions of iron in the crystalline structure. Kinetics of these carbonation reactions is very slow unless olivine and serpentine reactants are ground to fine powder heated and held at elevated pressures and temperature. Hence these granules were ground to very fine powder. A size distribution analysis revealed that major portion was within the range of 60-100 microns in size. A total of 3 grams of peridotite was fed into a 40 CC reactor along with 20CC of brine prepared by mixing 3 grams of laboratory grade NaCl in 20 CC of distilled water and brine was allowed to saturate the sample for about 2 days. CO_2 was then fed into the reactor at a pressure of 2000 psi, and the temperature was maintained at 100^0C. The reactor was isolated, and the experiment was carried out for 47 days. The pressure in the reactor first decreased and then stabilized around 1980 psi for the rest of the experiment with minimal fluctuations, which can be attributed to changes in ambient conditions. The pH change was very similar to the results in experimental set B. It increased from a value of 5.4 to about 5.7 after 28 days and 6.2 after 42 days.

Initial XRD analyses of the sample revealed that olivine was the major component in the sample, which was composed of 97.8 % olivine (by weight) and 2.2% pyroxene (Figure 46). Hence we can conclude from the reactions mentioned above that carbonation of this sample will mainly yield magnesite and serpentine. Because of the presence of excess CO_2 in the reaction setup, carbonation of peridotite will dominate hydration and hence magnesite precipitation should be omnipresent and formation of serpentine should be in trace amounts.

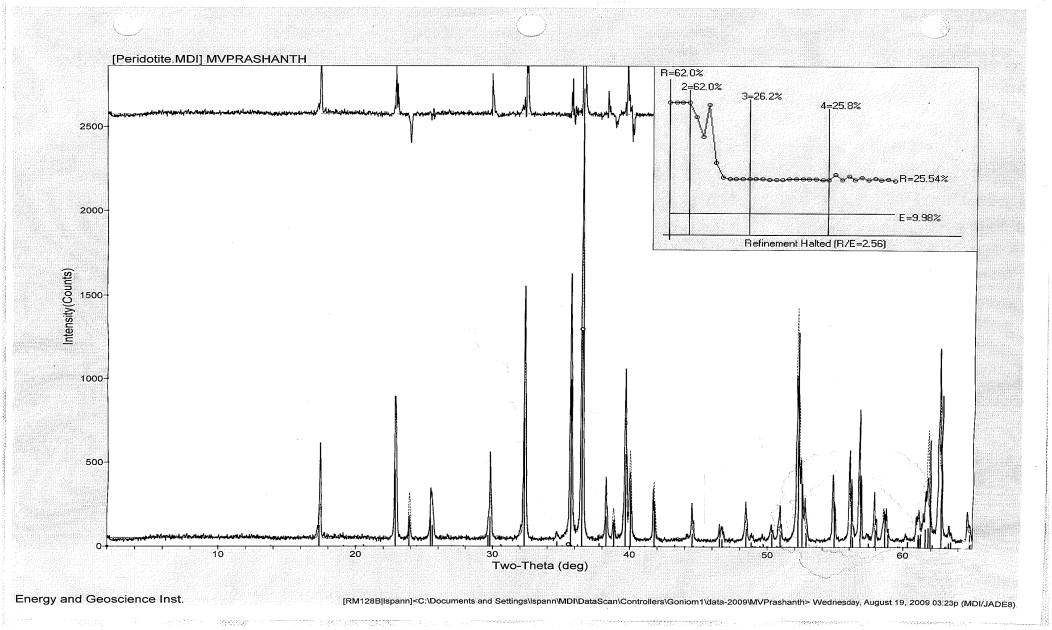

Figure 46. XRD analysis of the initial peridotite sample.

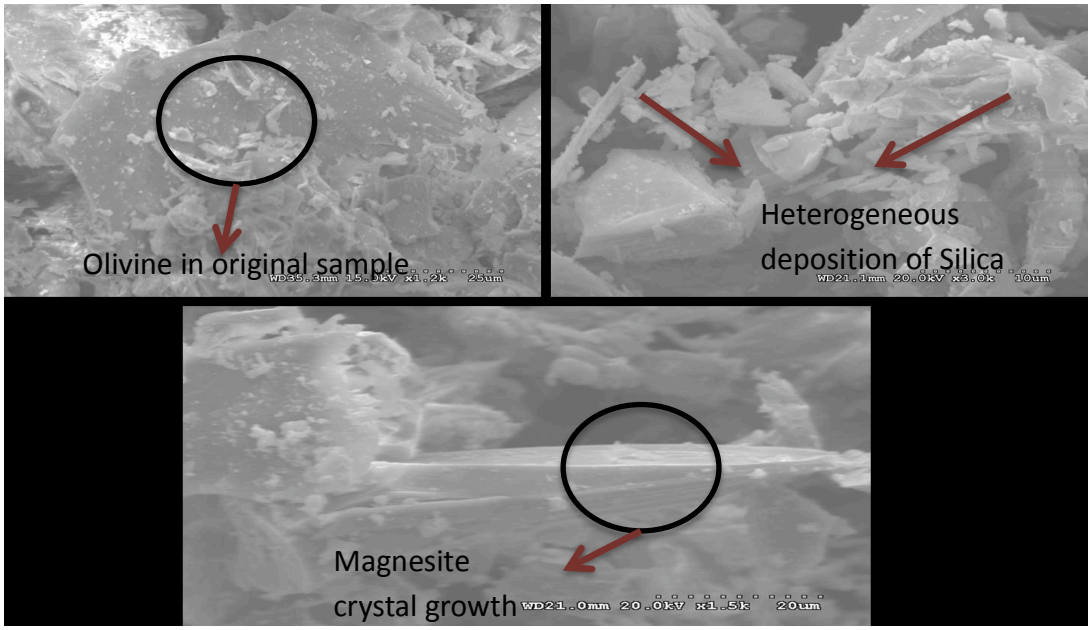

Figure 47. SEM (point) analyses of the initial rock (top left) reveals presence of olivine in the original samples. Figure (top right) showing trace amounts of silica mostly as fur draping across the surface of host peridotite. Figure (bottom) shows the growth of magnesite due to the carbonation reactions of peridotite.

The EDS analysis of the reacted rock (Figure 48) indicates the presence of $MgCO_3$ in the sample. This occurs due to the carbonation of the peridotite to form magnesite and silica. The presence of silica is also revealed in the analysis. The SEM analysis of the product revealed the precipitation of magnesite as

orthorhombic crystals with pitted rough faces. Depending on the shape of the crystal it can be concluded that by the time the experiment was concluded the brine was under saturated with respect to magnesite. The dissolution of the calcium and magnesium silicate minerals produces silica. This silica precipitates out (Figure 47) mainly as amorphous silica on the products when the experiment is terminated, and the temperature is decreased because the brine is supersaturated with respect to silica during the latter stages of the experiment.

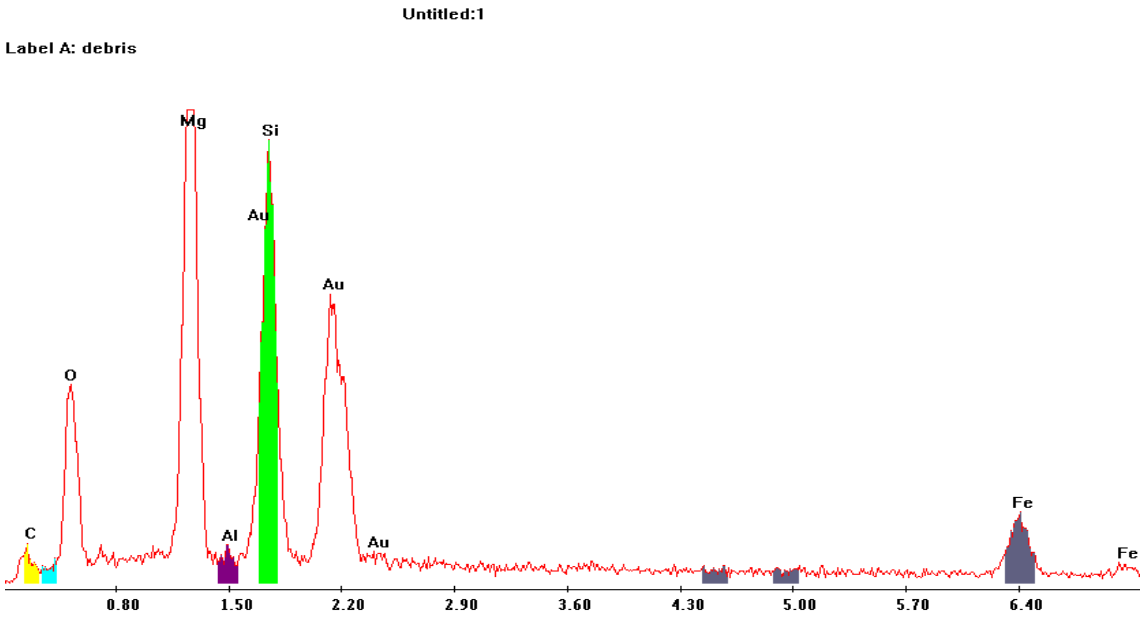

Figure 48. EDS analyses of the reacted rock.

The initial increase in the primary ions Mg, Ca and Si (Figure 49) indicates the dissolution of the aluminosilicates, which leads to a decrease in the pH of the solution. This leads to the carbonation reactions (favored at higher pH) dominating the hydration reactions. The carbonation of peridotite leads to the precipitation of magnesite and siderite. The steep increase in the concentration of Si is a result of the dissolution of the silicate minerals. The reacted samples were characterized with the deposition of silica, which precipitated from the brine when the reactor was degassed.

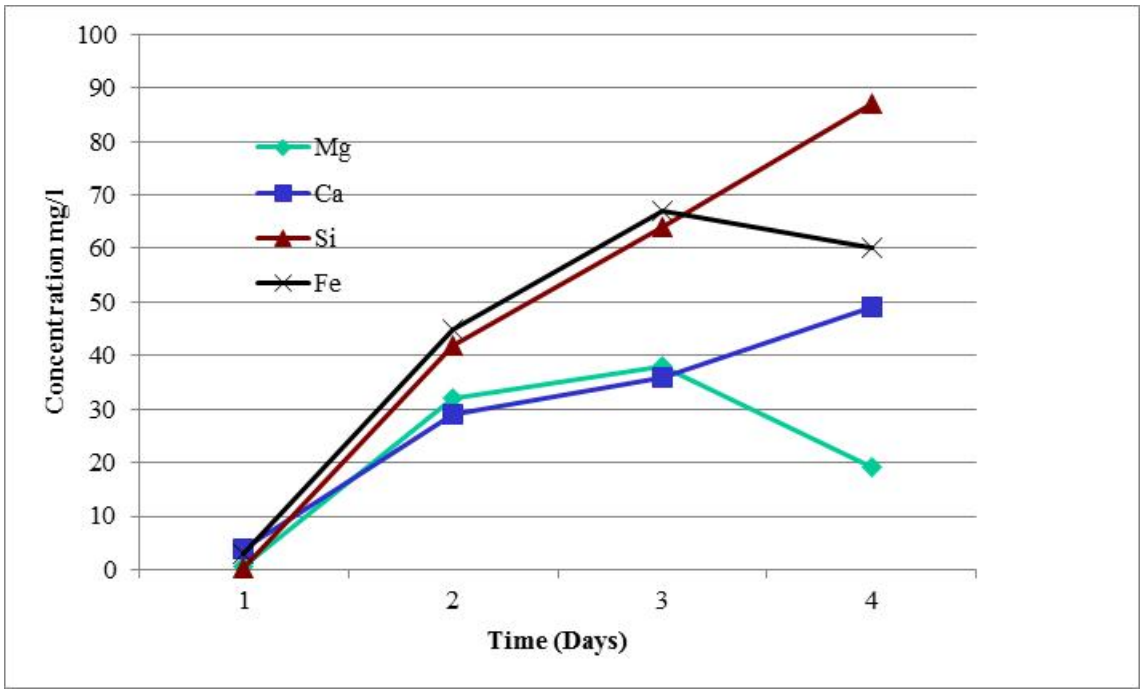

Figure 49. Principal changes in brine chemistry in peridotite experiments.

Set D: Experiments with Arkose

Experiments with arkose and CO_2 as feed gas have been described in detail in UC3 topical report.

Gas composition effects

To evaluate the effect of gas compositions on fluid-rock interaction reactions the following gas mixtures were selected.

1) CO_2+ SO_2
2) CO_2+NH_3

Regardless of flue gases treatment prior to injection and the application of new combustion technologies for pre-combustion capture of CO_2, the flue gas stream will contain some nitrogen, water vapor, carbon dioxide and small amounts of sulfur dioxide, carbon monoxide, ammonia and other trace gases. The most expensive part of pre-injection sequestration technology is CO_2 capture and purification. These costs can be significantly reduced if the flue gas mixtures can be injected into the geologic formation. Limited experimental work has been carried to investigate the changes that occur due to the introduction of these trace gases into the geochemical repository. Hence this experimental study contributes to understanding the effects of injecting CO_2 and the co-contaminant gases to reduce sequestration costs.

These experiments were also performed using the same experimental setup as described in Figure 28. A

90% CO_2 and a 10% SO_2 gas mixture provided by AIRGAS was used for these experiments. The results of these experiments were provided in the UC3 topical report. The solubility of NH_3 in the brine at the temperature and pressure of interest was calculated and was added to the autoclave.

The five experiments in this set were terminated at 14, 28 and 37 days, respectively with the experiments for 14 and 37 days being repeated for consistency. The rock was equilibrated with brine for a period of 36 days at the reaction temperature of 100^0C and then the gas was injected into the system. Comparison of the XRD analysis of the reacted sample after 37 days with the initial rock composition is shown in Figure 50. The XRD patterns show a nearly uniform distribution of the primary minerals in the host rock.

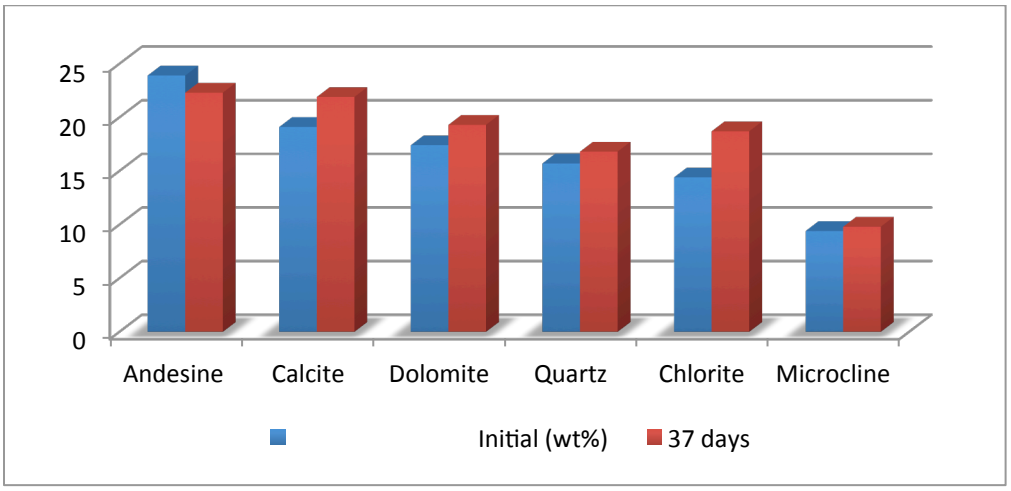

Figure 50. XRD analyses of initial and reacted samples in brines containing CO_2+NH_3.

In these experiments pH increased because of the presence of ammonia. This pH increase facilitates the precipitation of secondary carbonates. Calcite increases after 37 days, as does dolomite. These changes are interpreted on some precipitation and dolomotization reactions. The feldspars undergo dissolution in the initial stages of the experiment before their concentrations stabilize.

The reacted sample is characterized by the growth of ammonium zeolite as circular crystals (Figure 51). Zeolites are very commonly produced in reactions involving alkaline groundwaters.

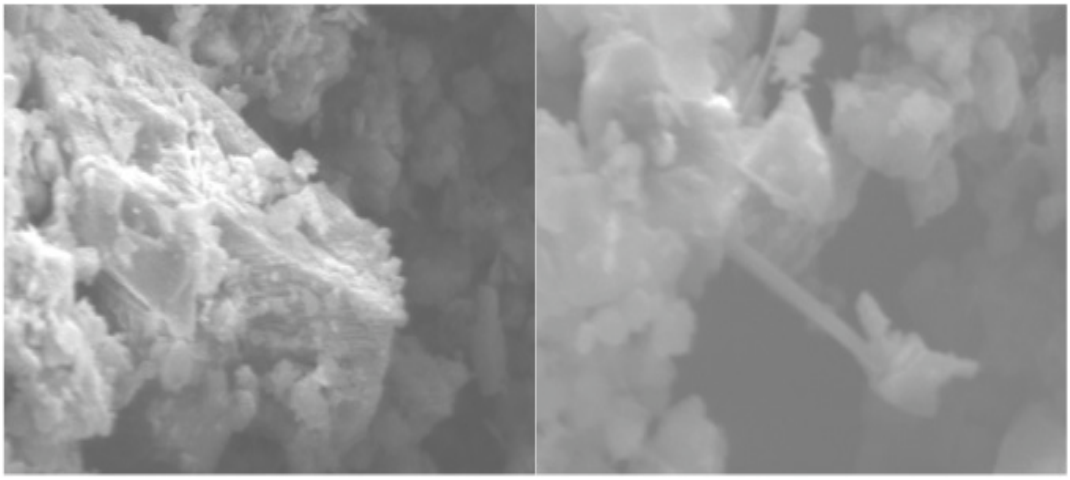

Figure 51. SEM images showing calcite in the initial samples (left) and an ammonium zeolite in the reacted sample (right) after 14 days.

Calcite growth is also observed in layers in the reacted samples after 37 days (Figure 52). This calcite can be from the carbonation of feldspar, a secondary precipitation reaction in alkaline environment.

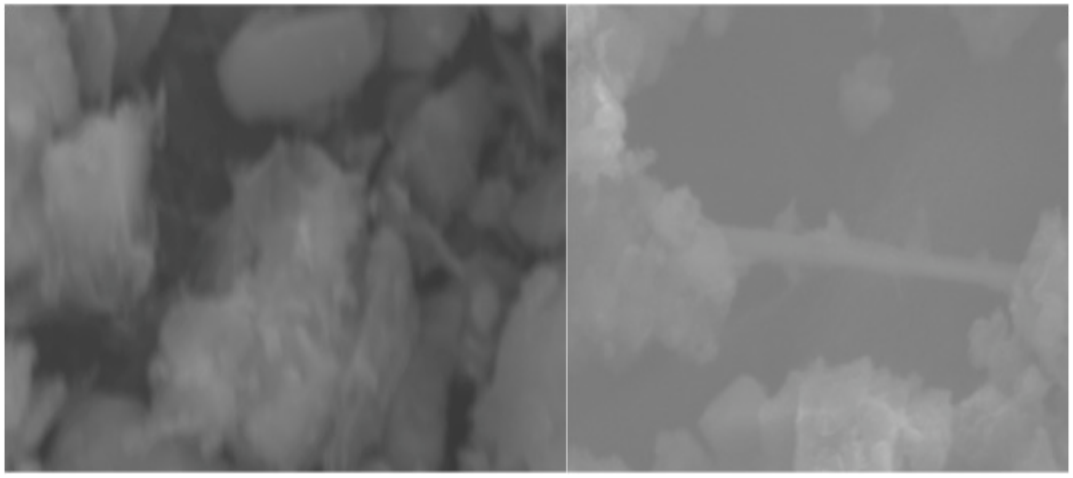

Figure 52. SEM images showing layers of calcite in the reacted samples and Ammonium zeolite in the reacted samples after 37 days.

Figure 53 shows the trend of Ca, K, Al and Si in the brine, with plagioclase feldspar and microcline being the primary alumino silicates in the initial mineral matrix and calcite and dolomite being the primary carbonate minerals. The decrease in Al suggests its precipitation in a solid phase, possibly as kaolinite. The Ca and Mg concentrations increase initially and then decrease, suggesting the precipitation of calcite and (or) dolomite.

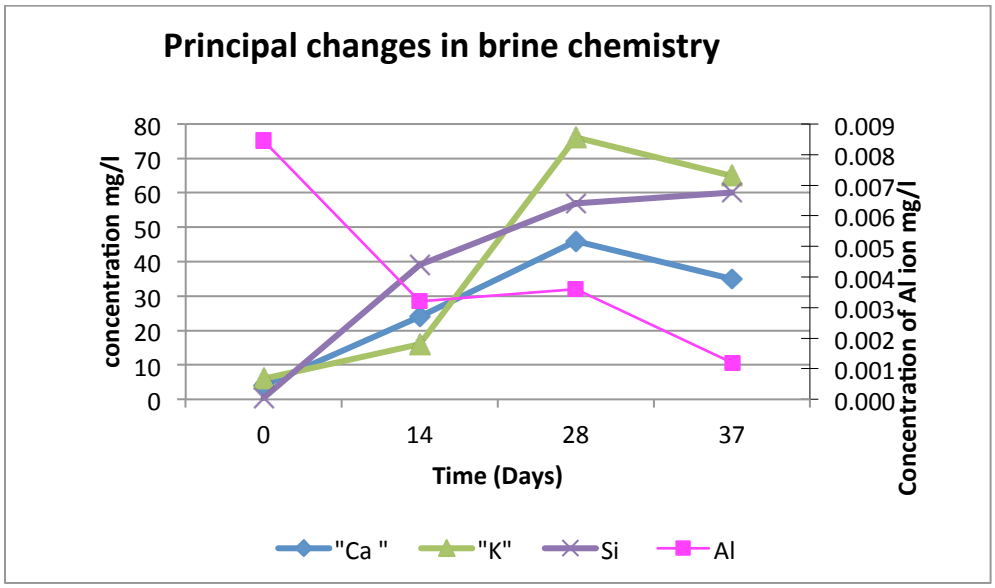

Figure 53. Changes in brine chemistry in CO_2+NH_3 experiments.

Effect of Brine to rock (B/R) ratio

To evaluate the effect of the brine to rock ratio (B/R) three different ratios of 10:1, 10.5:1 and 15.5:1 were employed. Zerai et al., (2006) carried out geochemical simulations using GWB to evaluate the effect of brine to rock ratios on the sequestration reactions and found that an increase in the brine to rock ratio increases the amount of CO_2 that is sequestered. This experimental study tests this conclusion. Brine to rock ratio governs the amount of rock in contact with the brine which indirectly effects the total reactive surface area of the geochemical system. Hence this study will be helpful in evaluating the extent of precipitation or dissolution (mineralization reactions in geological environments) with three brine to rock ratios.

The brine samples were prepared with the same brine shown in Table 2. Arkose was selected as the reacting material. The brine to rock ratio was varied by changing the amount of water used to prepare the brine and the quantity of rock was maintained at 3g (0.5 g of each constituent in the arkose). Experiments were carried out for 64 days with samples collected at 14, 32 and 47 days. CO_2 was used as a feed gas for all these experiments.

Figure 54 compares the three B/R ratios after 64 days. As the B/R ratio increases the dissolution of feldspars and carbonates increases. This can be attributed to more rock to fluid contact area, which enables enhanced reactive surface areas for these dissolution reactions. Chlorite exhibits a reverse trend, because as the B/R ratio increases, the osmotic barrier for the cation exchange between the clay and the brine increases, which inhibits the clay dissolution rates.

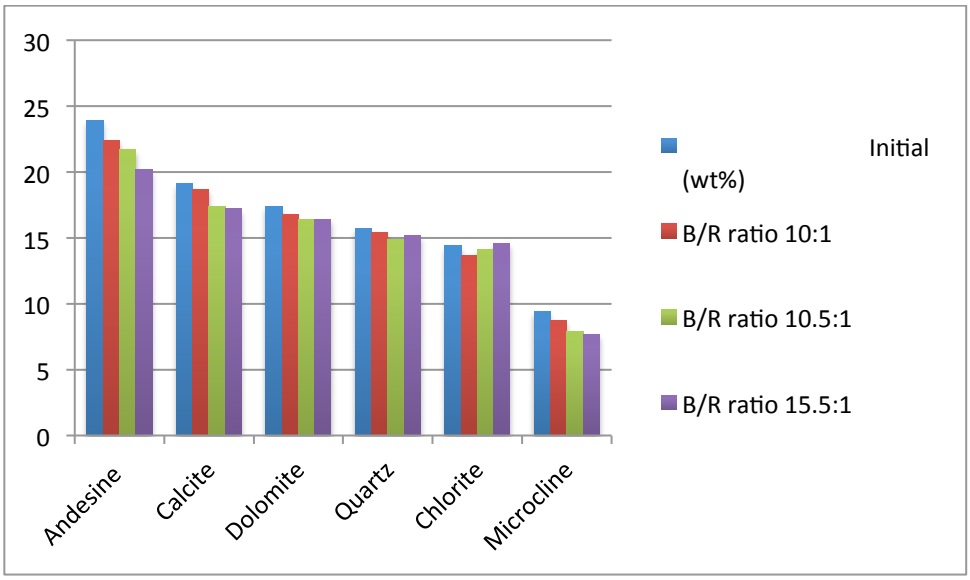

Figure 54. Quantitative XRD analysis of arkose for 3 B/R ratios after 64 days.

Figure 55 and Figure 56 show the concentrations of Ca and Mg in the brine through the duration of the experiments. These changes can be correlated with changes in rock chemistry. Calcite and dolomite dissolution rates increase with the increase in B/R ratio. Hence the concentrations of Ca and Mg also increase in the brine with increasing B/R ratio.

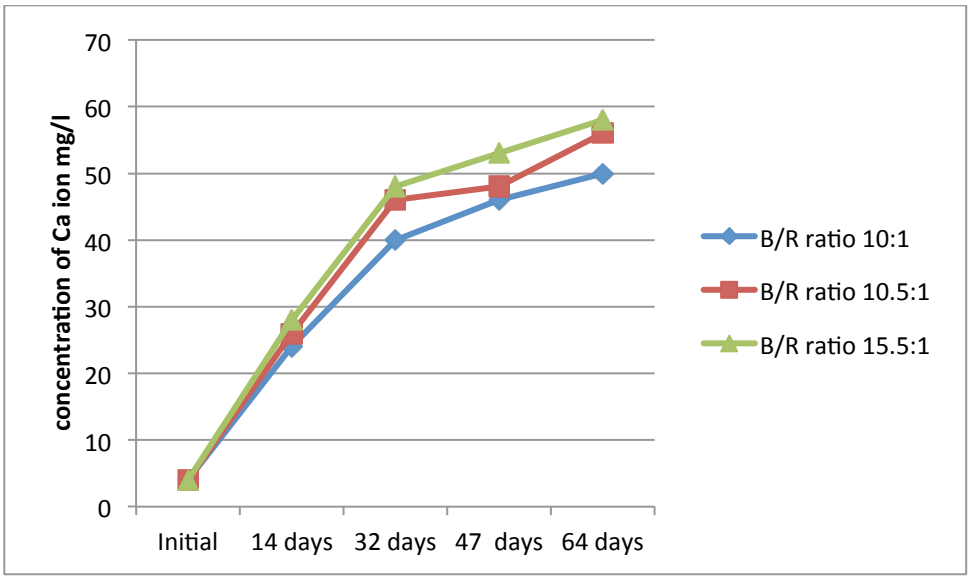

Figure 55. Ca concentration for three B/R ratios.

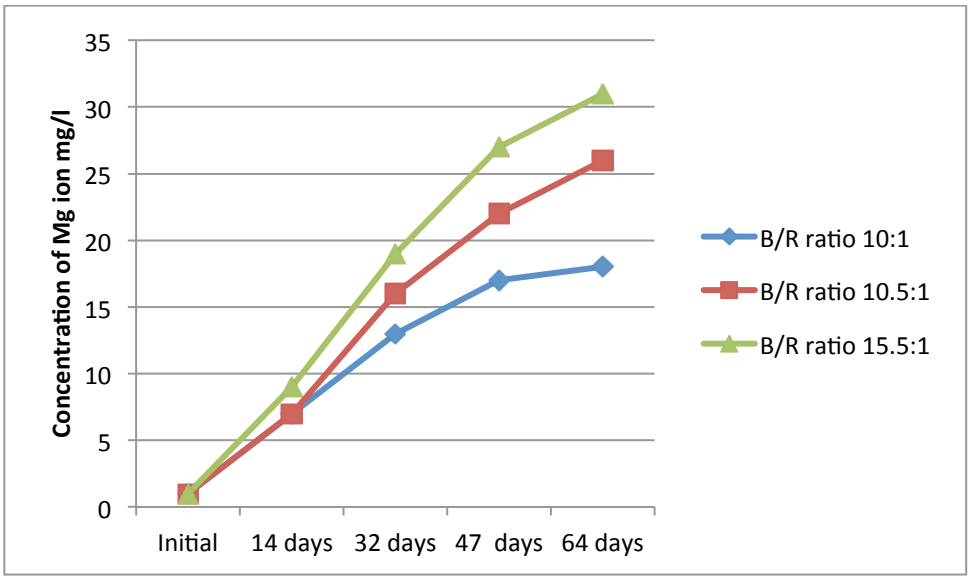

Figure 56. Mg concentration for three B/R ratios.

Mineral stability diagrams

This class of diagrams shows the relationship between mineral stabilities and the predominance of aqueous species. Species activity, gas fugacity, activity or fugacity ratio, pH, Eh, or pE may serve as an axis variable. These stability diagrams were plotted using Act2, a program that calculates and plots activity-activity diagrams. These diagrams are useful for determining he stability regimes in the experiments and for evaluating the reaction mechanisms for minerals of interest.

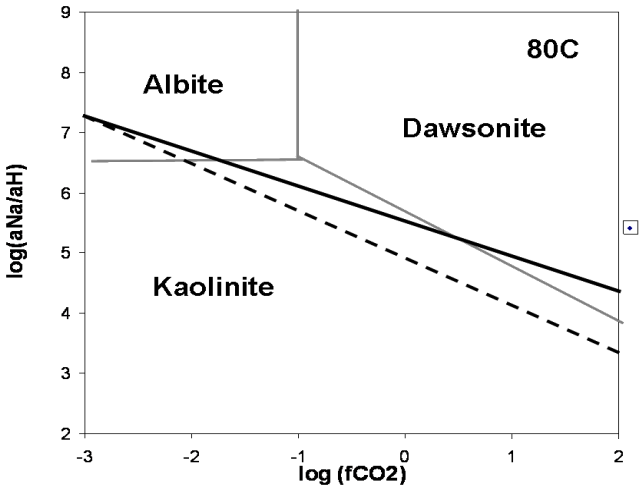

Figure 57. Log fugacity-activity diagram depicting mineral stability fields in the system Na_2O Al_2O_3 SiO_2 CO_2 H_2O at 80 °C. The dashed line was computed by equilibrating the formation water with varying CO_2 fugacities, whereas the solid line was computed by equilibrating seawater with calcite. (Hellevang et al. 2005).

Hellevang et al. (2005) calculated the relative stability of dawsonite with respect to other Na and Al bearing phases using logarithmic activity-fugacity diagrams such as those illustrated in Figure 57. The relationships presented in this figure illustrate phase relations in the system Na_2O Al_2O_3 SiO_2 CO_2 H_2O balanced on aluminum and with SiO_2 activity fixed by quartz saturation. The solid lines in this activity diagram represent fluid compositions in equilibrium with the two minerals adjoining these lines and are computed from the law of mass action for reactions among these minerals. For example, equilibrium between albite and dawsonite can be represented by

$NaAlSi_3O8 + H_2O + CO_2(aq) \leftrightarrow NaAl(OH)_2CO_3 + 3SiO_2(aq)$
(Albite) (Dawsonite) (quartz)

Increasing CO_2 fugacity in this system leads to calcite dissolution and consumption of some aqueous CO_2. At 40°C, dawsonite is stable in this fluid at all CO_2 fugacities greater than 0.1. At higher temperatures, higher CO_2 fugacities are required to stabilize dawsonite. At 80°C, dawsonite stability requires a CO_2 fugacity of approximately 6.3, corresponding to a partial pressure of 10 bars. The stability of dawsonite at elevated CO_2 pressures has led numerous scientists to propose dawsonite as a potential long-term CO_2 storage host, particularly in divalent-cation-poor sedimentary basins. In contrast, as injected CO_2 gas disperses, dissolves in, or leaks from the sequestrating formation following its injection, CO_2 fugacity would decrease, potentially destabilizing dawsonite relative to aluminosilicate phases. Thus the formation regimes of many minerals can be determined and the dissolution rates of the ephemeral phases can be calculated by laboratory measurements to be used as input for different geochemical calculations.

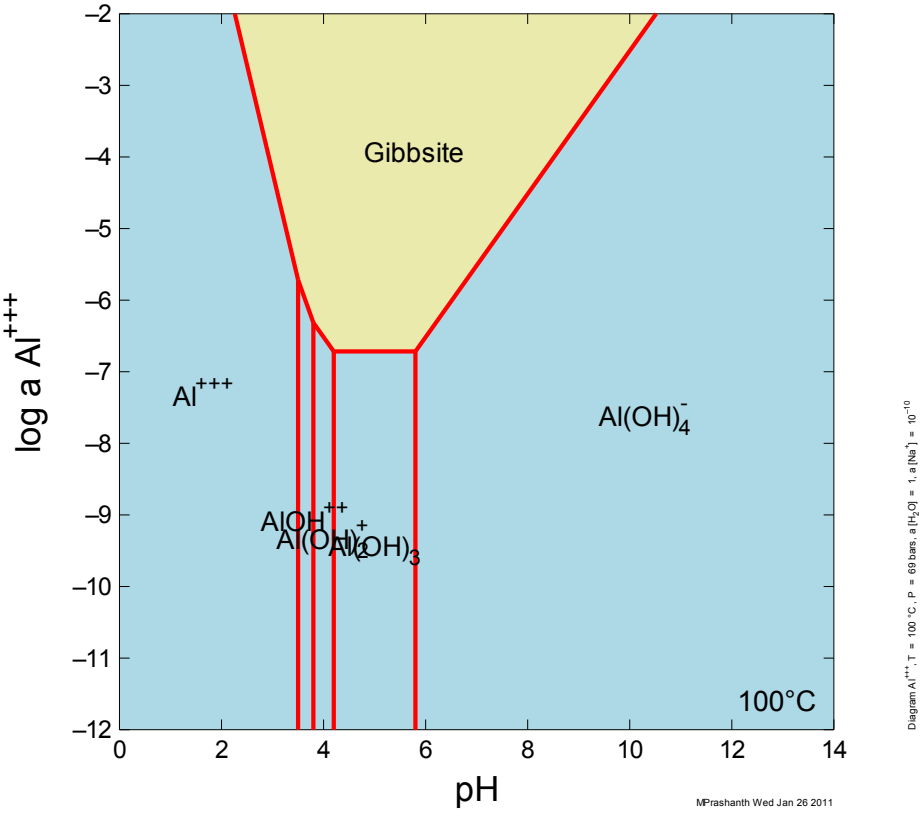

Figure 58. Stability regimes of different aluminum hydroxide species as a function of pH and activity of aluminum ion.

The solubility of aluminum hydroxide is complicated by the fact that dissolved aluminum can exist in several forms in solution. In the absence of other ligands, the most important are Al^{3+} and its hydrolyzed forms $Al(OH)_2$+, $Al(OH)^{2+}$, $Al(OH)_3$ and $Al(OH)_4^-$. The activity of Al^{3+} in equilibrium with gibbsite is given by

$$Al(OH)_3 + 3H^+ \rightarrow Al^{3+} + 3\ H_2O$$

The presence of feldspars (aluminosilicates) in arkose makes it necessary to identify the stable forms of aluminum in the solution in our experiments. The carbonation reactions of feldspars usually yield kaolinite, which is a stable mineral at high activities of H_4SiO_4 like those in our experiments ($10^{-4.4}$ at 100^0C). It is impossible to determine whether or not a particular solution is in equilibrium with kaolinite or any other mineral without knowing the dissolved aluminum concentration. Hence the activity diagram shown in Figure 58 provides an understanding of the stability regimes and the stable minerals like kaolinite at a known pH and Al^{3+} ion activity.

Another important system is that of K_2O Al_2O3 -SiO_2 -CO_2 -H_2O. Mineral pairs in this system include

$2KAl_3Si_3O_{10}(OH)_2 + 2\ H^+ + 3H_2O \leftrightarrow 3\ Al_2Si_2O_5(OH)_4 + 2\ K^+$
(muscovite) (kaolinite)

$2KAlSi_3O_8 + 2\ H^+ + 9\ H_2O \leftrightarrow Al_2Si_2O_5(OH)_4 + 2\ K_+ + 4H_4SiO_4$
(K-feldspar) (kaolinite)

$3\ KAlSi_3O_8 + 2\ H^+ + 12\ H_2O \leftrightarrow KAl_3Si_3O_{10}(OH)_2 + 2\ K^+ + 6\ H_4SiO_4$
(K-feldspar) (muscovite)

$KAl_3Si_3O_{10}(OH)_2 + 2\ H^+ + 12\ H_2O \leftrightarrow 3\ Al(OH)_3 + K^+ + 3\ H_4SiO_4$
(K-feldspar) (gibbsite)

The mineral stability diagram for these reactions is displayed in Figure 59 with the slopes of the lines determined by the stoichiometry of the equations.

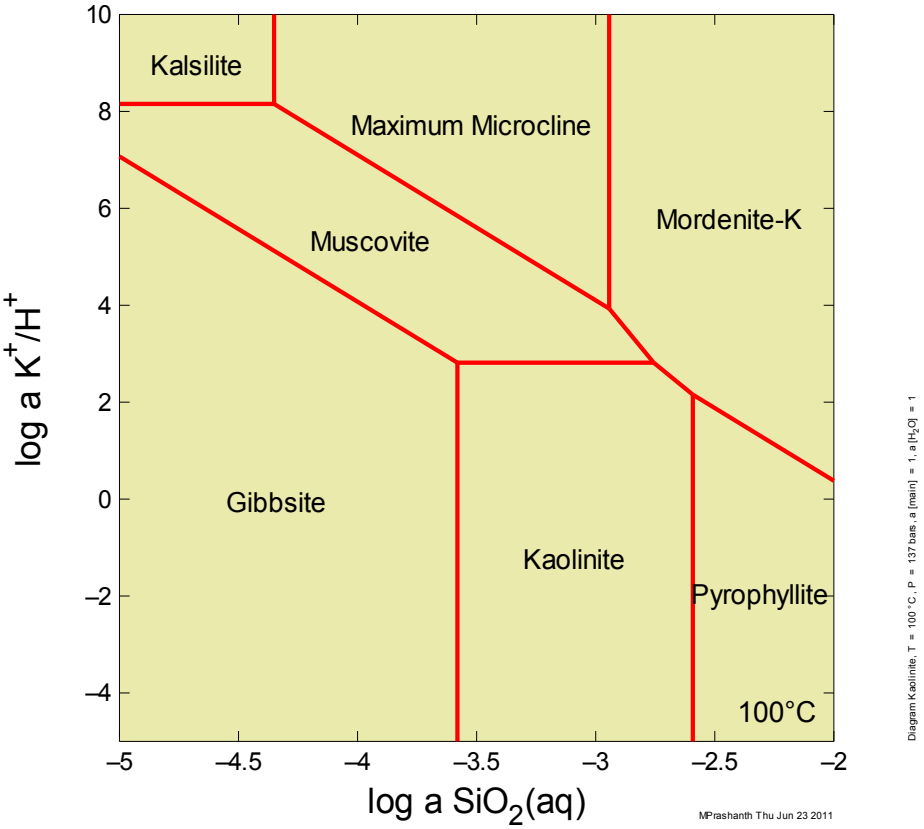

Figure 59. Stability relationships among some minerals in the system K_2O-Al_2O_3 -SiO_2 -CO_2 -H_2O at 100^0C.

The area kaolinite represents the solution composition in which kaolinite is the most stable of the minerals considered in constructing the diagram. It is conceivable that a mineral exists that would be more stable than kaolinite over part of the kaolinite field. The minerals used in these diagrams are the most common forms in natural environments. In our experiments with arkose, the log SiO_2 is around -3.37 and log aK+/H+ is around 0.9. This indicates that the most stable form of alumino silicate mineral in the system is kaolinite.

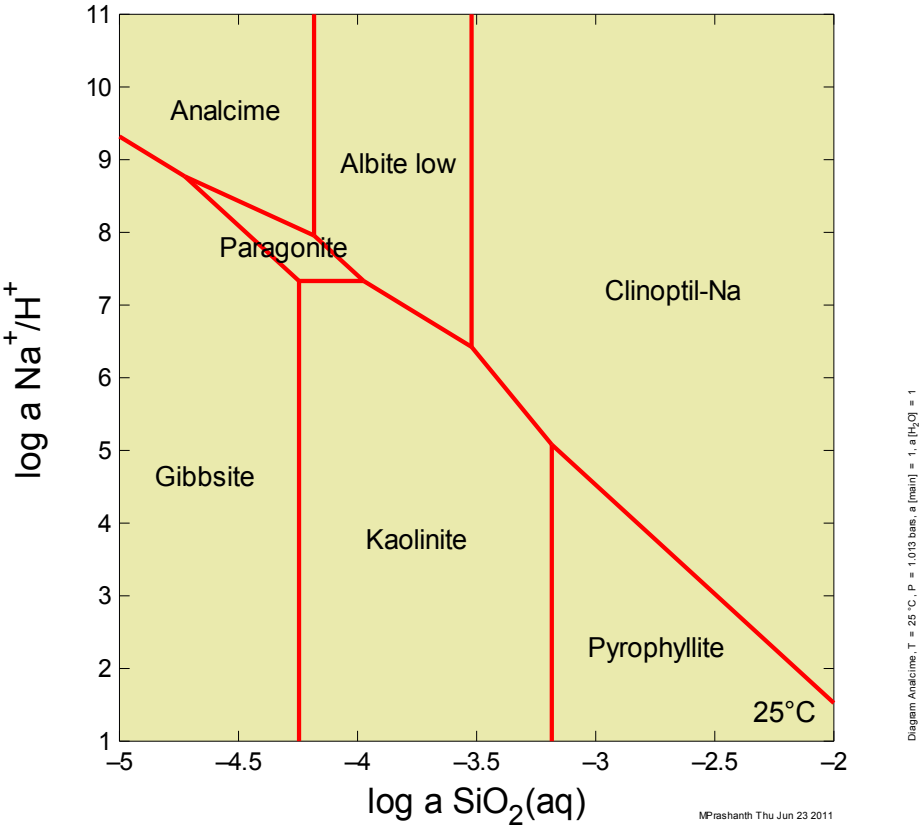

Figure 60. Stability relation ships among some minerals in the system Na_2O Al_2O_3 -SiO_2 -H_2O at 100 C.

Analogous stability diagrams can be constructed for system Na_2O Al_2O_3 -SiO_2 - H_2O. Na bearing feldspars like albite are an important source of cations required for secondary precipitation reactions of carbonates (Figure 60). Hence identification of stable phases in these environments is very important. Again for our experiments the most important stable aluminosilicate phase is kaolinite, which is the primary product in dissolution of orthoclase feldspar.

Modeling sequestration experiments

A batch geochemical model was developed using GWB version 7.0. The initial brine chemistry used for these models was identical to the brine used for experiments and described in Table 2. The temperature was assumed to be isothermal at 100^0C for all the simulations. The kinetic parameters and the parameter set used for the model are described in Table 10 and Table 9, respectively.

Table 9. Parameters used for simulation.

Parameters used	Description
Temperature	100^0C
CO_2	Dissolved in brine
Activity coefficient	B Dot equation
Reactive surface area	Table 4.2
Kinetic rate constants	Table 4.2
Fugacity coefficient	Based on Duan and Sun algorithm
CO_2 fugacity	113.08 bar

Table 10. Kinetic parameters for the simulations (Gaus et al. 2005).

Mineral	**Surface Area Cm^2/g**	**kinetic rate constant mol/cm^2sec**
Calcite	711	3.16E-14
Dolomite	635	4.17E-12
Quartz	686	1.86E-16
Chlorite	1130	2.34E-16
Microcline	720	1.60E-13
Andesine	637	1.80E-13

The following cases are discussed in the sections to follow

1. Arkose as the host rock and CO_2 as the feed gas
2. Arkose as the host rock and CO_2 + SO_2 as the feed gas
3. Limestone as the host rock and CO_2 as the feed gas
4. Sandstone as the host rock and CO_2 as the feed gas
5. Peridotite as the host rock and CO_2 as the feed gas

Degassing simulations

One of the main objectives of this study is to compare the experimental results with the results generated from the geochemical model in the GWB. Brine chemistry is used as the comparison parameter for the modeling and the experimental results. The rock chemistry was also quantified in the experiments using XRD. However, the intermediate (new) minerals precipitated could not be quantified since very small amounts of precipitates were detected and their composition was well within the range of uncertainty for XRD measurements.

All the experimental analyses were carried out at ambient conditions after the reactor was depressurized. This degassing process would lead to numerous retrograde reactions and also long-term quenching reactions. Several changes take place during this process like the change in the pH of the system because of a decrease in f_{CO2}, change in the saturation states of the minerals in the brine, spontaneous dissolution and precipitation of new phases. In order to compare the experimental results with the modeling a correction factor need to be introduced for this degassing process. Using the sliding fugacity module in GWB we can predict the changes that this change in f_{CO2} would introduce into the system. Following is the procedure that is followed for these simulations.

- The final output at the end of a particular time interval from the geochemical model is the input as the initial basis for the degassing simulation.
- The change in the concentrations of the principal ions is calculated and catalogued.
- The behavior of principal ions with their respective minerals in the event of a sudden decrease in f_{CO2} is used as a basis for calculating the in-situ elemental composition of the ion in the fluid.
- This concentration is then marked on the same plot as the modeling results.
- The concentrations of all the principal ions at the time intervals of degassing are calculated similarly and plotted.

Experiments with CO_2+Arkose

Arkose was reacted with CO_2 and brine (Table 2) at 100^0C and 2000 psi. The initial dissolution and re-precipitation of calcite and the precipitation of analcime were the key features in this experiment. The degassing simulations were conducted with the procedure mentioned above, and the experimental results were corrected for degassing. The model captured the initial increase in the Ca, which occurs due to the dissolution of the carbonate minerals calcite and dolomite and also the dissolution of plagioclase feldspar (Figure 61).

The Ca concentration was found to decrease in the latter stages of the reaction as seen in the experiments, which led to the precipitation of calcite. In spite of the degassing correction, there is a difference of about an order of magnitude for this case. The Mg concentrations increased due to dissolution of dolomite in the initial stages of the experiment. It should also be noted that the dissolution rate of dolomite is significantly higher (two orders of magnitude greater than calcite), which could have led to the immediate dissolution of dolomite. There was a very good agreement between the experimental and simulated values for Mg. K concentrations increased through out the experiment in response to the dissolution microcline. There was excellent agreement between the experimental and modeling concentrations for K. Fe concentration decreases rapidly in the latter stages because of the precipitation of iron carbonates like (Ankerite or siderite). Figure 62 shows the precipitation of analcime in the solid phase in the model.

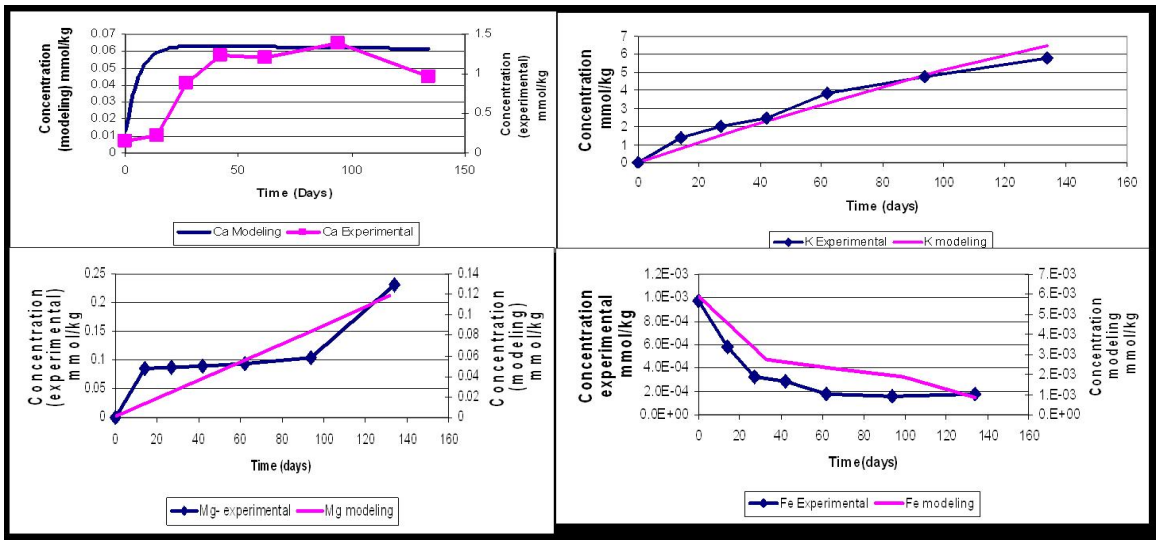

Figure 61. Comparison of experimental and modeling results for arkose + CO_2.

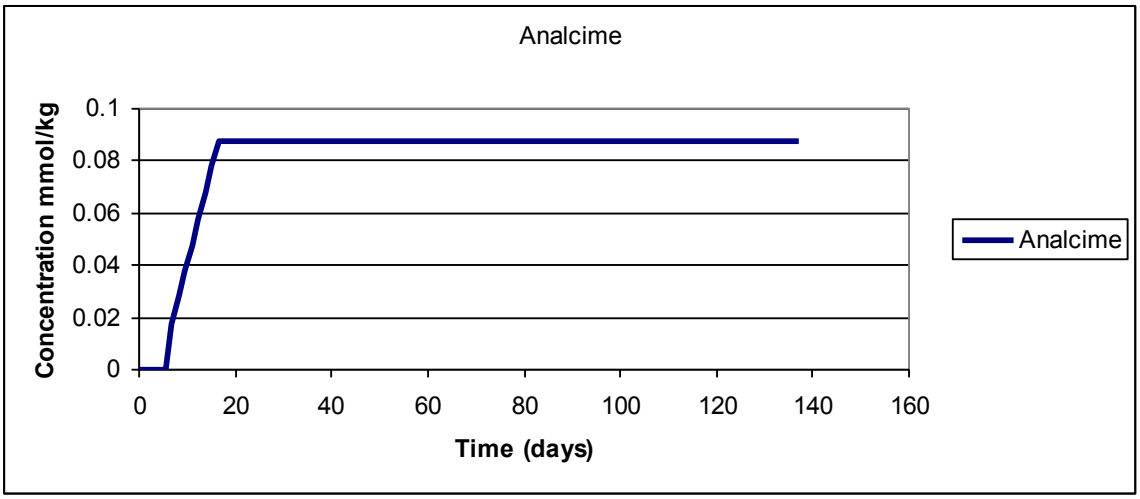

Figure 62. Precipitation of analcime in the model.

Experiments with CO_2+ SO_2Arkose

Arkose was reacted with 90% CO_2 and 10% SO_2 and brine (Table 1) at 100^{0}C and 2000 psi. Pronounced dissolution of all the minerals in the host rock and precipitation of anhydrite and kaolinite were the key features in this experiment. The degassing simulations were conducted with the procedure mentioned above and the experimental results were corrected for degassing. Figure 63 and Figure 64 show the output of the model for this case in both aqueous phase and solid phase.

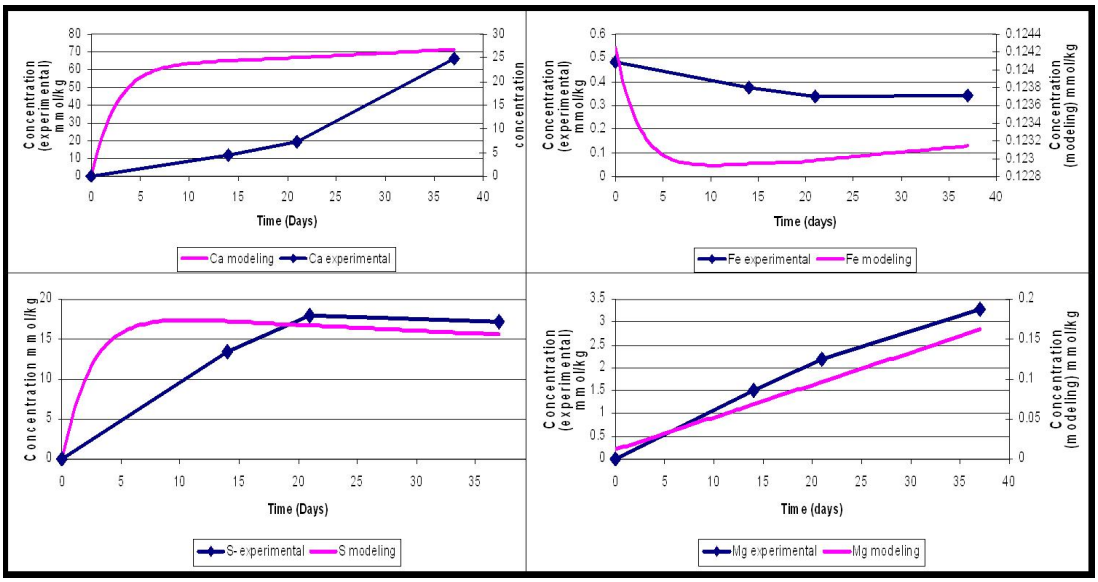

Figure 63. Comparison of experimental and modeling results for arkose $+CO_2$ $+SO_2$.

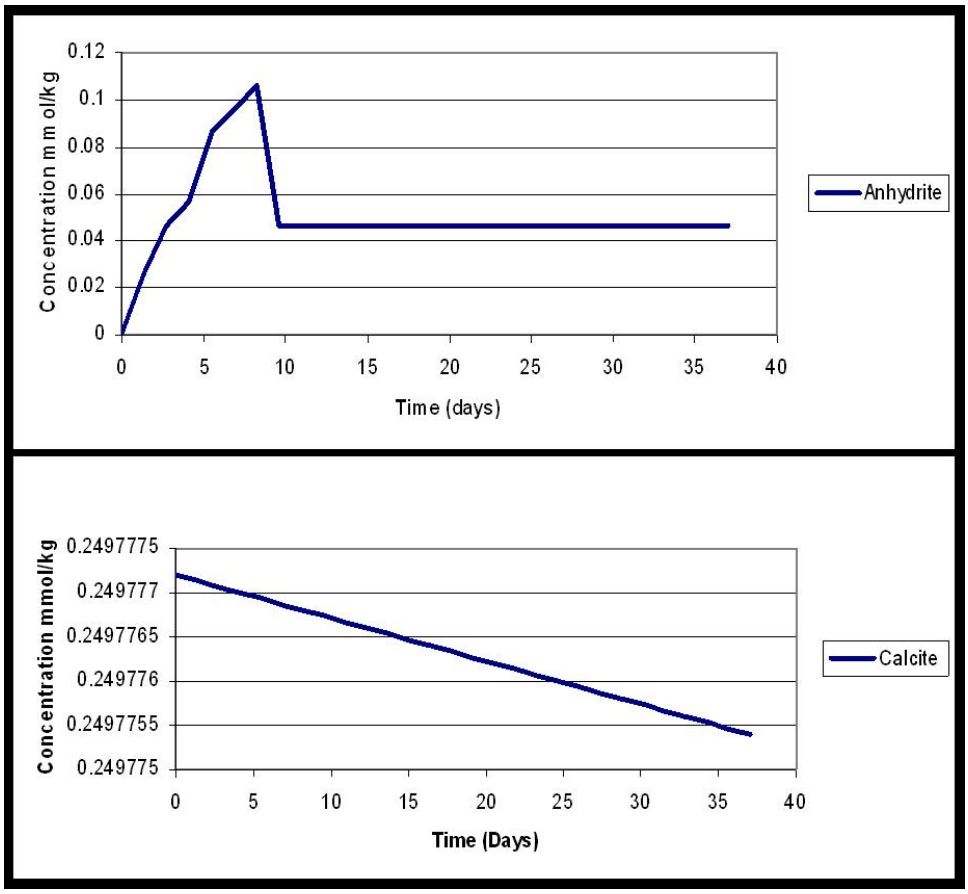

Figure 64. Precipitation of anhydrite and pronounced dissolution of calcite in the model.

In the model, the Ca ion concentration increases due to the dissolution of calcite and dolomite and also the silicate dissolution plagioclase feldspar. In this case the dissolution rate is fast due to the acidity of the brine (presence of SO_2 in the gas stream). There is good agreement between the simulations and the experimental results for Ca. The Mg concentrations increased in the experiment, and this increase is greater than that of Ca. This supports the "dolomotization of calcite" mechanism by Rosenbauer et al., (2005), brines with high sulfate concentrations. K ion concentration increases and continues to increase because of the dissolution of microcline. In the experiment the Al-bearing mineral kaolinite was found in trace amounts. Fe concentrations decreased, consistent with the experimental observations. Its decrease can be attributed to of the ankerite or siderite. The S concentrations increased in the initial stages of the experiment, but in the latter stages of the experiment S decreased because of the precipitation of anhydrite, gypsum or bassanite. These observations are consistent with the experimental results. Degassing corrections reduced the error to very acceptable value for geochemical simulations. The agreement in the sulfur ion concentration was very good because the only source of sulfur in the brine is the feed gas, whereas Ca in the brine can come from calcite, dolomite or plagioclase feldspar. The behavior of these minerals when f_{CO2} decreases is different. Hence when the correction factor is calculated, it leads to a marginally larger error in the case of cations, which are contributed by multiple minerals. Figure 25 shows the precipitation of anhydrite and dissolution of calcite in the experiments. Anhydrite is seen as euhedral crystals growing in the pore spaces of primary minerals. There were traces of gypsum and bassanite identified in the XRD analysis but the amount of these precipitates was very small.

Experiments with CO_2+ limestone

Limestone was reacted with CO_2 and brine at 100^0C and 2000 psi. Pronounced dissolution of the host rock was the key feature in this experiment. The degassing simulations were conducted with the procedure mentioned earlier, and the experimental results were corrected for degassing. The Ca concentration is the only comparison parameter used in this case. The agreement between the experimental and modeling values is very good (Figure 65). The Ca concentration increased because of the dissolution of limestone driven by the acidic brine. The absence of cations for secondary precipitation reactions precludes the chance of any mineral sequestration in this case. The rate of increase of Ca decreases with time temporally because the pH of the brine increases with calcite dissolution. But no precipitation reactions were observed in the time scale of this experiment.

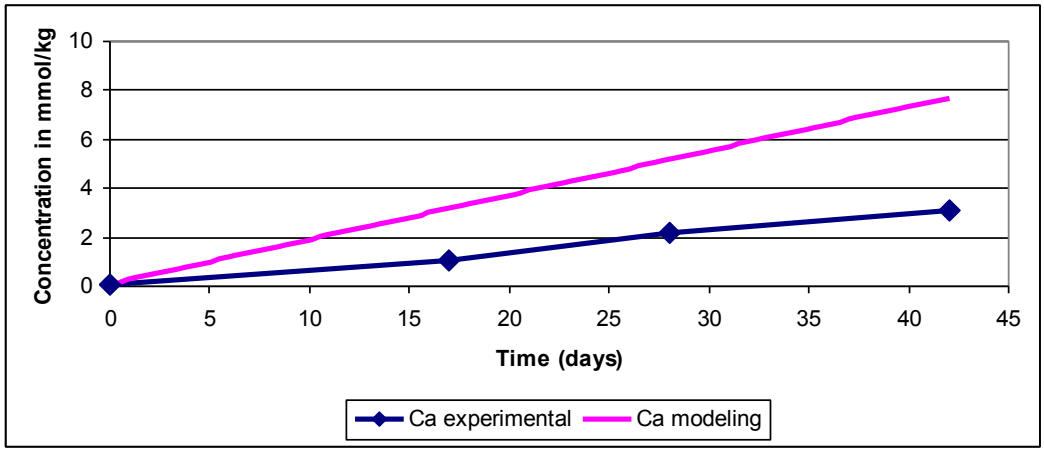

Figure 65. Comparison of experimental and modeling results for limestone experiments.

Experiments with CO_2+ sandstone

Brine chemistry is again chosen as the comparison parameter for this case (Figure 66). Ca concentrations progressively increased due to the dissolution of plagioclase feldspars. The experimental results agree very well with the modeling results. Dissolution of microcline leads to an increase in the K concentration in the brine. Kaolinite precipitation is observed in the experiments. As mentioned earlier, the mineral that is most stable in the activity regime in the experimental conditions is kaolinite. The silica saturation, driven by the dissolution of feldspars is the principal factor governing the mineral that would precipitate in this experiment. The deposition of amorphous silica is an indication of a very high silica activity in these experiments.

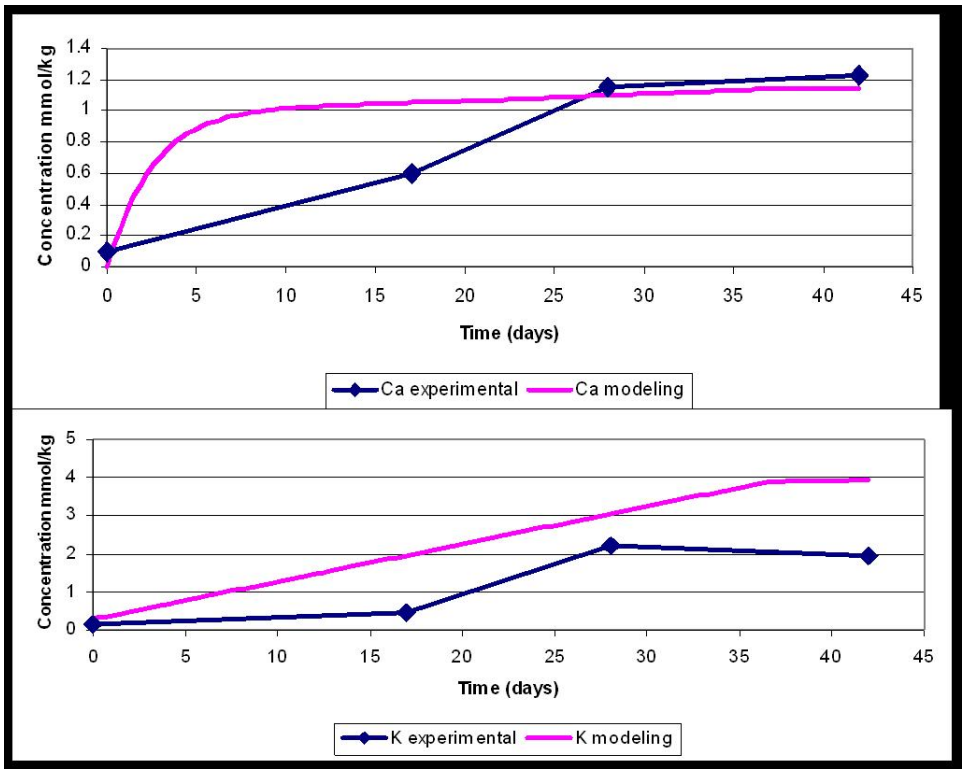

Figure 66. Comparison of experimental and modeling results for the sandstone experiments.

Experiments with CO_2+ peridotite

In the case of calcium, the model captured the increase in Ca, which occurs due to the dissolution of silicate minerals (Figure 67). The Mg ion concentration followed an increasing trend initially indicating dissolution of olivine in the initial stages of the experiment. The decrease in Mg in the latter stages of the experiment is a result of precipitation of magnesite ($MgCO_3$), which is a product of carbonation reactions. The precipitation of magnesite is shown in Figure 68. Due to the presence of excess CO_2 in the reactor, carbonation of olivine dominates the hydration reactions.

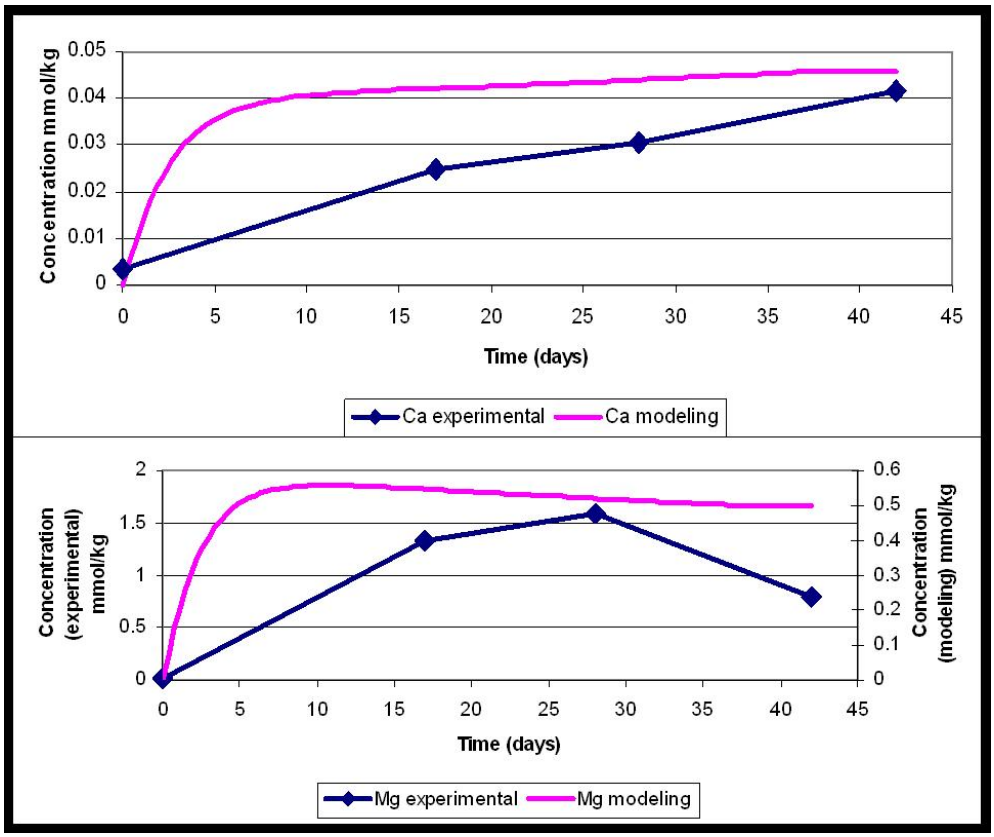

Figure 67. Comparison of experimental and modeling results for peridotite experiments.

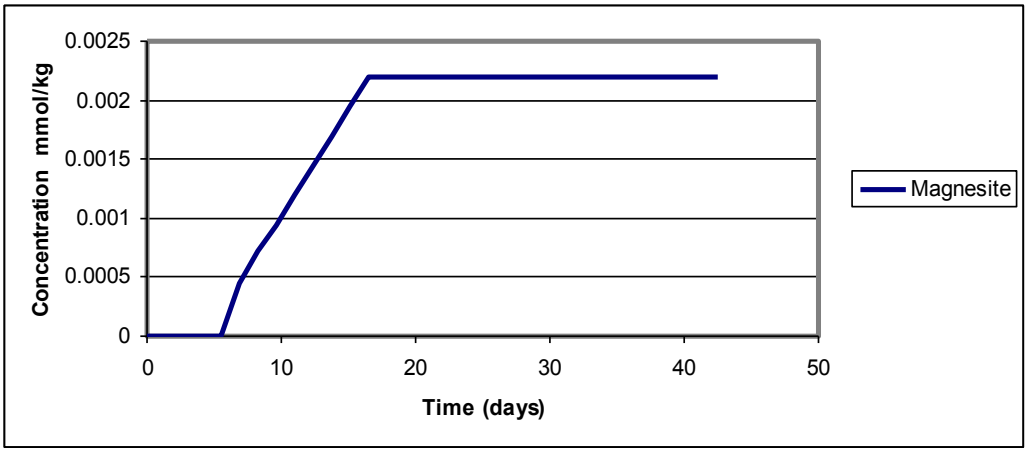

Figure 68. Precipitation of analcime in peridotite experiments.

Summary

This study examined controls on CO_2 mineralization processes by considering different mineral assemblages, limestone, sandstone, peridotite and arkose. The first step in the complex series of reactions in systems containing minerals, brine and CO_2 is CO_2 dissolution in water and subsequent deprotonation reactions. These reactions are shown in Table 11. The resulting carbonate system is highly pH dependent. The precipitation of thermodynamically stable carbonates depends on the pH of the brine in the geological repository. The pH depends on the composition of the rock in the aquifer. It is important to understand this interdependency, since it affects the thermodynamics and kinetics of the entire system.

Table 11. Protonation reactions.

Reaction	Explanation	Equilibrium constant (25ºC)
$CO_{2,g} + H_2O <====> H_2CO_3^*$	Dissolution of CO_2	$pK_H = 1.5$ (at 25ºC)
$H_2CO_3^* <====> HCO_3^- + H^+$	First deprotonation stage	$pK_1 = 6.3$ (at 25ºC)
$HCO_3^- <====> CO_3^{2-} + H^+$	Second deprotonation stage	$pK_2 = 10.3$ (at 25ºC)

As shown in Table 11, carbonate ion formation is favored at high pH. Due to the formation of carbonic acid, initially, the pH of the brine decreases. The bicarbonate and carbon ion formations are favored at much higher pH values, so the pH of the brine needs to increase to facilitate the precipitation of carbonates. This can only be achieved by buffering the brine. Hence the presence of alumino silicates (feldspars in arkose) or magnesium silicates (olivine or serpentine) in the mineral assemblages are necessary for carbonate precipitation. The dissolution rates of these minerals are very sensitive to changes in pH. They undergo fast (near instantaneous) dissolution in acidic environments and hence buffer the brine. In addition to this, these feldspars and magnesium silicates also provide the necessary cations for the carbonate precipitation. The kinetic rates of dissolution of these minerals increase with an increase in temperature, but the dissociation constant of carbonic acid decreases with an increase in temperature. This means that the initially weak carbonic acid will become increasingly weaker at higher temperatures. Zerai et al., (2006) used GWB to simulate the effect of the rock composition on the ultimate fate of CO_2 in the repositories. They reported that in a limestone reservoir continuous dissolution, and the CO_2 will remain in the aqueous phase or as free gas and would not contribute to mineral trapping of CO_2. In contrast it was reported that both sandstone and mixed assemblages (sandstone + carbonate) both accounted for mineral trapping of CO_2. The main minerals for trapping CO_2 are dawsonite and siderite. The precipitation of dawsonite was not observed in these experiments. Hellevang et al. [25] determined that dawsonite was a stable mineral phase only at high fugacities of CO_2 and was an ephemeral phase either converting into albite or other sodium aluminosilicate minerals at lower fugacities. Siderite precipitation was observed in experiments with peridotite. Another iron carbonate ankerite was found in as a precipitated phase in the experiments with arkose.

The behavior of individual minerals is different in a mineral assemblage. For example, let us consider calcite as an individual mineral and calcite in the arkose. The chemical composition of the mineral is the same, but the mineral assemblage it is placed within, plays the governing role in its ultimate fate. In the case of a limestone reservoir, calcite undergoes dissolution releasing Ca ion and CO_3^{2-} or HCO_3^- ion depending on the stage of deprotonation and pH. Thus it traps CO_2 in ionic phase or free gas phase. Hence addition of CO_2 to a carbonate reservoir will increase acidity and dissolve, not precipitate carbonate minerals. In a reservoir where arkose represents the principal mineralogy [26], the initial reactions of calcite are the same. The parallel reactions that take place are the dissolution of feldspars and chlorite. These reactions trigger a sequence of carbonation reactions. The cations added to the brine by the dissolution of feldspars combine with the carbonate or the bicarbonate ions and precipitate, thus bringing about the desired mineral sequestration. Hence the presence of feldspars or magnesium silicate minerals is necessary for mineral sequestration of CO_2.

In sandstone reservoirs the rapid dissolution of the silicate minerals overrides the relatively slow feldspar carbonation reactions, and hence the role of silicates in bringing about mineralization is not realized. The carbonation step in this sequence of reactions is usually the rate-controlling step since silicate dissolution rates are rapid. Silica is also released into the brine because of these dissolution reactions. The brine becomes sufficiently saturated with silica. When the sample is cooled down for analysis, the brine becomes supersaturated with silica at lower temperature. This silica undergoes heterogeneous deposition as amorphous silica on the surface of other host minerals, which was evident in the EDS analysis on all reacted samples.

Mineral stability diagrams are essential to identify the stable phases in the regime of interest in the experiments. The precipitation of dawsonite and its non-occurrence in most of the experimental findings can be adequately explained by the construction of a phase diagram and identifying that dawsonite is a stable phase at high fugacities of CO_2. Similar phase diagrams were constructed for the systems investigated in this study and kaolinite and analcime were identified as the stable aluminosilicate phases in the regime of interest of the experiments.

CONCLUSIONS

Three unique coal pyrolysis reactors have been assembled to realistically simulate pyrolysis under relevant in situ conditions. The FBR system has been demonstrated to give global kinetic data for both coal pyrolysis and gasification. A high-pressure rubblized bed reactor has been fabricated and will be used to study convective heating and subsequent product formation with rubblized beds and at high pressures during the coming year. The coal block reactor has been used to demonstrate unique aspects of heat and mass transfer within coal blocks, suggesting an increased importance of secondary pyrolysis in the global kinetics of pyrolysis at conditions relevant to UCTT.

A comprehensive review of available data on coal in-situ conversion shows it to be a promising technology (summary presented in Table 5). The following summary illustrates relevant design and operating parameters for UCTT.

Targeted Coal Rank: Preferably high volatile bituminous coals.

Conversion Approach: Conduction heating using an externally generated hot gas; or convection heating using an externally generated hot gas; or a combined approach.

Well Orientation: Parallel to the targeted coal seam

Rubblization: Not necessary

Presence of Oxygen: Not necessary and preferably not.

Temperature: The temperatures that favor the formation of different products are:

j. Maximum 600-700°C (1100-1300°F), a temperature range at which the volatile yield approaches an asymptotic value;
k. Coal-bed methane, less than 300°C (570°F);
l. Liquid Products, less than 390°C (730°F);
m. Moisture, less than 400°C (750°F);
n. Methane, 400-500°C (750-930°F);
o. Hydrogen, above 500°C (930°F);
p. Tar, above 400°C (750°F) and peak at 550°C (1020°F);
q. Tar gasification, above 550°C (1020°F);
r. Syngas (H_2+CO), 450-700°C (840-1300°F).

Pressure: The pressure for underground gasification should be maintained below the lithostatic pressure to prevent outleakage of gas and contamination of groundwater. Lithostatic pressures of 3.5MPa to 15-30MPa (500 to thousands of psi) are not uncommon. The effects of pressure on yield are:

c. Liquid products are maximized at low pressure;
d. Gas products are maximized at high pressure;

Heating Sources:

a. Fossil fuel is currently the major energy source for heating;
b. In the future, solar, wind and renewable are possible alternatives;
c. The process can be made self-sufficient in energy by using product gas as the heat source;
d. Heating requirements can be reduced by aggressive heat management, such as using the waste heat in the coal ash product.

Well Orientation: Parallel to the targeted coal seam

Rubblization: Not necessary

Presence of Oxygen: Not necessary and preferably not.

Temperature: The temperatures that favor the formation of different products are:

s. Maximum 600-700°C (1100-1300°F), a temperature range at which the volatile yield approaches an asymptotic value;
t. Coal-bed methane, less than 300°C (570°F);

u. Liquid Products, less than 390°C (730°F);
v. Moisture, less than 400°C (750°F);
w. Methane, 400-500°C (750-930°F);
x. Hydrogen, above 500°C (930°F);
y. Tar, above 400°C (750°F) and peak at 550°C (1020°F);
z. Tar gasification, above 550°C (1020°F);
aa. Syngas (H_2+CO), 450-700°C (840-1300°F).

Pressure: The pressure for underground gasification should be maintained below the lithostatic pressure to prevent outleakage of gas and contamination of groundwater. Lithostatic pressures of 3.5MPa to 15-30MPa (500 to thousands of psi) are not uncommon. The effects of pressure on yield are:

e. Liquid products are maximized at low pressure;
f. Gas products are maximized at high pressure;

Heating Sources:

a. Fossil fuel is currently the major energy source for heating;
b. In the future, solar, wind and renewable are possible alternatives;
c. The process can be made self-sufficient in energy by using product gas as the heat source;
d. Heating requirements can be reduced by aggressive heat management, such as using the waste heat in the coal ash product.

The UCTT simulation subtask focused on developing a simulation tool that captures the relevant physical processes and data from a large-scale UCTT system. By developing a geometry creation strategy for a representative section of a rubblized coal bed, appropriate boundary conditions, and a new solution algorithm to take advantage of the differing time scales, we can obtain a long-term thermal history of the coal particles. The results also indicate the importance of convective heat transfer, which greatly decreases the time required to heat the coal to the production temperature.

The purpose of this sequestration subtask was to analyze the effect of rock and injection gas composition on sequestration reactions experimentally and using simulations. In the case of limestone (carbonate reservoir) the absence of any buffering media results in continuous dissolution. No matter how much CO_2 is added to the system, the precipitation of any new phases is ruled out. In sandstone reservoirs the relative abundance of cations and presence of silicate minerals leads to precipitation of new phases. Carbonation of feldspars and phase alteration of albite lead to precipitation of carbonates and analcime. Kaolin deposition is also evident. The silicate dissolution reactions are much faster, and this overrides the carbonation reactions. In peridotite experiments carbonation of olivine leads to formation of magnesite, which is observed to grow as crystals. In arkose, the relative geochemical complexity leads to chain of series and parallel reactions and complex results. Carbonate growth as calcite is seen in latter stages if the experiment where dissolution patterns of both silicate and carbonate minerals dominate in the earlier stages of the experiment. The growth of analcime and deposition of silica are also observed. These results

are correlated with the brine chemistry in each of the cases, and a comprehensive picture of the geochemical interactions taking place between CO_2-brine and the host rock is provided. A comparison of experimental and modeling results (which has not been reported in the literature yet) has also been presented in this study.

PEER-REVIEWED PUBLICATION

Mandalaparty, P.; Deo, M.; Moore, J. 2011. Gas-Compositional Effects on Mineralogical Reactions in Carbon Dioxide Sequestration. *SPE J*. SPE-124909-PA (in press; posted 15 July 2011).

REFERENCES

Agarwal, A.K. Assessment of Solid Waste Characteristics and Control Technology for Oil Shale Retorting, United States Environmental Protection Agency. 1986, pp. 136–138. EPA 600/1–96–019.

Angelova, G. K.; Minkova, V. N. and Goranova, M. D. Thermal degradation of solid fuels at atmospheric pressure in the presence of steam, *Izvestiya po Khimiya*, 1981, 14, 251-257.

Angelova, G. K. and Minkova, V. N. Pyrolysis of solid fuels in a stream of water vapor: Bulgarian coals and shales, *Khimiya Tverdogo Topliva* (Moscow, Russian Federation), 1986, 3, 94-99.

Anthony, D. B.; Howard, J. B.; Hottel, N. C.; and Meissner, H. P. Rapid Devolatilization of Pulverized Coal, *Proceedings of Combustion Institute*, 1975, 15, 1303.

Avid, B.; Purevsuren, B.; Born, M.; Dugarjav, J.; Davaajav, Ya., and Tuvshinjargal, A. Pyrolysis and TG Analysis of Shivee Ovoo Coal from Mongolia, *Journal of Thermal Analysis and Calorimetry*, 2002, 68, 877-885.

Bartis, James T.; LaTourrette, Tom; Dixon, Lloyd; Peterson, D.J.; Cecchine, Gary Oil ShaleDevelopment in the United States. Prospects and Policy Issues. Prepared for the National Energy Technology Laboratory of the United States Department of Energy, The RAND Corporation. 2005, http://www.rand.org/pubs/monographs/2005/RAND_MG414.pdf.

Bethke C.M. Geochemical Reaction modeling, University press, Newyork, 1998.

Berchenko, I.; et al. In Situ Thermal Processing of An Oil Shale Formation Using A Pattern of Heat Sources, U.S. Patent 6991032 B2, January 31, 2006.

Berry, Kay L.; Hutson, Roy L.; Sterrett, John S.; Knepper, Jay C. Modified In-Situ Retorting Results of Two Field Retorts, *SPE Annual Technical Conference and Exhibition*, 1982. New Orleans: Society of Petroleum Engineers.

Biagini, E. and Tognotti, L. Comparison of Devolatilization/Char Oxidation and Direct Oxidation of Solid Fuels at Low Heating Rate, *Energy and Fuels*, 2006, 20, 986-992.

Brandt, Adam R. Converting Oil Shale to Liquid Fuels: Energy Inputs and Greenhouse Gas Emissions of the Shell in Situ Conversion Process, *Environmental Science and Technology*, 2008, 42, 7489-7495.

Burnham, Alan K. Slow Radio-Frequency Processing of Large Oil Shale Volumes to Produce Petroleum-like Shale Oil, Lawrence Livermore National Laboratory, 2003, UCRL-ID-155045.

Burnham, Alan K.; McConaghy, James R. Comparison of the acceptability of various oil shale processes, *26th Oil shale symposium*, Golden, Colorado, 2006, UCRL-CONF-226717.

Businessweek, Bringing good things to sunlight, October 11th, 2010.

Calderon, Albert; Laubis, Terry J. Method for recovering energy in-situ from underground resources and upgrading such energy resources above ground, Can. Pat. Appl. 2010. CA 2666145 A1 20100903.

Campbell, J.H. Pyrolysis of subbituminous coal in relation to in-situ coal gasification, *Fuel*, 1978, 57, 217-224.

Carlson, R. D.; Blase, E. F.; McLendon, T. R. Development of the IIT Research Institute RF heating process for in situ oil shale/tar sand fuel extraction–an overview. *14th Oil Shale Symposium Proceedings*, 1981, (Golden, Colorado: Colorado School of Mines): 138–145.

Cha, Z. The Linde Group, personal communication, 2010.

Chemical & Engineering News, Chemistry Energizes China, v88(40), pp 10-16, October 4, 2010.

Chen, Haokan; Li, Baoqing; Zhang, Bijiang Effects of mineral matter on products and sulfur distributions in hydropyrolysis, *Fuel*, 1999, 78, 713-719.

Chevron USA, Inc. Oil Shale Research, Development & Demonstraction Project. Plan of Operation, 2006.

Christsora, C. T.; Muhlen, H. J.; van Heek, K. H.; Juntgen, H. The Influence of Pyrolysis Conditions on the Reactivity of Char in H2O, *Fuel Processing Technology*, 1987, 15, 17.

Colorado Division of Reclamation and Mining Safety, Department of Natural Resources Designated Mining Operation Reclamation Permit Application, for the Shell Frontier Oil and Gas, Inc., Oil Shale Test Project, Denver, CO, 2007.

Covell, J.R., Fahy, J.L., Schreiber, J., Sudduth, B.C., and Trudell, L. Indirect In Situ Retorting of Oil Shale Using the TREE Process, *17th Oil Shale Symposium*, 1984, Golden, Colorado: Colorado School of Mines, CONF-8404121.

Crawford, Peter M.; Biglarbigi, Khosrow; Dammer, Anton R.; Knaus, Emily Advances in World Oil Shale Production Technologies, *2008 SPE Annual Technical Conference and Exhibition*, Denver, Colorado.

Cypres, R. and Furfari, S. Low-Temperature Hydropyrolysis of Coal under Pressure of H_2-CH_4 mixtures, *Fuel*, 1982, 61, 721-724.

Duan, Z.; Sun, R. An improved model calculating CO2 solubility in pure water and aqueous NaCl solutions from 273 to 533 K and from 0 to 2000 bar. *Chem. Geol*. 193, 257–271, 2003.

E.G.L. Resources, Inc. Plan of Operation for Oil Shale Research, Development and Demonstration (R,D/D) Tract, Submitted to Bureau of Land Management, 2006.

Earth Search Sciences, Inc. General Synfuels International Announces Formation Of Technology Fund For Oil Shale Development. Press release, 2010. http://www.earthsearch.com/general-synfuels-international-announces-formation-of-technology-fund-for-oil-shale-development-2/.

Farage, D. L.; Williford, C. W., Jr.; and Clemmer, J. E. Pyrolysis of Mississippi Lignite in a Fixed Bed, *Fuel Processing Technology*, 1987, 16, 35-43.

Gaus I.; Azaroual, M.; Czernichowski-Lauriol I. Reactive transport modeling of the impact of CO2 injection on the clayey cap rock at Sleipner (North Sea), *Chem Geol* (217) 319-337, 2005.

Global Resource Corp. Global Resource Reports Progress on Oil Shale Conversion Process, Press release, 2007. http://www.downstreamtoday.com/news/article.aspx?a_id=1943.

Graff, R. A.; and Brandes, S. D. Coal liquefaction by steam pyrolysis, *Preprints of Papers -American Chemical Society*, Division of Fuel Chemistry, 1984, 29(2), 104-111.

Green Car Congress Chevron and Los Alamos Jointly Research Oil Shale Hydrocarbon Recovery, 2006, http://www.greencarcongress.com/2006/09/chevron_and_los.html

Green Car Congress General Synfuels to Test In-Situ Oil Shale Gasification Technology in Wyoming and Colorado, 2009, http://www.greencarcongress.com/2009/05/gsi-sha-20090503.html.

Halliburton, Halliburton Hydraulic Fracturing, Over 60 Years of Successful Performance Focused on the Environment, 2008, http://www.halliburton.com/public/pe/contents/Data_Sheets/web/H/H06640.pdf

He, Y. G. Mining and utilization of Chinese Fushun oil shale, *Oil Shale*, 2004, 21(3), 259-264.

Hellevang, H.; Aagaard, P.; Oelkers, E.H.; Kvamme, B. Can dawsonite permanently trap CO_2? *Evniron. Sci.Technol*. 2005, 39, 8281-8287.

Howard, J.B. Fundamentals of coal pyrolysis and hydropyrolysis. *Chemistry of Coal Utilization.* 1981, 2nd Supl. Vol, 665-784.

Hulsebos, J.; Pohani, B.P.; Moore, R.E.; Zahradnik, R.L. Modified-In-Situ Technology Combined with Aboveground Retorting and Circulating Fluid Bed Combustors Could Offer a Viable Method to Unlock Oil Shale Reserves in the Near Future, *21st Oil Shale Symposium*, Golden, Colorado: Colorado School of Mines, 1988, p440-447.

Johnson, H.R.; Crawford, Peter M.; Bunger, James W. Strategic significance of America's oil shale resource. Volume II: Oil shale resources, technology and economics, Office of Deputy Assistant Secretary for Petroleum Reserves; Office of Naval Petroleum and Oil Shale Reserves; United States Department of Energy, 2004.

Kellemen P.B.; Matter, J. In situ carbonation of peridotite for CO_2 storage. *PNAS* 2008, vol 105, no 45 17295-17300.

Khan, M. R. A Literature Survey and An Experimental Study of Coal Devolatilization at Mild and Severe Conditions: Influences of Heating Rate, Temperature, and Reactor Type on Products Yield and Composition, *Fuel*, 1989, 68, 1522-1531.

Khan, M. R. and Hshieh, F. Y. Influence of Steam on Coal Devolatilization and on the Reactivity of the Resulting Char, *Preprints of Papers - American Chemical Society*, Division of Fuel Chemistry, 1989, 34(4), 1245-55.

Kinzer, D. Past, Present, and Pending Intellectual Property for Electromagnetic Heating of Oil Shale, *28th Oil Shale Symposium*, Golden, Colorado: Colorado School of Mines, October 13-15, 2008.

Kimber, G.M.; Gray, M.D. Rapid devolatilization of small coal particles. *Combust. Flame.* 1967, 11, 360-362.

Lasaga, A.C. Fundamental approaches in describing mineral dissolution and precipitation rates. In: White, A.F., Brantley, S.L. (Eds.), Chemical Weathering Rates of Silicates Minerals, *Reviews in Mineralogy*, vol. 31. BookCrafters, Chelsea, MI, pp. 23–86, 1995.

Lee, S.; Speight, J.G.; Loyalka, S.K. *Handbook of Alternative Fuel Technologies*, CRC Press. 2007, p. 286.

Lekas, M.A. Progress Report on the Geokinetics Horizontal Retort Process, *12th Oil Shale Symposium*, 1979, pp.229-236.

Lewis, A. E.; Rothman, A. J. Rubble In Situ Extraction (RISE): A Proposed Program for Recovery of Oil from Oil Shale, Lawrence Livermore National Laboratory. UCRL-51768, 1975.

Liao, H.; Li, B.; and Zhang, B. Co-Pyrolysis of Coal with Hydrogen-Rich Gases 1. Coal Pyrolysis under coke-oven gas and synthesis gas, *Fuel*, 1998, 77, 847-851.

Liu, D.X.; Wang, H.Y.; Zheng, D.W.; Fang C.H.; Ge, Z.X.世界油页岩原位开采技术进展 (World Progress of Oil Shale In-situ Exploitation Methods, *天然气工业 (Natural Gas Industry)*, 2009, 29(5), 128-132.

McCown, M. S.; and Harrison, D. B. Pyrolysis and Hydropyrolysis of Louisiana Lignite, *Fuel*, 1982, 61, 1149.

Minkova, V.; Razvigorova, M.; Goranova, M.; Ljutzkanov, L. and Angelova, G. Effect of Water Vapour on the Pyrolysis of Solid Fuels 1. Effect of Water Vapour during the Pyrolysis of Solid Fuels on the Yield and Composition of the Liquid Products, *Fuel*, 1991, 70, 713-719.

Moon, Ted Oil-shale extraction technology has a new owner. *The Journal of Petroleum Technology* (Soc. Petro. Eng), 2008, http://www.spe.org/jpt/2008/02/oil-shale-extractiontechnology-has-a-new-owner/

Mutyala, S.; Fairbridge, C.; Pare, J.R.; Belanger, J.M.R.; Ng, S.; Hawkins, R. Application of microwaves to oil sands and petroleum: A review. *Fuel.Proc.Tech.* 2010, 91, 127-135.

Nair, Vijay; Ryan, Robert; Roes, Guus Shell ICP – Shale Oil Refining, *26th Oil Shale Symposium*, Golden, Colorado: Colorado School of Mines, 2006.

Neavel, R.C. Origin, petrography and classification of coal. *Chemistry of Coal Utilization.* 1981, 2nd Supl. Vol, 91-158.

Oil and Gas Journal Political Fracturing, *Oil & Gas Journal*, Nov 17, 2008, page 20

Peters, W. and Bertling, H., Kinetics of the rapid degasification of coals. *Fuel*, 1965, 44, 317-331.

Petroleum Research Center, University of Utah, Gas Solubility Tests in Oil Shale, 2008.

Qian, Jialin; Wang, Jianqiu World Oil Shale Retorting Technologies, *International Conference on Oil Shale*, Recent Trend in Oil Shale, 7-9 November 2006, Amman, Jordan.

Raytheon Radio Frequency/Critical Fluid Oil Extraction Technology, 2006, http://www.raytheon.com/businesses/rids/products/rtnwcm/groups/public/documents/content/rtn_bus_ids_prod_rfcf_pdf.pdf.

Reuters Mountain West Energy's In-Situ Vapor Extraction Technology Wins the Clean Technology and Energy Utah Innovation Award, 2008, http://www.reuters.com/article/pressRelease/idUS56731+23-May-2008+BW20080523.

Rosenbauer, R. J.; Koksalan, T; Palandri, J.L Experimental investigation of CO_2 -brine-rock interactions at elevated temperature and pressure : Implications for CO_2 sequestration in deep-saline aquifers, *Fuel Process. Tech.* 2005, 86, 1581–1597.

Rothman, A. J. Research and Development on Rubble In-Situ Extraction of Oil Shale (RISE) at Lawrence Livermore Laboratory, *8th Oil Shale Symposium*. Golden, Colorado: Colorado School of Mines, 1975.

Savage, M.T. Geothermic Fuel Cells, *26th Oil Shale Symposium*, Golden, Colorado: Colorado School of Mines, 2006.

Sharma, D.K.; Sulimma, A.; van Heek, K. H. Hydropyrolysis of Coal in the Presence of Steam, *Fuel*, 1986, 65, 1571-1574.

Sharma, D.K.; Sulimma, A.; van Heek, K. H. Comparative Studies of Pyrolysis of Coal in Inert Gas, Steam, and Hydrogen Under Pressure, Erdoel Kohle, Erdgas, *Petrochem*, 1986, 39(4), 173.

Shell Frontier Oil and Gas, Inc. Oil Shale Test Project, Oil Shale Research and Development Project. Plan of operation, Submitted to Bureau of Land Management, 2006.

Shih, S. M.; Sohn, H. Y. Nonisothermal determination of the intrinsic kinetics of oil generation from oil shale. *Ind. Eng. Chem. Process. Des. Dev.* 1980, 19 (3), 420–426.

Shurtleff, Kevin, Doyle, Dave. Single well, single gas phase technique is key to unique method of extracting oil vapors from oil shale. *World Oil Magazine* (Gulf Publishing Company), 2008. http://www.worldoil.com/March-2008-Single-well-single-gas-phase-technique-is-key-to-unique-method-ofextracting-oil-vapors-from-oil-shale.html. Retrieved 2009-09-27.

Suuberg, E. M.; Peters, W. A.; Howard, J. B. Product Compositions in Rapid Hydropyrolysis, *Fuel*, 1980, 59, 105.

Suuberg, E.M. Rapid pyrolysis and hydropyrolysis of coal. *Sc.D thesis, Dept. of Chem.Eng. MIT.* 1977.

Symington, Williams A.; Olgaard, David L.; Otten, Glenn A.; Phillips, Tom C.; Thomas, Michele M.; Yeakel, Jesse D. ExxonMobil's Electrofrac Process for In Situ Oil Shale Conversion, *AAAPG Annual Convention*. San Antonio: American Association of Petroleum Geologists, 2008.

Taiyuan University of Science and Technology: 太原理工大学高温烃类气体对流加热油页岩开采油气的方法, patent, China: E21B43/24. 200710139353. X. (P). 2006-09-06.

Tyler, R. J., Flash pyrolysis of coals. Devolatilization of bituminous coals in a small fluidized-bed reactor, *Fuel*, 1980, 59, 218-226.

United States Department of Energy, Office of Naval Petroleum and Oil Shale Reserves Secure Fuels from Domestic Resources: The Continuing Evolution of America's Oil Shale and Tar Sands Industries, 2007.

United States Department of Interior. Bureau of Land Management. White River Field Office. Environmental assessment. Chevron Oil Shale Research, Development & Demonstration, 2006, CO-110-2006-120-EA. http://www.blm.gov/pgdata/etc/medialib/blm/co/field_offices/white_river_field/oil_shale/chevron_u_s_a__inc.Par.26834.File.dat/CO1102006120EAwofigures.pdf.

United States Office of Technology Assessment, An Assessment of Oil Shale Technologies, 1980, DIANE Publishing.

Vanderborgh, N.E.; Bertino, J.P.; Cort, G.E.; Wagner, P. Convective Heat Transfer Through Coal Blocks. *In Situ*. 1978, 2, 217-228.

Wall, T.F.; Liu, G.S.; Wu, H.W.; Roberts, D.G.; Benfell, K.E.; Gupta, S. The effect of pressure on coal reactions during pulverized coal combustion and gasification. *Prog.Ener.Comb.Sci.* 2002, 28, 405-433.

Wellington, S.L.; Vinegar, H.J.; Berchenko, Ilya I.; Maher, K.A.; deRouffignac, E.; Karanikas, J.M.; Zhang, E. Emissionless energy recovery from coal, Patent, U.S. Provisional Application No. 60/199,213, 2001.

Westmoreland, P.R.; Dickerson, L.S. Pyrolysis of Blocks of Lignite, *In Situ*, 1980, 4(4), 325-343.

White, A.F.; Peterson, M.L. Role of reactive surface area characterization in geochemical models. Chemical modeling of aqueous systems II. In: Melchior, D.C., Bassett, R.L. (Eds.). *Am. Chem. Soc. Symp. Ser.* 1990, 416, 416–475.

Wu, Naniel M.P.; Harrison, Douglas P. Volatile products from lignite pyrolysis and hydropyrolysis, *Fuel*, 1986, 65, 747-751.

Yardim, M. F.; Ekinci, E.; Minkova, V.; Razvigorova, M.; Budinova, T.; Petrov, N. and Goranova, M. Formation of Porous Structure of Semicokes from Pyrolysis of Turkish Coals in Different Atmospheres, *Fuel*, 2003, 82, 459-463.

Yu, J.; Lucas, J.A.; Wall, T.F. Formation of the structure of chars during the devolatilization of pulverized coal and its thermoproperties. *Prog.Ener.Comb.Sci.* 2007, 33, 135-170.

Zerai, B.; Saylor, B.Z.; Matisoff, G. Computer simulation of CO_2 trapped thorough mineral precipitation in the Rose Run Sandstone, Ohio. *Applied Geochem*. 2006, 21, 223-240.

Zheng, D.; Wang, H.; Liu, D.; Li, J.; Ge, Z.大庆柳树河油页岩特点及干馏工艺选择 (Oil Shale Features and the Retorting Process for Oil Shale In the Liushuhe Basin in Daqing), *天然气工业 (Natural Gas Industry)*, 2008, 28(12), 1-3.